5-2023

Partitioning and Microdosimetry of Plutonium-239 and 55-Iron in Environmental Bacteria Grown in Liquid Cultures

Lisa Manglass
lmangla@clemson.edu

PARTITIONING AND MICRODOSIMETRY OF PLUTONIUM-239 AND IRON-55 IN ENVIRONMENTAL BACTERIA GROWN IN LIQUID CULTURES

A Dissertation
Presented to
the Graduate School of
Clemson University

In Partial Fulfillment
of the Requirements for the Degree
Doctor of Philosophy
Environmental Engineering and Earth Sciences

---

by
Lisa M Manglass
May 2023

Accepted by:

Dr. Nicole Martinez, Committee Chair

Dr. Mark Blenner
Dr. Timothy DeVol
Dr. Cindy Lee
Dr. Lindsay Shuller-Nickles

ABSTRACT

The work presented herein provides quantitative data related to bacteria exposed *in situ* to two radionuclides relevant to nuclear sensing: plutonium-239 (^{239}Pu) and iron-55 (^{55}Fe). Originally motivated by the fundamental science underlying biosensing, liquid cultures of *Pseudomonas putida* and *Escherichia coli* were exposed to radionuclides over the course of 15-day experimental periods with the intent of gaining insight into the response of these bacteria. An essential component of characterizing or utilizing this response in a meaningful way is an understanding of the dose leading to that response. This dissertation narrows the knowledge gap associated with dose-response of microorganisms at environmentally relevant radionuclide concentrations through consideration of factors that influence the local dose, i.e., microdosimetry, experienced by the bacteria. These studies found that ^{239}Pu accumulation in *P. putida* cells increased initially but plateaued after about 5 days, whether or not complexed with citrate. Moreover, ^{239}Pu concentration in *E. coli* cells was greater than that in *P. putida* cells which may be the result of a stronger complexing agent made by *E. coli* for the purpose of Fe uptake. In cultures grown with ^{55}Fe, over 75% of ^{55}Fe was located in cell samples because of internal and external accumulation. When *P. putida* cultures were grown with ^{239}Pu and ^{55}Fe in combination, as well as ^{239}Pu in combination with stable Fe, results indicate that ^{239}Pu inhibited the uptake of ^{55}Fe, and that the presence of Fe in cultures may promote pathways for Fe accumulation that are used by ^{239}Pu. Finally, consideration of RNA extractions specifically suggested that ^{239}Pu and ^{55}Fe detected in RNA extraction samples is the result of binding to RNA prior to the time of extraction, as opposed to flow through or binding after cell lysis, and it highlights the practical importance of nucleic acid sample characterization to radiation protection, more generally. The

work presented in this dissertation supports a more robust understanding of the behavior of ^{239}Pu and ^{55}Fe in bacteria systems and provides the groundwork necessary for the development of appropriate microdosimetric models for bacteria as well as more informed interpretation of transcriptomic analysis.

DEDICATION

"We were looking out the window and I said to Jean 'Wow, imagine inventing a car.'

Jean said nobody invented the car from nothing. So many people had to invent so many things."

- @JortsTheCat

To the three generations of working women who raised and inspired me: my Aunt Kim,

Aunt Linda, grandmother, Aunt Cheryl, Aunt Liz, sister-in-law Sharla,

and especially my mother,

to my father, for making sure I always had a computer,

to my brother, for telling me that I applied the torque,

and to all my students (past, present, and future)

for giving me the greatest job in the world.

ACKNOWLEDGMENTS

An acknowledgement isn't sufficient for the thanks owed to my adviser, Dr. Nicole Martinez. She is the model adviser that all aspiring graduate students should search for. She gave me emotional support when I needed an ear to listen and academic support when I needed a project to give me drive. She gave me the chance to do the things I loved, even if it slowed me down sometimes, and considered my unique needs as she guided me, always. She provided criticism when I needed to be pushed, but even when she was tough, she was also fair and kind. She mentored me actively by elevating my voice, finding opportunities for me, and sharing details about her methods and processes any time I asked. And she did all of this while navigating the tenure review process herself. I am a better scientist, teacher, and person because of the role that Dr. Martinez has played in my life, and I will forever be thankful for this opportunity to work with her.

I'd also like to acknowledge the many mentors who have enriched my career. Thank you to my committee members, Drs. Shuller-Nickles, Blenner, and Lee, for taking time to advise me and having patience as I worked to complete my degree. Professionally, I'm so thankful for Dr. Tom Johnson at Colorado State University who never stopped cheering on my career as a health physicist, and my former bosses, Steve Brown and Dr. Doug Chambers, who gave me an amazing career to draw from as I have embarked on this next journey. I will also forever appreciate Phil Egidi for encouraging my career in health physics with a fresh and honest perspective. And, of course, my department chair at Francis Marion University, Dr. Derek Jokisch, who has been patient, supportive, and a joy to work for.

I have also been supported by many peers. At Clemson, Dr. Megan Hoover for being my first Clemson friend, Dr. Mara Watson for understanding me, Dr. Dawn Montgomery for being someone to talk about life with, Merritt Earle for letting me kool-aid-man into his life and be wonderfully weird together, Dr. Connor Parker for bringing joy to my workspace, and Dr. Kathryn Peruski for always taking time to help me with whatever weird thing I wanted to try next. While I am surrounded by wonderful colleagues at Francis Marion, I am especially grateful for the invaluable support provided by Drs. Ginger Bryngelson, Brittany Baker, and Hunter Sims.

There are too many friends to name but I am here today because of the constant support of many pocket friends, my Denver girls, the football girls, my "family" of nonsense and shenanigans, my Frands, nuclear twitter, and my group chat of women that has gone by varying names, none of which would be appropriate to print in a dissertation. Of all these friends, a few must be mentioned by name, however. Jenni, my oldest best friend who provided me a safe space to be loved when I needed it most. Jim, who made room for me to be candid and cared for with abundant comfort. Lee, for giving me a place to game and laugh. Amber, for growing with me in ways that neither of us ever expected and for being the best person to talk out my ideas with. And last, but certainly not least, Lauren, my lobster and my "sister", who I would be lost without.

The most unexpected part of my PhD journey was meeting my husband, Trell. He has been the definition of a partner in life and has surrounded me with the kindest love that I have ever known. Because of him, I also received the incredible gift of my stepdaughters Gabby and Charlotte, who are so different, so special, and so wonderful. I love them more than they will ever know. My life today doesn't look anything like I pictured that it would when I went back to

school in 2016, but I wouldn't change a thing. Thank you, Trell, for building a home with me where I am loved so wholly and have been so very supported as I completed my dissertation.

Perhaps this is unconventional, but I'd also like to take a moment to offer absolutely no thanks at all to COVID-19, my gallbladder, my aging body, and both of my landlords in Anderson. You all made this much harder on me, and it would have been much easier without you.

TABLE OF CONTENTS

LIST OF TABLES

LIST OF FIGURES

CHAPTER ONE

INTRODUCTION

The work presented in this dissertation originated from efforts to evaluate the potential of common microorganisms to act as biosensors and aid efforts related to the non-proliferation of nuclear weapons. The use of common environmental microorganisms as biosensors is appealing for their potential use in scenarios where traditional electronic or passive radiological detection devices cannot be used. The potential for microorganisms to maintain a record of past exposure based on analysis of gene expression is of particular interest. For microorganisms to serve as effective aids in non-proliferation efforts, we must be capable of relating changes in gene expression to absorbed dose and the specific radionuclides to which the microorganisms were exposed so we can differentiate between exposures to materials related specifically to the production of nuclear weapons and radiological exposures from natural radioactivity and peaceful applications of nuclear technology.

The work presented herein is a subset of data collected in the Martinez and Blenner laboratories examining the response of different bacteria and yeasts to alpha, beta, gamma, and neutron radiation. Specifically, this dissertation examines physical, radiological data from *Pseudomonas putida* and *Escherichia coli* grown in liquid culture with ^{239}Pu and ^{55}Fe, both alone in combination. Both radionuclides are metals and have similarities in their expected behavior in liquid bacteria cultures, however ^{239}Pu provides the opportunity to examine exposures to high Linear Energy Transfer (LET) alpha radiation, while ^{55}Fe provides the opportunity to examine low-LET, low-energy beta and gamma radiation.

The task of evaluating microorganisms for their potential use as discriminating biosensors of radiological exposure is challenging and cannot be evaluated without examining more fundamental questions regarding the exposure of microorganisms to different sources of radiological material in various environments. As such, beyond the goals of the project related to the non-proliferation of nuclear weapons, the chapters to follow provide support for the utility of this data for a variety of other radiological science applications. In particular, the work supports efforts to describe the biological response of *P. putida* and *E. coli* by developing dose estimates that reflect the specific conditions of radiological exposure in the form of a dose response model.

A first step in the process of understanding a dose-response was to determine the fractionation of ^{239}Pu and ^{55}Fe between the growth media and the cells. In the following studies, dose estimates to bacteria were used to determine the quantities of radionuclides to add to each culture. The dose estimates were based on absorbed dose in water, where the water was both the source and receptor, assuming a homogenous distribution of radionuclides in the water. Because of the, relatively, local deposition of energy from ^{239}Pu and ^{55}Fe emissions, any accumulation of the ^{239}Pu or ^{55}Fe on the cell surfaces or inside the cells (via uptake) would render the assumption of a homogenous distribution inaccurate. As expected, ^{239}Pu and ^{55}Fe both concentrated in the cells justifying the need for more rigorous examination of dose via microdosimetry as opposed to an absorbed dose calculation in a fluid. The work presented in this dissertation attempts to characterize the similar and dissimilar ways that ^{239}Pu and ^{55}Fe concentrate in cells over a 15-day experiment.

When samples of ribonucleic acid (RNA) extractions were analyzed for radioactivity for the purpose of radiological materials handling, the results were unexpected. The RNA extraction

process is highly selective for RNA to maintain sample purity, so it was not expected that these samples would contain detectable concentrations of ^{239}Pu or ^{55}Fe. Instead, the observation that the RNA extracts did, in fact, contain ^{239}Pu and ^{55}Fe indicated that further analysis was warranted. In the chapters to follow, analysis of RNA extracts for radiological content is undertaken to examine their utility as a tool for comparing uptake versus sorption of radionuclides in the cells. The analysis of RNA extractions includes an experiment designed to examine the extraction process itself, because of the possibility that process flowthrough was responsible for the results observed.

In Chapter 2, ^{239}Pu accumulation with and without citrate was examined in *P. putida* cultures, and the fractionation of ^{239}Pu when complexed with citrate was examined in *P. putida* and *E. coli* cultures. The accumulation of ^{239}Pu in *P. putida* cells was found to increase both with and without citrate complexation for the first five days and then plateau until the end of the study period (15 days). Citrate complexation was found to sufficiently increase the solubility of ^{239}Pu in *P. putida* cultures. The activity concentration of ^{239}Pu in *E. coli* cells was greater than that in *P. putida* cells which may be the result of a stronger complexing agent made by *E. coli* for the purpose of Fe uptake. In Chapter 3, ^{239}Pu accumulation was considered in combination with ^{55}Fe and stable Fe. In cultures grown with ^{55}Fe, over 75% of ^{55}Fe was located in cell samples because internal and external accumulation. When *P. putida* cultures grown with ^{239}Pu and ^{55}Fe in combination, as well as ^{239}Pu in combination with stable Fe, and the results support hypotheses regarding uptake of both radionuclides with supporting data from the analysis of ribonucleic acid (RNA) extractions. Results indicate that ^{239}Pu inhibited the uptake of ^{55}Fe, and that the presence of Fe in cultures may promote pathways for Fe accumulation that are used by ^{239}Pu. Chapter 4 investigates the hypothesis that radiological content in RNA extractions presented in Chapter 3

were the result of process flow-through. RNA extractions were performed on bacteria growth media with and without bacteria cells (i.e., with and without RNA) at several different concentrations of ^{239}Pu and ^{55}Fe. Results of the study suggest that ^{239}Pu and ^{55}Fe detected in RNA extraction samples during long term cell studies is the result of binding to RNA prior to the time of extraction, as opposed to flow through or binding after cell lysis, and it highlights the practical importance of nucleic acid sample characterization to radiation protection more generally. Chapter 5 provides an overall summary of the dissertation conclusions and a discussion of future work. The final five appendices provide supplemental information for Chapters 2, 3, and 4.

The data presented herein has undergone peer review and published in the literature prior to the publication of this dissertation. Chapters 2, 3, and 4, are adaptations of papers published under the same titles as the chapter titles as provided below.

- Chapter 2: Health Physics Journal, Volume 121(5), Pages 484-493
- Chapter 3: Journal of Radiological Protection, Volume 41(4), 1199
- Chapter 4: Journal of Radiological Protection, Accepted January 4th, 2023

CHAPTER TWO

PLUTONIUM-239 ACCUMULATION IN *E. COLI* AND *P. PUTIDA* GROWN IN LIQUID CULTURES

Abstract

Understanding of the behavior and effects of plutonium (Pu) in the environment is an important aspect of developing responsible and effective strategies for remediation and environmental stewardship. This work studies the sorption and uptake of ^{239}Pu by common environmental bacteria, *Escherichia coli* DH10β and *Pseudomonas putida* KT-2440. Plutonium was directly incorporated into growth media prior to inoculation (0.12 kBq mL^{-1}), and samples from the liquid cultures of *E. coli* and *P. putida* were analyzed over a 15-d growth period through liquid scintillation counting (LSC) of Pu in cell pellets and cell culture media following centrifugation. To improve its solubility in the liquid cultures, Pu was complexed with citrate prior to inoculation. *P. putida* cultures were also grown without citrate to examine potential impact of *P. putida*'s ability to use citrate as a food source. The accumulation of Pu in *P. putida* cells was found to increase both with and without citrate complexation for the first 5 d and then plateau until the end of the study period (15 d). A higher activity concentration of Pu was found in *P. putida* cells grown with citrate complexation than without. The activity concentration of Pu in *E. coli* cells was greater than that in *P. putida* cells, which may be the result of a stronger complexing agent made by *E. coli* for the purpose of iron uptake. There are a variety of factors that influence Pu behavior in bacterial systems, and results confirm that even in a simple system, multiple mechanisms are at play.

Introduction

Plutonium in the Environment

Plutonium (Pu) is primarily found in the environment anthropogenically, released through nuclear weapons production and testing, nuclear fuel reprocessing and storage, nuclear accidents, and the re-entry of satellites powered by radioisotope thermoelectric generators[1–4] . Environmental stewardship requires effective strategies for management and remediation of such actual or potential releases, and responsible decision-making necessitates understanding of the behavior and effects of Pu in the environment. Although Pu has long been studied in ecosystems[5–7] there are still many knowledge gaps regarding its environmental behavior[8] that continue to be of interest due to the long-term human and environmental health concerns associated with legacy Pu contamination as well as potential future contamination. This study considers exposure of *Escherichia coli* and *Pseudomonas putida* to ^{239}Pu ($t_{1/2}$ = 24,110 y) which is a fissile nuclide that is used in the production of nuclear weapons. Plutonium-239 is also present in high-level radioactive waste, and its mobility is a significant factor influencing long-term risk of geological disposal [9].

Bacteria of Interest

E. coli and *P. putida* are both gram-negative, rod-shaped bacteria that are commonly found in a variety of environmental habitats. The *E. coli* strain used in this work was derived from a K-12 strain which is a model organism that has been studied over the nearly one-hundred years since the first isolation of K-12 *E. coli* in 1922 [10]. *E. coli* is a versatile model organism that has held a key role in understanding many foundational principles of genetics[11]. The specific strain selected for this work, *E. coli* DH10β, is a non-pathogenic strain that is frequently selected

for laboratory experiments and is primarily used for DNA cloning because of its suitability as a host for large foreign DNA fragments[12]. *E. coli* cells are approximately 1-2 μm long with a radius of 0.5 μm [13], as seen in **Figure 1**a.

P. putida is ubiquitous in soil and fresh water ecosystems and has a versatile metabolism that allows it to grow in a variety of environments[14]. The strain of *P. putida* selected, KT2440, is a biological safety strain of that has been fully sequenced since 2002 and has been used in a wide variety of research activities, so it is well characterized and suited for bioinformatic investigations[15]. *P. putida* are generally found to have a length of about 2 μm and a radius of about 0.5 μm[16] as seen in **Figure 1**b.

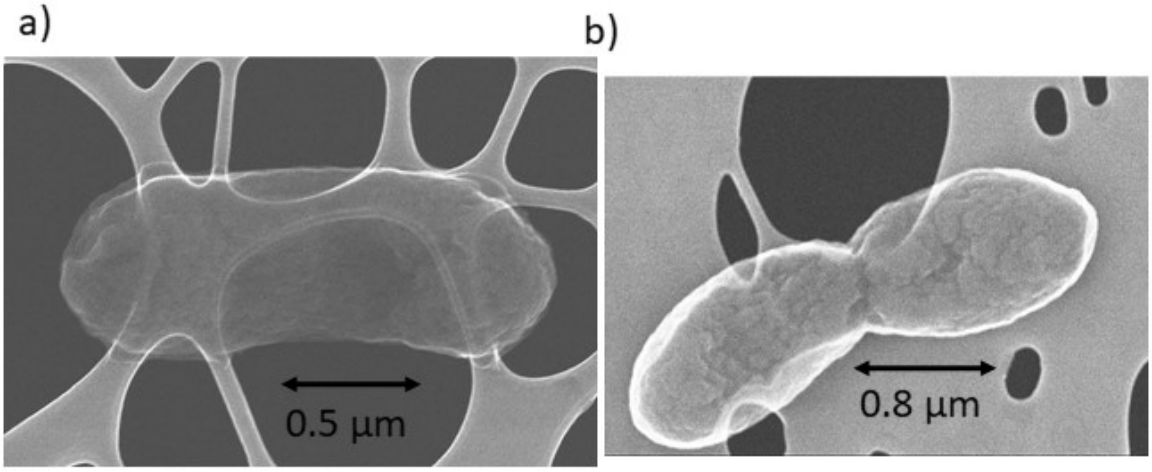

Figure 1 Images of (a) *E. coli* and (b) *P. putida* collected from liquid cultures. Images were collected by at the Clemson Electron Microscopy Facility in June 2019 via Transmission Electron Microscopy (Hitachi HD 2000).

Plutonium in liquid cultures of bacteria

For practical purposes, absorbed dose is typically averaged over a volume of interest[17]. It is conventionally assumed that deoxyribonucleic acid (DNA) is the primary and critical target for induction of dose-related effects, whether directly or indirectly produced. As summarized in a

thorough review paper by Dauer et al.[18], the current literature suggests that while this assumption is warranted in many cases, interactions with the cell membrane, proteins, mitochondria, cell signaling pathways, and other organelles may also be responsible for inducing effects as a result of ionizing radiation, and these effects may be highly relevant to understanding the mechanisms of effect of chronic low doses of radiation.

Plutonium-239 decay results primarily in the emission of 5.14 MeV alpha particles [19] which travel about 49 μm on average in water or tissue, depositing energy along their path of interaction. Plutonium-239 concentrated within the cells internally (via uptake) or externally on the cell surfaces (sorption) would mean that a larger portion of alpha interactions will occur at sensitive locations within the cells including, but not limited to, bacterial DNA, the cell membrane, and other organelles.

The influence of citrate on plutonium chemistry

To utilize ^{239}Pu in an aqueous solution, previous work in the Martinez lab using citrate with Pu indicated that a complexing agent would be required to maintain proper solubility.[20] While many complexing agents are capable of making this oxidation state change, the use of citrate was determined to meet my needs in this experiment as the biological impact was assumed to be minimal as compared to other options such as ethylenediaminetetraacetic acid (EDTA). The use of citrate as complexing agent transforms Pu(V) into Pu(IV), which is generally soluble at near neutral pH when complexed with an organic ligand like citrate[21]. There is ample evidence in the literature that Pu will readily bind to the surfaces of cells or other organic matter[22]. Although Pu has many interactions with cells that are similar to those of other metals, Pu also has many unique behaviors because of its complicated variety of oxidation states at near-neutral pH ranges and large physical size, and as such, Pu is generally more likely to

bond to surfaces than be transported through the cell membrane [23]. A complicating factor in Pu transport, however, is siderophore complexes that are produced by bacteria for the purpose of transporting iron across the cell membrane. Biotransformation of Pu(IV) organic complexes is expected in the presence of *Pseudomonas* bacteria[24]. Evidence of Pu transport through the cell membrane has been observed in *P. putida* by a variety of siderophore complexes including via hydroxamate complexes which are the strongest natural Pu chelating compounds [25]. The use of citrate as a complexing agent provides an interesting scenario when examining partitioning of Pu in *P. putida* cultures. While both bacteria studied herein have pathways to transport iron and presumably Pu across the cell membrane, *P. putida*'s robust metabolism allows it to use citrate as an energy source providing further pathways for Pu mobility in and around the cells [26] whereas *E. coli* cannot use citrate as an energy source under aerobic conditions [27].

Our work, therefore, starts by examining the impact of citrate complexation on the partitioning of Pu in *P. putida* cell cultures so that this information can be utilized to improve dose modeling efforts, an important step in the development of dose-response relationships. While the assumption that the addition of citrate would maintain sufficient solubility, I found it prudent to examine activity of cell culture samples as compared to the expected activity of the samples to ensure that the ^{239}Pu remained soluble during the work. General chemical models can determine the solubility of ^{239}Pu based on the quantity of complexing agents, but the less predictable factor of siderophore production by bacteria could alter the oxidation state ratios of ^{239}Pu. I found that comparing cultures with ^{239}Pu not complexed with citrate as well as ^{239}Pu complexed with citrate would provide more confidence in this and future analyses.

Motivation

The work described herein was part of a larger effort that sought to identify transcriptional changes in ribonucleic acid (RNA) expressed by model environmental microorganisms that were exposed to low radiation dose rates (~9 mGy d^{-1}) of select radionuclides relevant to anthropogenic, nuclear-related activities. This process afforded the opportunity to gain fundamental knowledge concerning the (1) low dose effects to model microorganisms, and (2) influence of these organisms on Pu behavior in a simple aquatic system. The utility of this knowledge can be applied to the broad environmental problems inherent with the use and disposal of materials that contain Pu. The study of common microorganisms provided insight into the effects of ionizing radiation at low-doses in environmental settings as these organisms are often indicators of environmental health and can provide pathways to the food-chain via low-trophic level organisms[28].

A long-term goal of my study is to combine the results regarding the accumulation of radionuclides with microdosimetric modeling to ensure that accurate doses are connected to observed changes in gene expression. The system of interest was environmental bacteria grown in liquid culture, and the first step in developing an appropriate dose response model for this system was to examine the partitioning of the radionuclide between the growth media and the organism to enable the development of microdosimetric models. Specifically, the objectives of the study were

- To examine the impact of citrate complexation on Pu accumulation in *P. putida* over an exposure duration of 15 days (as *P. putida* can use citrate as a food source) and
- To examine Pu accumulation in the common environmental bacteria *E. coli* and *P. putida* over an exposure duration of 15 days.

Materials and Methods

Bacteria culture

Non-pathogenic strains of bacteria, *P. putida* KT-2440 (Nelson et al., 2002) and *E. coli* DH10β[12], were grown from glycerol stocks in 100 mL of M9 minimal media (recipe provided in Appendix C) in 250 mL baffled flasks on a New Brunswick I24R (Eppendorf AG, Hamburg, Germany) temperature-controlled shaker/incubator at 215 rpm and 28 °C for 15 days. M9 minimal media was supplemented with 0.5% glucose, 1% thiamine hydrochloride, and 1% casamino acids. As mentioned previously, these microbes were chosen because they would be expected to be exposed to radioisotopes in their natural ecologies, and as they are ubiquitous in nature, would make excellent sentinels. The health of the bacteria cultures was monitored with routine optical density (OD) measurements on all sampling days at 600 nm.

Radiological treatments

Three treatment groups (control, ^{239}Pu, and ^{239}Pu complexed with citrate), each in biological triplicate, were used in investigating Pu accumulation in *P. putida*. For investigations of *E. coli*, two treatment groups (control and ^{239}Pu complexed with citrate) also in biological triplicate, were considered. At the time of experimentation with *E. coli*, it was already determined that ^{239}Pu complexed with citrate would provide sufficient solubility to conduct the experiments. While a set of data including *E. coli* grown with ^{239}Pu not complexed with citrate would have been ideal for my work, this exposure scenario was not determined to serve the overall project's goals and was not authorized at the time because of limited space on the incubation platform.

Prior to inoculation with bacteria, radionuclide treatments were added to growth media from an in-house stock solution of ^{239}Pu in 0.01M HCl with a concentration of 69.9 kBq mL^{-1} (30.4 ppm). The Pu solution was provided by the radiochemistry group at Clemson University and contained 99.919% ^{239}Pu by mass as of 07 July 2015 as per personal correspondence (B. Powell, August 28th, 2017). The oxidation state was assumed to be primarily Pu(V) (~75%) with some Pu (IV) and Pu(VI) prior to the addition of citrate, based on oxidation state analysis of the stock solution. Based on oxidation state measurements of growth media spiked immediately prior to inoculation, the oxidation state of Pu in treatment groups where citrate was added was found to be primarily Pu(IV) (75-80%) with the remainder mostly comprised of Pu(V). Additional information regarding oxidation state analysis can be found in Appendix B.

All treatment groups were spiked to a concentration of Pu that would yield a uniform absorbed dose rate to the growth media (including bacteria) of approximately 9 mGy d^{-1}, assuming homogenous distribution of Pu (specifically, 0.12 kBq mL^{-1} or 0.05 ppm). For treatment groups containing Pu-citrate, citrate was added to an aliquot of ^{239}Pu stock solution with which each Pu-citrate group was treated to ensure consistency between replicates. The citrate-to-Pu mass ratio was approximately 1000:1. A citrate treatment was considered because citrate acts as a chelating agent, and the propensity of Pu to bind with other organic substances including cell surfaces may be limited as compared to Pu that is not complexed and more readily available for binding[23].

The dose rate was selected to be just below Department of Energy's upper end of environmental dose rate guidelines (10 mGy d^{-1} for terrestrial biota) which are considered safe levels of exposure with respect to biota population effects [29]. The DOE dose rate guidelines are based on seeing "no effect" on population attributes in terrestrial biota including mammals and

birds, which are much more radiosensitive than bacteria[30]. Although these guidelines do not specifically address microorganisms or individual response, we consider these values to be representative of "low dose rate" because they are appropriately conservative for the study of bacteria, where the goal of our study is to observe individual responses in gene expression without expression being dominated by DNA repair. The dose-rate of 10 mGy d^{-1} is also relevant when compared to dose-rates at sites of historic environmental contamination. For example, the average radiation doses in the top 1 cm soil layer at Kyshtym, the primary site of contamination from a nuclear accident at the Mayak Pu production facility in Russia, were on the order of 5-12 mGy d^{-1} [31].

Sampling method for cell cultures

Sampling (0.5 mL aliquot) was conducted 24-hours post inoculation (day 1) such that the bacteria had sufficient time to reach a stationary phase prior to sampling and then approximately 36- and 48-hours post-inoculation (days 1.5 and 2, respectively) and at days 5, 10, and 15. Samples were centrifuged at 5500 relative centrifugal force (RCF) for 5 minutes at room temperature. The supernatant was eluted from each sample and collected in a liquid scintillation vial. Cell pellets were rehydrated in 0.5 mL of M9 minimal growth media and resuspended by vortexing. Resuspended pellet samples were treated with 25-50 µL of H_2O_2 (30%) depending on the amount of organic matter in the sample and lightly vortexed. The addition of H_2O_2 (30%) was used to break down organic material and reduce potential effects of physical quenching during liquid scintillation analysis. Samples were left (uncapped) with added H_2O_2 for least 30 minutes prior to transferring samples to liquid scintillation vials for analysis. A graphical depiction of this method is provided in **Figure 2**.

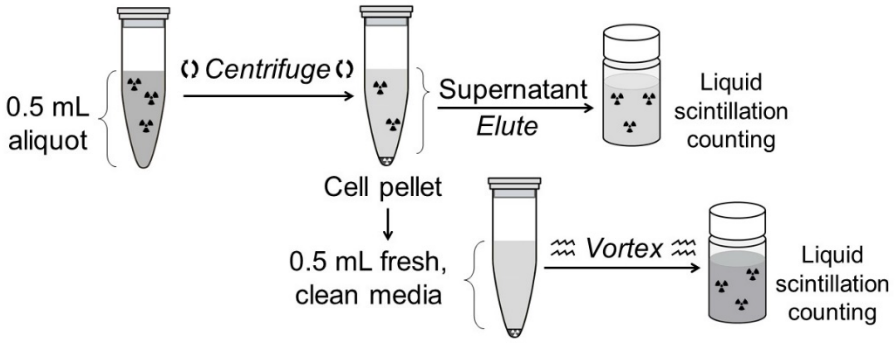

Figure 2 Conceptual model depicting an overview of the sampling and analysis process.

Sample masses were collected for the total sample, cell pellet, and supernatant for the purpose of mass balance calculations. All liquid scintillation vial samples were prepared for liquid scintillation counting (LSC) analysis with the addition of 10 mL of Optiphase HiSafe 3 liquid scintillation cocktail (PerkinElmer, Waltham, MA, USA). The sampling process is a destructive testing process such cells cannot be recovered from cell pellet samples after the addition of H_2O_2.

Determination of radioactivity content

Samples were analyzed for radioactivity using a Tri-Carb 4910 TR liquid scintillation analyzer (PerkinElmer, Singapore). We assumed an efficiency of 100% for alpha emissions from Pu decay, which is the expected and manufacturer recommended efficiency for alpha counting. To ensure proper quantification of Pu in the samples, potential contributions to total activity were considered based on the reported isotopic ratios of ^{239}Pu (99.919%), ^{240}Pu (0.055%), ^{238}Pu (0.002%), ^{241}Pu (0.012%), and ^{242}Pu (0.012%) as well as all potential ingrowth products: ^{234}U, ^{235}U. ^{236}U, ^{238}U, and ^{241}Am. The Pu stock used routinely undergoes a Pu separation process to remove U and Am ingrowth products. Using the date of the last Pu separation, the date of the

experiments, and the isotopic ratios at the certification date, the only isotopes with an expected contribution of more than 0.1% of total activity were alpha emitters ^{239}Pu (84.59% of total activity), ^{239}Pu (0.46%), and ^{240}Pu (0.17%) and the beta emitter ^{241}Pu (14.73%). The resolution of the LSC method was insufficient to differentiate alpha peaks from the different Pu isotopes, and as such an alpha peak region was used to collectively count all activity from ^{239}Pu, ^{238}Pu, and ^{240}Pu. While the peak resulting from ^{241}Pu beta emissions could be differentiated from the alpha peak, we were unable to obtain a counting efficiency for these beta emissions to allow for true quantification of ^{241}Pu. To determine total Pu in samples, we used the assumption that the total counts from the alpha region accounted for approximately 85% of total sample Pu activity, such that the reported Pu concentrations are the result of the net counts from the alpha region divided by 0.85. An example calculation to demonstrate this is provided in Appendix D.

All samples were normalized to a 1 mL sample volume for direct comparison by using the total mass of each sample and the simplifying assumption that the density of the liquid cultures was 1 g cm^{-3}. The net activity concentration of Pu was determined by using the average of three biological replicate control samples for the given sampling day for background subtraction.

Assumptions

As proof of principle that citrate improved Pu solubility, the measured activity of the samples was normalized to 1 mL and compared to the expected activity of a 1 mL sample of culture. The expected concentration was calculated assuming homogenous distribution of Pu in solution such that the expected net total activity in the entire 100 mL flask was 120 kBq, and a 1 mL would contain 0.12 kBq. As such, the expected activity concentration would be 0.12 kBq mL^{-1}. If the Pu did not remain in solution, one would expect sorption to the flask surface which

would reduce the concentration of Pu to less than 0.12 kBq mL^{-1}. A simplifying assumption applied was that liquid bacteria cultures retain both a constant volume (accounting for sampling) and density. The latter assumption of 1 g mL^{-1} is likely a source of error in these calculations as the density of individual cells varies between live, dead, and stressed cells[32], and therefore, likely varied over the course of the experiment. The density assumption was applied for the entire volume of culture; while cell density will vary non-uniformly over the duration of a 15-day experiment period, the density of the growth media will not, and as such we expect that this assumption will result well below 10% error in all cases.

Terminology

In the analysis of data provided in the next section, the following terms are utilized.

- **Expected Activity**- The expected activity of any sample is based the assumptions that 120 kBq of ^{239}Pu will be distributed homogeneously in 100 mL of growth media and that there is no loss of ^{239}Pu via sorption to the flask walls. As such, the expected activity of a 1 mL sample was determined to be 0.12 kBq and the Expected Activity Concentration of the solution is thus 0.12 kBq mL^{-1} because

$$\frac{Total\ ^{239}Pu\ added\ to\ flask(kBq)}{Volume\ of\ growth\ media\ in\ flask(mL)} = Expected\ Activity\ Concentration$$

- **Cell Pellet Activity** The cell pellet activity is defined as the activity determined when the cell pellet sample was analyzed by LSC as described in the above sections (**Figure 2**, Bottom LSC vial)
- **Media Activity** The media activity refers to the activity of sample comprised of eluted growth media during sample processing (**Figure 2**, top vial).

- **Total Sample Activity** The total sample activity is the activity of the entire sample collected, which was defined as the sum of the cell pellet activity and media activity.

$$Total\ Sample\ Activity = Cell\ Pellet\ Activity + Media\ Activity$$

As described in detail in the previous sections, results in all cases were normalized based on the sample mass to account for variation in pipetting. All results presented have been normalized for direct comparison.

Statistical analysis

Statistical analyses were conducted with Minitab (Minitab18, State College, PA, USA) and JMP Software (SAS Institute Inc., Cary, NC, USA). In all cases, significance was taken as $p < 0.05$. Simple linear regression models and associated confidence / F-tests were computed using JMP. All other analysis was completed with Minitab. Analysis of variance (ANOVA) statistical tests were used to determine the significance of the effects of predictor variables such as treatment duration or bacteria species on useful activity metrics (e.g., cell pellet activity concentration). In such cases that treatment duration was a significant contributor to variation in an activity metric of interest, additional analyses were conducted to provide further insight into this variation. For example, comparisons of the means of relevant activity metrics on specific sampling days were completed with two-sample, one-tailed t-tests without the assumption of equal variance. Multiple linear regression was used to determine the statistical significance of temporal trends and to compare trends as appropriate. Reported errors are standard error of the mean.

Results and Discussion

Citrate and Solubility in P. putida Cultures

The purpose of this portion of the experiment was to justify if a complexing agent was needed by examining if the addition of citrate significantly increased solubility of ^{239}Pu in the cell cultures. To determine the impact of citrate on the solubility of ^{239}Pu in solution, total sample activity as a fraction of expected activity was computed.

$$Fraction\ of\ Expected\ Activity = \frac{Total\ Sample\ Activity}{Expected\ Activity}$$

It was expected that samples without citrate would have a lower total activity, and thus a lower fraction of expected activity, compared to the citrate samples because as Pu precipitates it is likely to sorb to the surface of the flasks containing the culture, even with constant mixing on the incubator platform. The time series of fraction of expected activity found in samples is shown in **Figure 3**.

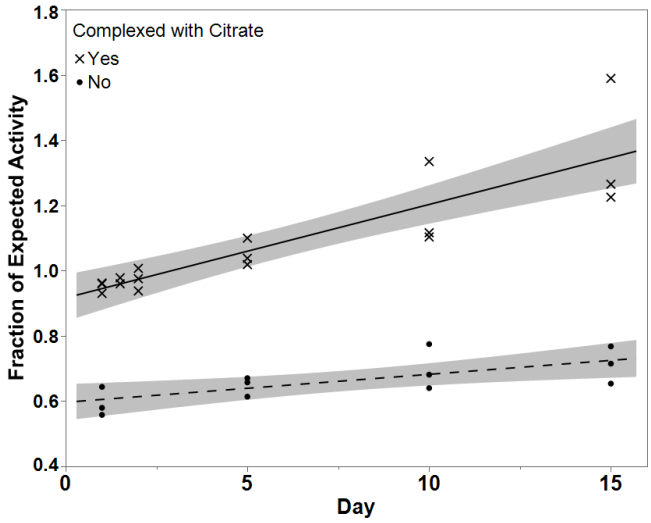

Figure 3 Fraction of expected activity (where expected activity was 0.12 kBq) vs sampling day for *P. putida* where treatment groups with citrate are indicated with "x" and treatment groups without citrate are indicated with "•". Data were fit with simple linear regression models and the shaded area shows the 95% confidence interval for the model.

As presented, the data indicates that samples from cultures containing ^{239}Pu with citrate contain a larger percent of the expected activity, justifying the use of a complexing agent. Because the flasks are constantly mixed on the incubator platform, samples of the cell cultures would still be expected to contain insoluble ^{239}Pu unless the insoluble form sorbed to the flask walls, removing it from the solution. The simple linear regression models in **Figure 3** were added to determine if sample day was a significant predictor of the fraction of expected activity and, if so, provide a quantitative analysis of the interaction. The linear regression models for ^{239}Pu without citrate ($y=0.5968+0.008553x$) and with citrate ($y=0.9163+0.02865x$) both demonstrate that sample day was a significant predictor of the fraction of expected activity via F-test ($p = 0.0094$ and $p \leq 0.001$, respectively). The appropriate interpretation of these models in terms of the experiments is that when citrate is not present samples contained an average of 59.7% of the expected activity at a theoretical "day 0", and that the percent of expected activity increases at a rate of 0.9% per day. Similarly, when citrate is present, the model explains that samples contained an average of 91.6% of the expected activity at a theoretical "day 0" with an increase of 2.9% per day. The observation that the fraction of expected activity increases as a function of time was unexpected from the perspective of ^{239}Pu sorption to the flask walls. If the amount of ^{239}Pu that sorbed to the walls remained constant, day would not be a significant interaction term. If the amount of ^{239}Pu that sorbed to the walls increased over time, then a negative relationship with sample day would be expected, as ^{239}Pu is removed from the solution. Because the amount of ^{239}Pu sorbed to the walls was not directly measured, it is not possible to statistically test for interaction between sorption to the flask walls and fraction of expected activity.

The positive relationship between fraction of expected activity and day indicates that another factor is present, which I hypothesize was the result of the evaporation of water from the cell cultures as evaporation was qualitatively observed during the experiment. A fifteen-day exposure period is a long duration for bacteria studies of this nature, and evaporation of water from the liquid cultures over time is expected. Evaporation, which would increase the concentration of ^{239}Pu relative to the decreasing water content in the flasks, is also indicated by both the positive relationship between fraction of expected activity and sample day, as well as by the multiple observations where the fraction of expected activity was greater than one in the case of ^{239}Pu complexed with citrate. The value used for expected activity in **Figure 3** assumed that the only liquid removed from the culture was for sampling purposes, and the expected activity, accordingly, remained constant throughout the analysis. If evaporation were occurring, the expected activity would increase as evaporation occurred. However, as there was no practical way to ascertain the remaining volume of each culture on a given day without introducing a risk of contamination of the cultures or an unacceptable level of stress to the bacteria, so the evaporation rate was not quantitatively assessed. An additional complication related to evaporation of liquid during the experiment is that the evaporation rate was not consistent across the entire incubation platform, so a proxy flask could not be used to determine an evaporation rate.

With no quantitative assessment of evaporation, any attempt to provide a correction would be best described as a pseudo-correction, however I provided such a pseudo-correction to examine the data further. If the concentration of ^{239}Pu is increasing as a function of time due to evaporation, as hypothesized, then the total sample activity will also increase with time as the same volume is sampled at each timepoint considered. When the total sample activity for both

^{239}Pu with and without citrate were plotted as a function of time and fit with a simple linear regression model, the relationship between sample activity and time is determined to be y=4936+79.19x for ^{239}Pu without citrate (p=0.0078 based on F-test) and y=3583+127.5x (p<0.001 based on F-test).

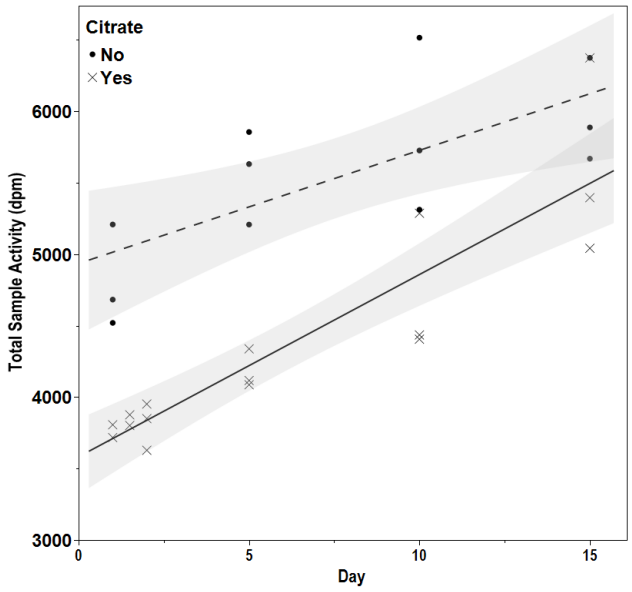

Figure 4 Total sample activity of ^{239}Pu as a function of day, with simple linear regression models. The shaded area indicated the 95% confidence interval for the model. Treatment groups with citrate are indicated with "x" and treatment groups without citrate are indicated with "•".

The correction factors determined from these models were "pseudo" corrections because, to use them, I was required to assume that the increase in activity over time is primarily attributed to evaporation and that there was no significant change in the amount of ^{239}Pu sorbed to the walls of the flask over time. The assumptions needed were reasonable, but the experiment did not provide the quantitative data required to prove that they are justified, therefore the corrections presented should be considered of utility for illustrative purposes only. The slopes of the linear regression models (79.19 dpm d^{-1} for no citrate and 127.5 dpm d^{-1} with citrate) show

the rate of change for activity of the samples per day of the experiment. They were applied as pseudo-correction factors for the expected activity of samples:

^{239}Pu without Citrate

$$Expected\ Activity + (79.19 \times Day) = Pseudo - corected\ Expected\ Activity$$

^{239}Pu with Citrate

$$Expected\ Activity + (127.5 \times Day) = Pseudo - corected\ Expected\ Activity$$

Finally, a pseudo-corrected fraction of expected activity can be computed as such:

$$Pseudo - corrected\ Fraction\ of\ Expected\ Activity = \frac{Total\ Sample\ Activity}{Pseudo - corrected\ Expected\ Activity}$$

The pseudo-corrected fraction of expected activity is plotted as a function of time in **Figure 5.**

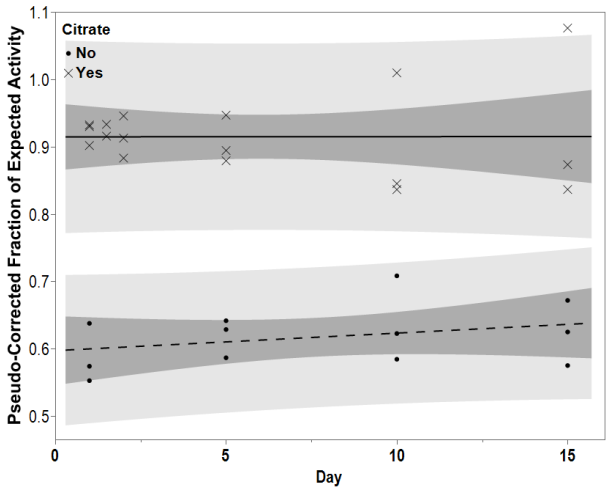

Figure 5 Pseudo-corrected fraction of expected activity as a function of time for cell culture samples containing ^{239}Pu with and without citrate complexation using correction factor for evaporation. The darker shaded area indicated the 95% confidence interval for the model, while the lighter shaded area indicates the 95% confidence interval for observations. Treatment groups with citrate are indicated with "x" and treatment groups without citrate are indicated with "•". There is no significant interaction between fraction of pseudo-corrected fraction of expected activity and day.

When the pseudo-corrected fraction of expected activity is statistically analyzed, there is no longer any significant interaction with sample day (p= 0.3147 for no citrate and p=0.9920 for

citrate). The average pseudo-corrected fraction of expected activity for samples without citrate was found to be 0.617±0.012 and for samples with citrate the average was 0.905±0.013, indicating that the citrate greatly improved the solubility of ^{239}Pu in the cultures and was necessary for future work. The pseudo-corrected averages further support the use of a complexing agent in our cultures. Note that because one replicate in the ^{239}Pu with citrate exposure scenario on Day 15 was found to be a statistical outlier as it was outside of the predicted region for observations (visually presented in **Figure 5**), it was excluded when the average and associated standard error was calculated.

Accumulation of ^{239}Pu in P. putida cells with and without citrate

The accumulation of Pu in *P. putida* cells was examined in two different ways. The first was by looking at the fraction of total Pu activity in the liquid culture sample that was found in cell pellet sample such that:

$$\text{Fraction of Total Activity in Cell Pellet} = \frac{\text{Cell Pellet Activity}}{\text{Cell Pellet Activity} + \text{Media Activity}}$$

A comparison of the fraction of total activity in cells pellets between *P. putida* cultures grown with and without citrate complexation is found in **Figure 6**a. In addition, the accumulation of Pu in *P. putida* cells was examined based on the activity concentration of the cell pellet sample, where:

$$\text{Activity Concentration } \left(\frac{\text{Bq}}{\text{g}}\right) = \frac{\text{Cell Pellet Activity (Bq)}}{\text{Mass of Cell Pellet (g)}}$$

The activity concentration of cell pellet samples from *P. putida* with and without citrate over the sampling period is provided in **Figure 6**b.

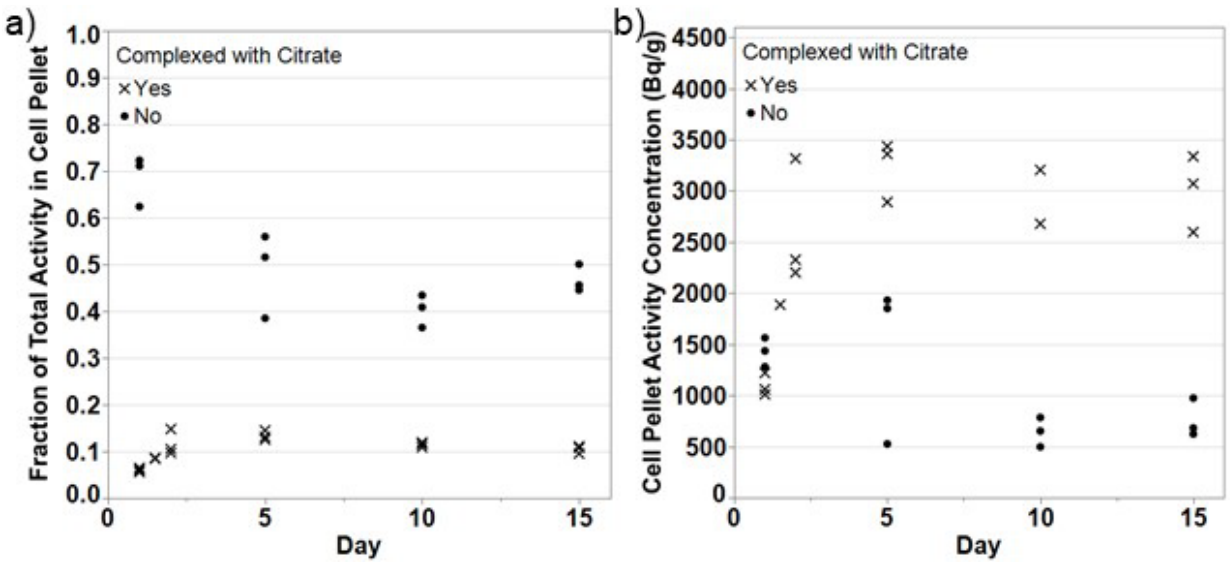

Figure 6(a) Fraction of total sample activity found in sample cell pellet vs sample day for *P. putida*. (b) Activity concentration of cell pellets vs sample day for *P. putida* where activity concentration is the activity of Pu in Bq of the pellet sample divided by the mass of the pellet sample (g). Treatment groups with citrate are indicated with "x" and treatment groups without citrate are indicated with "•".

In **Figure 6**b, the *P. putida* cells in cultures without citrate showed a high fraction of total Pu activity in cell pellet samples, where most samples had more than 40% of Pu in cell pellet samples with a range of 36.5-72.3% even though the cells only accounted for 2.8-8.1% of the total samples by mass. Because there was no chelating agent added to the cultures, this high accumulation fraction was likely the result of adsorption directly to the cell membrane surface. However, some of the accumulation of Pu in the cells grown without citrate may also have been the result of complexation with pyoverdines, which are produced by *Pseudomonas* bacteria that aid iron uptake[33]. Comparatively, in *P. putida* cultures grown with citrate complexation for ^{239}Pu, a much smaller fraction of total activity was found in the cell pellets with a range of 5.6-14.8% of total activity in cell pellets (where cell pellets made up 0.5-0.9% of the samples by mass).

The activity concentration of cell pellets was larger for cultures grown with citrate than without. As discussed in the previous section, because the ^{239}Pu with citrate was more soluble in the growth media than the ^{239}Pu without citrate, the total activity of the samples when citrate was not present was much lower than the total activity of samples with citrate. The higher activity concentration in cultures grown with citrate may be due, in part, to the higher activity of the total samples, such that more Pu was available for sorption or uptake, but the difference is not fully explained by higher total activity alone and may be the result of *P. putida* metabolizing citrate. Linear regression analysis was used to determine if activity concentration increased over time (i.e., if the slope of the line is statistically different than zero) for treatments with and without citrate. Considering the entire treatment duration, the rate of change of activity concentration over time was significantly different than zero for both treatment groups ($p = 0.02$ for citrate and $p = 0.03$ for no citrate). However when I considered only sampling days 5, 10, and 15 there was no statistically discernable change ($p = 0.52$ for citrate and $p = 0.14$ for no citrate), statistical confirmation of the visually apparent plateau that starts around day 5 as seen in **Figure 6**b. While *P. putida* cultures should continue to produce pyoverdine for the entire study duration, the majority of this siderophore is produced in the first four days[34], and this may account for the apparent plateau of activity concentration in both cases after day 5 of the experiment period.

Accumulation of plutonium in E. coli vs P. putida

In **Figure 7**, the fraction of total activity in cell pellets as well as the activity concentration of Pu in cells is shown for *E. coli* and *P. putida* grown with ^{239}Pu

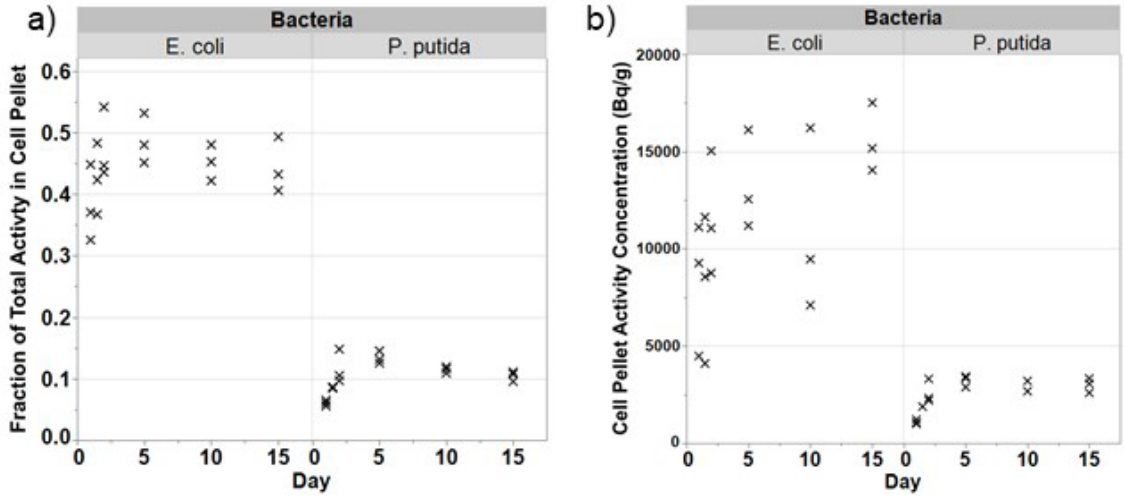

Figure 7(a) Fraction of total sample activity found in the cell pellet for *E. coli* (left) and *P. putida* (right) treated with ^{239}Pu complexed with citrate. (b) Activity concentration of ^{239}Pu complexed with citrate in cell pellets vs sample day for *E. coli* (left) and *P. putida* (right) where activity concentration is the activity of Pu in Bq of the pellet sample divided by the mass of the pellet sample (g).

complexed with citrate. A two-way ANOVA was run to examine the effect of sampling day and bacteria species on both pellet activity concentration and pellet activity fraction in Pu-citrate treated cultures. In both cases, the bacteria species and sampling day were significant contributors to variation in these activity metrics, with no significant interaction terms. This suggests that it is reasonable to consider and analyze our two bacteria species separately for further analysis. Of note is that the fraction of activity in the cell pellet and the activity concentration were much larger for *E. coli* than *P. putida* samples, which was confirmed with a one-tailed, two sample t-test of the means ($p \leq 0.001$). In all cases, the pattern of plateau at about day 5 remains consistent suggesting that siderophore production in *E. coli* follows a similar timeline to production of siderophores in *P. putida*.

While *P. putida* produces pyoverdine as its primary siderophore[33,34], *E. coli* produces enterobactin to mediate iron transfer[35]. Considering the higher quantities of Pu found in *E. coli* cells as compared to *P. putida* both as a fraction of sample activity and as an activity

concentration, it is likely that the enterobactin produced by *E. coli* is more efficiently assisting the uptake of Pu by cells than pyoverdine does for *P. putida* cells. Enterobactin is one of the strongest natural chelators of iron and shares this high affinity for Pu, and the use of enterobactin has been proposed as a mechanism for sequestration of Pu from living systems[36]. The hypothesis that *E. coli* has increased uptake of Pu as compared to *P. putida* is also supported by the data presented in **Figure 8**.

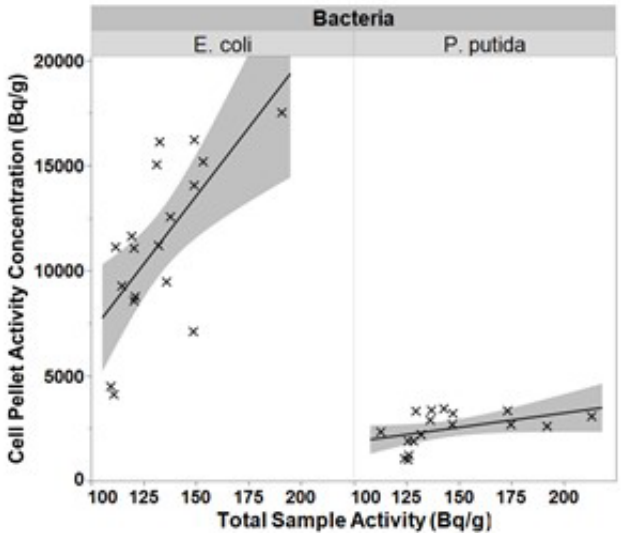

Figure 8 Pellet activity concentration (Bq ^{239}Pu per gram of cell pellet) vs total sample activity, normalized to Bq per mL sample, for *E. coli* (left) and *P. putida* (right) for all samples collected during the 15-day sampling period. Graphs show linear regression lines where the shaded region is the 95% confidence interval for fit. ^{239}Pu was complexed with citrate in both cultures.

In **Figure 8**, the pellet activity concentration is plotted as a function of total sample activity (Bq mL^{-1}). When fit with a linear model, *E. coli* has a positive relationship where activity concentration of Pu in cell pellets increases with total sample activity (p = 0.009), however *P. putida* does not show any statistically significant relationship between the two quantities

Conclusions

This study was designed to consider the accumulation of Pu by *P. putida* and *E. coli*; the results suggest that there may be uptake of Pu in the cells in addition to sorption to the surface, especially in the case of *E. coli*, although work remains to definitively differentiate between internal and external accumulation. Regardless, these results will be useful in developing appropriate microdosimetric models for bacteria species as well as in informing hypotheses when considered with the on-going body of work produced by this project, including ongoing transcriptomic data processing. There are a variety of factors that influence Pu behavior in bacterial systems [8] and these results confirm that, even in a simple system, multiple mechanisms are at play. The information provided by the study, including its implications on dosimetry, will provide a necessary bridge to translate the results of transcriptomic analysis into implications regarding effects of low doses of ionizing radiation on bacteria.

CHAPTER THREE

ACCUMULATION OF RADIO-IRON AND PLUTONIUM, ALONE AND IN COMBINATION, IN *PSEUDOMONAS PUTIDA* GROWN IN LIQUID CULTURES

Abstract

The impact of low doses of ionizing radiation on biological and environmental systems have been historically difficult to study. Modern biological tools have provided new methods for studying these mechanisms but applying these tools to a dose-response relationship may require refinement of dosimetric techniques that incorporate a detailed understand of radionuclide accumulation in biological cells, particularly when assessing the impact of low doses of ionizing radiation. In this work *Pseudomonas putida* (KT2440) grown in liquid culture was exposed to low dose rates (10-20 mGy d^{-1}) of ^{239}Pu and ^{55}Fe, both alone and in combination, for a period of 20 days, and the accumulation of ^{239}Pu and ^{55}Fe in cell pellets was analyzed via liquid scintillation counting. The study also considered of cells grown with ^{239}Pu and stable Fe (primarily ^{56}Fe). In addition to the analysis of cell pellet and media samples, this work includes analysis of the radiological content of RNA extraction samples to examine uptake of radionuclides. Results indicate that ^{239}Pu inhibited the uptake of ^{55}Fe, and that the presence of stable and radioactive isotopes of Fe in cultures may promote pathways for Fe accumulation that are used by ^{239}Pu. The work herein provides foundational insight into future dosimetric models for our work with environmental bacteria.

Introduction

Motivation

In this work, *Pseudomonas putida* has been exposed to ^{239}Pu ($t_{1/2}$ = 24,110 y) and ^{55}Fe ($t_{1/2}$ = 2.7 y), as well as stable Fe, in liquid culture. *P. putida* is ubiquitous in soil and fresh water ecosystems and has a versatile metabolism that allows it to grow in a variety of environments[37]. Specifically, the strain selected, KT2440, is a biological safety strain of *P. putida* that has been fully sequenced since 2002 and has been used in a wide variety of research activities, so it is well characterized and suited for bioinformatic investigations [15]. The work in this chapter supports the larger project goals of develop a discriminating biosensor for detection of weapons-related activities and additionally it affords the opportunity to gain fundamental knowledge concerning the (1) low dose effects to model microorganisms, and (2) influence of a micronutrient, Fe, on ^{239}Pu behavior in a simple aquatic system.

Plutonium-239 is an alpha emitting radionuclide with alpha energies of 5.156 (73.1%),5.143 (15%), and 5.105 (11.8%) MeV [19]. Iron-55 is a common activation product that undergoes electron capture [38]. Iron-55 produces x-rays (5.9 (25%) and 6.5 (3.7%) keV), as well as Auger electrons with energies 6.1 (140%) and 5.2 (61%) keV [19]. Ionizing radiation emissions from both radionuclides that have a concentration of either radionuclide on or in cells (i.e., internal or external accumulation) would increase the dose received because of the short range of the ^{239}Pu and ^{55}Fe emissions in water (as compared to a dose estimate based on a homogenous distribution of these radionuclides in liquid culture). The radionuclides selected provide the opportunity to examine both a high Linear Energy Transfer (LET) (^{239}Pu) and low LET (^{55}Fe) source of radiological exposure.

The objective of the presented study is to determine the relative activity of ^{239}Pu and ^{55}Fe in the common environmental bacteria *P. putida* to inform future efforts to characterize the dose from ionizing radiation received by the bacteria in our cultures.

Relevance

The study of both high and low-LET ionizing radiation at low doses is poorly characterized in biological systems such that even exposures of *P. putida* to ^{239}Pu and ^{55}Fe alone is of relevance[39]. However, when studied in combination, the effects of Fe in stable and radioactive forms on ^{239}Pu accumulation and ^{239}Pu presence on ^{55}Fe accumulation must be considered to compare the results to studies where ^{239}Pu and ^{55}Fe are used singly because of their shared pathways and chemical manipulation by siderophores. The utility of this knowledge is not exclusive to applications related the non-proliferation of nuclear weapons and can be applied to the broad environmental problems inherent with the use and disposal of materials that contain Pu. The study of common microorganisms provides insight into the effects of ionizing radiation at low-doses in environmental settings as these organisms are often indicators of environmental health and can provide pathways to the food-chain via low-trophic level organisms [28].

Material and Methods

Bacteria culture information

P. putida KT-2440 ATCC 47054 was grown from glycerol stocks in 100 mL of M9 minimal media in 250 mL baffled flasks on a New Brunswick I24R (Eppendorf AG, Germany) temperature-controlled shaker/incubator at 215 rpm and 28 °C for 20 days. The recipe for M9 minimal media is provided in Appendix C. The dose rates selected for this study were selected to

provide radiological exposures that did not result in population-level effects. The health of *P. putida* cultures was routinely assessed at all sampling days by measurement of optical density to ensure appropriate comparison to expected values based on growth curves. All cultures had reached stationary phase by the first sampling point (24 hours after inoculation).

Radiological treatment

Radiological treatment groups utilizing different combinations of ^{239}Pu and ^{55}Fe were considered for this study. Radionuclide treatments were added to growth media prior to inoculation. For treatments with ^{239}Pu, ^{239}Pu was added from a stock solution in 0.01M HCl with a concentration of 30.4 mg L^{-1} (69.9 kBq mL^{-1}). The the solution contained 99.919% ^{239}Pu by mass as of July 7th, 2015.

The use of ^{239}Pu in this study necessitated the addition of citrate in a ratio of approximately 1000:1 to ensure sufficient complexation of the ^{239}Pu such that it maintained solubility in the near-neutral bacteria cultures. Modeling efforts showed that a full complexation of all ^{239}Pu would not be achieved at this ratio, however the addition of more citrate than this resulted in complications with aerated media in past experiments, and this was found to be the ideal ratio for biological investigations [40].

The cultures studied in this chapter come from three different experiments because of limited space on the incubator platform, though some exposure scenarios were repeated between experiments to ensure that our results could be replicated. All experiments had associated control groups, the use of which is discussed in further detail later in this section. Based on oxidation state measurements of growth media spiked immediately prior to inoculation in similar experiments, the oxidation state of Pu in treatment groups where citrate was added was found to be primarily Pu(IV) (75-80%) with the remainder mostly comprised of Pu(V). After 1 day of

culture growth, the oxidation state of Pu in treatment groups was primarily Pu(V) (73 to 96%), with the remainder Pu(IV), with similar results after 5 days of growth (90-95% Pu(V), remainder Pu(IV)). Beginning with day 1 of this experiment, it was assumed that Pu was in a reasonably soluble form.

The concentration of ^{239}Pu and ^{55}Fe in the liquid cultures was determined based on target absorbed dose rates that were determined assuming a homogeneous mixture of radionuclides. The experiment considered exposures from ^{239}Pu and ^{55}Fe, individually, at a dose rate of approximately 10 mGy d^{-1}. Combinations of the two radionuclides were considered at two different total dose rates of approximately 10 mGy d^{-1} (5 mGy d^{-1} from ^{239}Pu exposure and 5 mGy d^{-1} from ^{55}Fe exposure) and 20 mGy d^{-1} (10 mGy d^{-1} from ^{239}Pu exposure and 10 mGy d^{-1} from ^{55}Fe exposure). All solutions, including the control, included the same quantity of citrate and Fe chloride (regardless of radiological or stable form) to be able to distinguish between radiological and chemical impact, except for one ^{239}Pu exposure group that had no Fe chloride added. The various treatment groups are summarized in **Table 1**.

For treatment groups that included exposures to ^{55}Fe, a solution of $^{55}FeCl_3$ (Perkin Elmer) in 0.5M HCl was used. The stock solutions were shipped with a specific activity of 12.6 to 21.0 mg L^{-1} (1110 to 1850 MBq mL^{-1}) and diluted with deionized and distilled water (DDI) to a concentration of 0.42 mg L^{-1} (37 MBq mL^{-1}) immediately prior to spiking the treatment flasks. Both $FeCl_3$ and citrate (used for complexation of ^{239}Pu) have the potential to chemically influence the sorption and uptake of contaminants in the system, as well as the overall health of the bacteria. As such, all treatment groups without ^{239}Pu included the addition of citrate in a

Table 1 Concentration of all contaminants in all exposure scenarios.

Treatment Group	Dose Rate (mGy d^{-1})	^{239}Pu (mg L^{-1})	Citrate (mg L^{-1})	^{55}Fe (mg L^{-1})	^{56}Fe (mg L^{-1})
Control	0	0	60	0	2.1×10^{-3}
$^{239}Pu + {}^{56}Fe$	10	5.2×10^{-2}	60	0	2.1×10^{-3}
^{239}Pu	10	5.2×10^{-2}	60	0	0
^{55}Fe	10	0	60	2.1×10^{-3}	0
$^{239}Pu + {}^{55}Fe$	10	2.7×10^{-2}	60	1.0×10^{-3}	1.0×10^{-3}
$^{239}Pu + {}^{55}Fe$	20	5.2×10^{-2}	60	2.1×10^{-3}	0

working solution consisting of 0.01 M HCl, including the control group. The working solution contained approximately 35 mg L^{-1} citrate.

All but one treatment group without ^{55}Fe included the addition of stable $FeCl_3$; in one treatment group, ^{239}Pu with citrate was added without any Fe to examine the influence of the presence of Fe on ^{239}Pu accumulation in and on bacteria. A stable $FeCl_3$ working solution was made with 0.5 M HCl and $FeCl_3$ in solid powder form via serial dilution to produce a working solution of 1.75×10^3 mg L^{-1} Fe. This solution was diluted with 0.5M HCl to create a working solution with a concentration that matched the ^{55}Fe solution shipped from the supplier. The working solution was diluted with DDI in the same volumes as the ^{55}Fe solution immediately prior to spiking to mimic the process completed for the radioactive treatments.

Cell culture sampling

Cell cultures were sampled in 500 µL aliquots from each culture at 24, 32, and 48 hours post inoculation. Samples were then collected at Day 5 post-inoculation and every 5 days after

for a 20-day growth period (days 5, 10, 15, and 20). The 500 µL samples were centrifuged for 7 minutes at 6000 RCF to form cell pellets. The supernatant fluid was eluted and collected in liquid scintillation counting (LSC) vials. The cell pellets were centrifuged for a second time (3 minutes, 6000 RCF), and the elution step was repeated, where the eluted supernatant was collected in the same LSC vial as the first step. The remaining cell pellets were resuspended in 500 µL of M9 minimal growth media by vortexing. To prevent physical quenching during LSC, approximately 25 to 40 µL of 30% H_2O_2 was added to each sample to breakdown remaining organic material. A graphical summary of how cell culture samples were prepared for LSC analysis is provided in **Figure 9**. The total activity of the sample consisted of the addition of the results of LSC analysis for both the elutant LSC vial and cell pellet LSC vial.

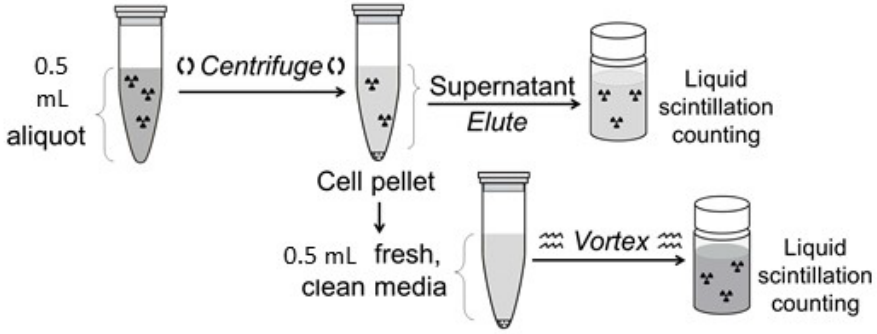

Figure 9 Visualization of sample collection process

RNA extraction

The presented work is part of a larger study to examine transcriptional changes in *P. putida* as a result of low-dose radiological exposure. Extractions of ribonucleic acid (RNA) were collected from cell culture samples and analyzed for radiological content for the purposes of controlling potential contamination of sequencing equipment with radiological materials. After

determining that RNA samples contained radiological materials, we opted to collect samples for radiological characterization to determine if they could be instructive regarding uptake of ^{239}Pu or ^{55}Fe. Internal investigations of the RNA extraction process with ^{239}Pu and ^{55}Fe determined that the presence of these radionuclides in RNA samples is not the result of process flow through and should be attributed to ^{239}Pu or ^{55}Fe bound to RNA prior to the extraction process.

RNA was extracted using the RNEasy kit following manufacturer's instructions (Qiagen, Maryland, USA). RNA extractions were transferred from the collection vessel (centrifuge tube) to an LSC vial with 10 mL of Optiphase HiSafe 3 cocktail. RNA extraction samples were collected, in many cases, retrospectively from samples frozen at -80ºC immediately after collection and processing. I collected samples to represent the experiment period, however samples were collected based on availability when concerns for replicates for bioinformatic analysis was considered. As such, samples from Day 10 were analyzed for some exposure scenarios, but other scenarios used Day 15 samples, but samples from Days 1 and 5 were collected for all exposure scenarios.

Determination of radiological content

Samples were analyzed for radioactivity using a Tri-Carb 4910 TR liquid scintillation analyzer (PerkinElmer, Waltham, MA). The average of 3 (biological replicate) control samples for the given sampling day was used for background subtraction. All cell culture samples were normalized to a 0.5 mL sample volume for direct comparison by using the total mass of each sample and the simplifying assumption that the density of the liquid cultures was 1 g cm^{-3} to account for any variation in sample volume. RNA samples were also normalized to a 0.5 mL sample because the RNA extraction process dictates sample volumes based on measurement of optical density of the cultures to assure that the ideal amount of RNA is collected for

transcriptomic analysis. As such sample volumes ranged from 150 to 300 µL and required this normalization to be directly compared.

LSC was used as a counting method because of its ability to detect low concentrations of alpha and weak beta emitting radionuclides. When calculating activity from count rate data, an efficiency of approximately 100% for alpha emissions from ^{239}Pu and 42.5% for electron emissions from ^{55}Fe was applied. Efficiencies were calculated prior to data analysis by using aliquots of ^{239}Pu and ^{55}Fe stock solutions and dividing counts by the known activity of the aliquot.

Statistical Methods

Pearson's correlation coefficients (r) were calculated to determine the correlations between exposure duration, pellet mass, treatment, pellet fractional activity, and pellet activity concentration. Pearson's correlation coefficients are used to show the strength of correlation between two variables with values between -1.0 (when one variable increases, the other decreases) to 1.0 (both variables increase in response to the other increasing) where 0 indicates no correlation [41]. For the purpose of this work, two variables are considered to be highly correlated when the Pearson's correlation coefficient is $r > 0.9$ or $r < -0.9$, moderately correlated when $r \geq 0.5$, and weakly correlated if $r \leq 0.5$.

Linear regression analysis was conducted to determine if pellet activity concentrations varied with total sample activity day or total sample activity for different treatment groups to gain insight into the rate of uptake or sorption. The slopes of linear regression models were compared using Analysis of Covariance (ANCOVA) which allows for the comparison of models based on categorical values (treatment group) with adjustment for the covariate, a continuous and independent variable (sampling day or total sample activity). The coefficient of determination,

R^2, is provided in some cases to indicate the amount of variation in the dependent variable that can be explained by the independent variable. In all cases, significance was taken as $p < 0.01$ unless otherwise noted. All statistical analyses were conducted with Minitab (Minitab18, State College, PA, U.S.), and JMP (SAS Institute, Cary, NC, U.S.) was used to generate all plots and associated uncertainties.

Results and Discussion

Fraction of total ^{239}Pu and ^{55}Fe activity in cell pellets

Figure 10 and **Figure 11** show the time series of relative ^{239}Pu and ^{55}Fe concentration in cell pellets, respectively. The fraction of total sample mass that the cell pellet comprises is also included for comparison. A greater fraction of the radionuclides used was found in the pellet portion of the sample than would be predicted by mass; while the mass of cell pellets made up 0.25-4.4% of the mass of the samples collected, 5.6-23.4% of ^{239}Pu and 57.6-93.3% of ^{55}Fe in (individual) cell culture samples was found in the cell pellets. This indicates that the radionuclides are not homogeneously mixed in the growth media, but instead concentrate on or in the cells via uptake and/or sorption pathways.

Average relative activity of ^{239}Pu in the cell pellet gradually increases over the course of the 20-day time series to 12-20% (**Figure 10**), whereas average relative activity of ^{55}Fe in the cell pellet is relatively constant at around 80% (**Figure 11**). The higher relative activity of ^{55}Fe compared to ^{239}Pu is to be expected, as Fe is an essential micronutrient.

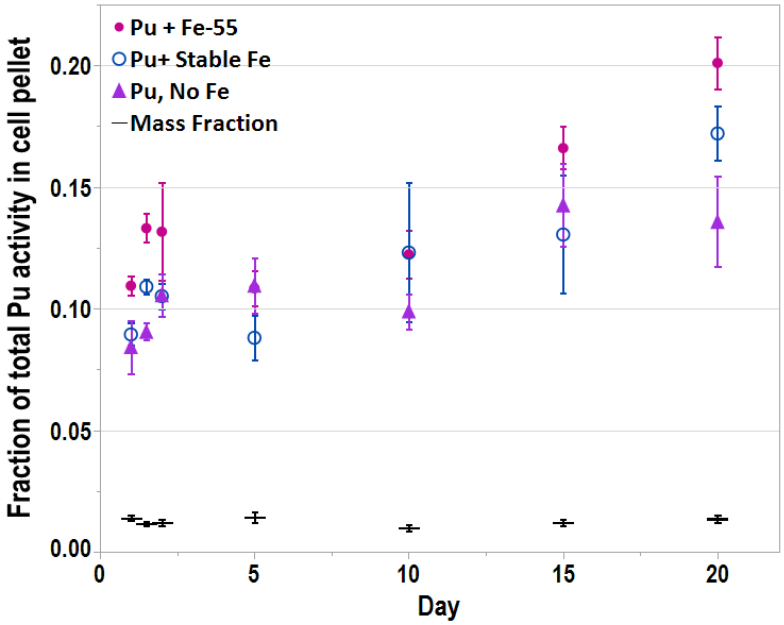

Figure 10 Data presented are means of total sample ^{239}Pu activity in cell pellets at each sample time. Error bars represent the standard error of the mean. The fraction of the total sample mass that consists of the cell pellet after centrifuging and supernatant elution is provided for reference and is denoted with the "–" symbol.

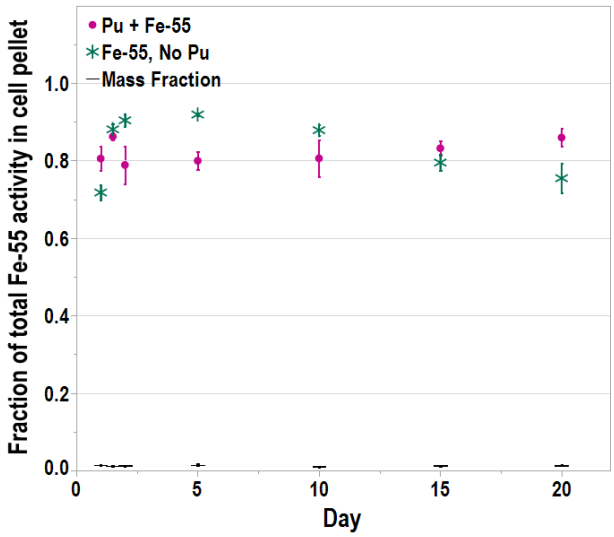

Figure 11 Data presented are means of total sample ^{55}Fe in cell pellets at each sample time. Error bars represent the standard error of the mean. The fraction of the total sample mass that consists of the cell pellet after centrifuging and supernatant elution is provided for reference and is denoted with the "–" symbol.

Activity Concentration of ^{239}Pu in Cell Pellets

While these results demonstrate accumulation of both ^{239}Pu and ^{55}Fe in *P. putida*, there is not a clear indication of any difference between the exposure conditions on the relative activities. To gain insight into potentially unobserved differences, we considered the concentration of radionuclides in/on the cells as an activity concentration expressed as Bq of radionuclide per milligram (mg) cell pellet. For ^{239}Pu activity, differences in the patterns of activity concentration, **Figure 12**, are difficult to determine. While there may exist some difference between treatment groups over the sampling time, ANCOVA tests indicate that the slopes of treatment group models are statistically indistinguishable except that of the ^{239}Pu + ^{55}Fe at 10 mGy d^{-1} and ^{239}Pu + stable Fe treatment groups.

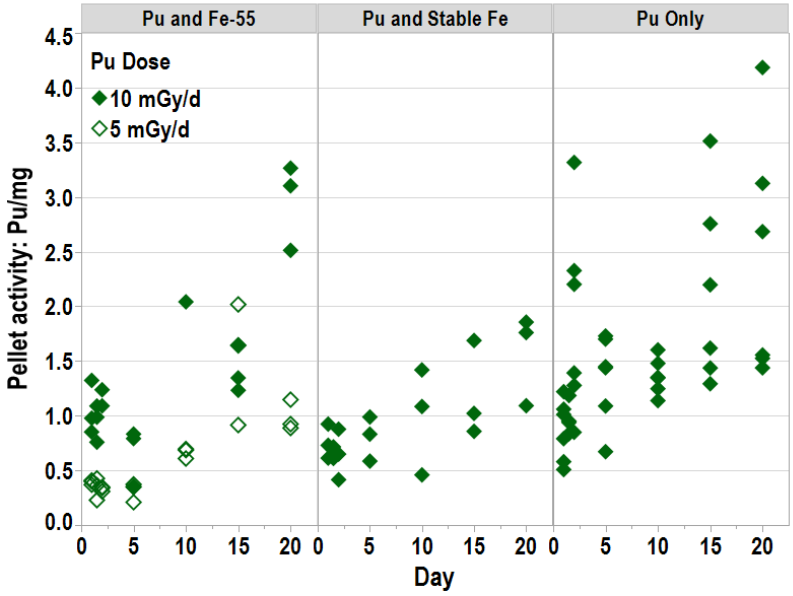

Figure 12 Activity concentration in cell pellets expressed as Bq ^{239}Pu per mg of cell pellet are shown as a time series based on sampling time collected 1, 1.5, 2, 5, 10, 15, and days after inoculation. Bacteria cultures contained approximately 122 Bq mL^{-1} or 61 Bq mL^{-1} to result in 10 mGy d^{-1} or 5 mGy d^{-1} dose rates from ^{239}Pu, respectively.

Activity Concentration of ^{55}Fe in Cell Pellets

When examining ^{55}Fe activity concentration in cell pellets there is a difference between ^{55}Fe activity concentration as a function of time when ^{239}Pu is present and when it is not (**Figure 13**). When ^{239}Pu is not present, the ^{55}Fe activity concentration rises steeply for the first 5 days, and then appears to plateau, suggesting that the cells have reached a point of saturation. When ^{239}Pu is present, however, ^{55}Fe activity concentration is about a factor of 4-5 lower and only rises toward the end of the sampling period, which may be explained by stressors in the bacteria culture related to evaporation of the liquid cultures. The cell pellet activity concentration is different than the activity concentration of the total cell culture because the cell pellet activity concentration is based on results after the cell culture samples were separated into media and cell pellet samples (**Figure 9**), while the activity concentrations of the cell cultures given in the Methods and Materials section were part of the experiment setup conditions.

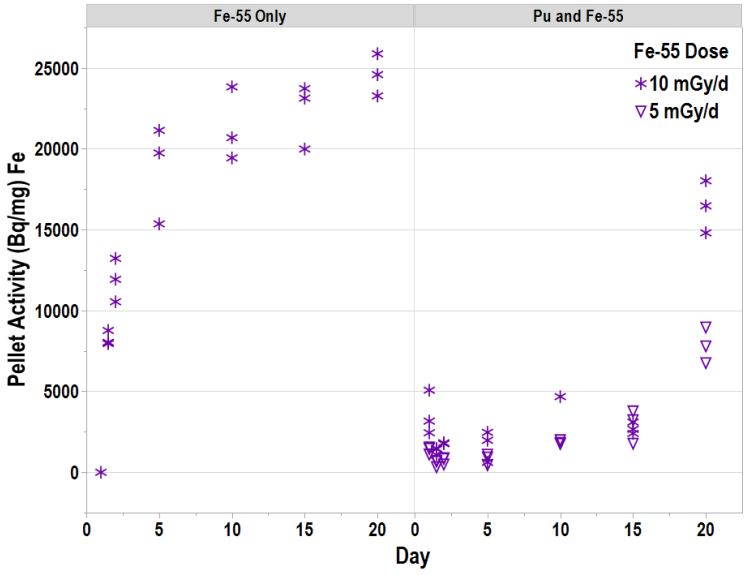

Figure 13 Activity concentration in cell pellets expressed as Bq ^{55}Fe per mg of cell pellet. Bacteria cultures contained approximately 181 kBq mL^{-1} or 90.5 kBq mL^{-1} to result in 10 mGy d^{-1} or 5 mGy d^{-1} dose rates from ^{55}Fe, respectively.

The large differences between activity concentration warranted further investigation, as the fraction of total ^{55}Fe activity in the pellet samples was generally 70-85% regardless of if ^{239}Pu was present or not (**Figure 11**). The activity concentration of ^{55}Fe in cell pellets is plotted as a function of the total ^{55}Fe sample activity in **Error! Reference source not found.**. Data were fit with a linear model to examine the relationship of ^{55}Fe uptake and sorption in the presence of ^{239}Pu. Linear regression models indicated that variation in activity concentration was well accounted for in all three cases by total sample activity: ^{55}Fe only (R^2 =0.84), 10 mGy d^{-1} ^{55}Fe+ ^{239}Pu (R^2 = 0.97), and 5 mGy day^{-1} ^{55}Fe + ^{239}Pu (R^2 =0.94) (for all models, $p \leq 0.0001$). The slope (β) for the model of ^{55}Fe without ^{239}Pu (β =0.167) was about 2x the slope of both the 10 mGy d-1 (β =0.080) and 5 mGy d-1 (β =0.087) models and the results of ANCOVA tests between the different treatment groups confirm that the slopes of both linear regression models for ^{239}Pu+^{55}Fe and ^{55}Fe only are statistically different. The ANCOVA test indicated that the models for 10 mGy d^{-1} and 5 mGy d^{-1} are statistically the same. These results indicate that the presence of ^{239}Pu hinders or competes with the accumulation of ^{55}Fe in cells.

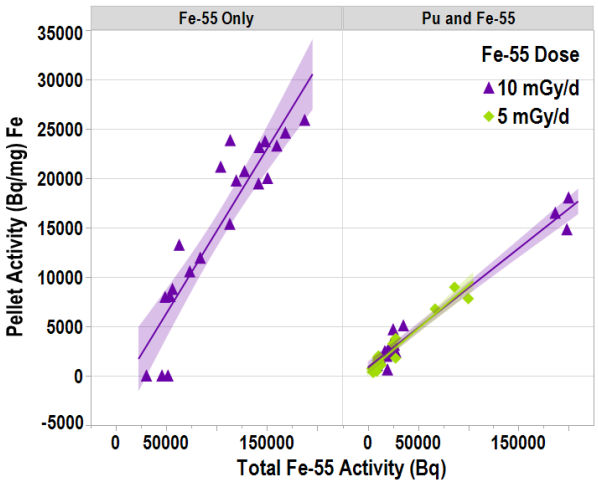

Figure 14 Cell pellet activity concentration shown in Bq ^{55}Fe per mg cell pellet plotted as a function of total sample ^{55}Fe activity (normalized to the same sample volume). Plotted data was fitted with a linear regression model, where shaded areas show model uncertainty with a 95% confidence interval.

Analysis of correlation

Pearson correlation coefficients (r) were calculated for several combinations of variables because statistically significant ($p<0.01$ unless otherwise noted) correlations provide insight into potential dependencies or confounding factors. The most instructive statistically significant coefficients are included in Table 2.

Table 2 Pearson correlation coefficients for different sets of variables. All values were statistically significant where $p<0.01$ unless otherwise noted.

		Exposure Scenario				
Correlation Variables		**^{55}Fe Only**	**^{239}Pu Only**	**^{239}Pu Stable Fe**	**^{239}Pu+^{55}Fe 20 mGy d^{-1}**	**^{239}Pu+^{55}Fe 10 mGy d^{-1}**
^{239}Pu Pellet Bq mg^{-1}	Day	-	0.573	0.745	0.806	0.732
^{239}Pu Pellet Bq mg^{-1}	^{239}Pu Pellet Activity Fraction	-	0.781	0.839	0.835	0.732
^{239}Pu Pellet Bq mg^{-1}	Total ^{239}Pu Sample Activity	-	0.343*	0.622	0.901	0.886
^{55}Fe Pellet Bq mg^{-1}	Total ^{55}Fe Sample Activity	0.937	-	-	0.948	0.986
^{55}Fe Pellet Bq mg^{-1}	^{239}Pu Pellet Bq mg^{-1}	-	-	-	0.936	0.596
^{55}Fe Pellet Activity Fraction	^{239}Pu Pellet Activity Fraction	-	-	-	0.757	0.493

* *p=0.028*

While radionuclide activity concentration is correlated with the total sample activity of that radionuclide in all cases, ^{55}Fe activity concentration is highly correlated with total sample

^{55}Fe activity in all cases (r=0.937, r=0.948, and r=0.986 for ^{55}Fe Only, ^{239}Pu+^{55}Fe 10 mGy d^{-1}, and ^{239}Pu+Fe^{55} 5 mGy d^{-1} respectively). Interestingly, however, the strength of correlation is much less for ^{239}Pu activity concentration, and total ^{239}Pu sample activity as compared to ^{55}Fe, though the correlation is stronger when Fe is present (r=0.622 ^{239}Pu+Stable Fe; r=0.901 ^{239}Pu+^{55}Fe 10 mGy d^{-1}; r=0.886 ^{239}Pu+^{55}Fe 5 mGy d^{-1}) than when it is not (r=0.343). Plutonium activity concentration in cell pellets is also more strongly correlated with day (i.e. Bq mg^{-1} ^{239}Pu in cell pellets increased over the duration of the experiment) when Fe is present (r=0.745 ^{239}Pu+Stable Fe; r=0.806 ^{239}Pu+^{55}Fe 10 mGy d^{-1}; r=0.732 ^{239}Pu+^{55}Fe 5 mGy d^{-1}) than when it is not (r=0.573).

Several metals, including Fe, are essential micronutrients for bacteria and other living organisms. Aerobic organisms, such as *P. putida*, may have difficulty with obtaining Fe from the environment because of its poor solubility at near-neutral pH. *P. putida* and other microorganisms produce siderophore complexes (high-affinity chelating compounds) to aid the uptake of insoluble Fe from their environment [42]. Most microorganism produce a range of siderophores with different affinities for Fe, but a unique feature of *P. putida* is that its siderophore production is exclusively in the form of pyoverdines [33] which have an "extremely high" affinity for Fe [43] such that it binds with Fe in a 1:1 stoichiometric ratio [44]. In addition to their high affinity for Fe, however, pyoverdine hydroxamate compounds are some of the strongest natural Pu chelating compounds [45]. Plutonium has a wide range of oxidation states and a large physical size, such that it is often more likely to bond to cell surfaces than undergo transport across the cell membrane in many cases [23]. In the case of *P. putida*, however, the production of pyoverdine siderophores has previously been shown in the literature to effectively transport Pu across the cell membrane [46]. As such, it is expected that ^{239}Pu will use binding sites

and pathways designed for Fe uptake and sorption when accumulating in cells, but the stronger correlation of ^{239}Pu activity to total activity and ^{239}Pu activity concentration to sample day when Fe is present in some form suggest that the presence of Fe may activate additional pathways that are used by ^{239}Pu.

There is a correlation between ^{55}Fe activity concentration and ^{239}Pu activity concentration in cell pellets at both 20 mGy d^{-1} and 10 mGy d^{-1} dose rates, however the strength of correlation is much higher for the higher dose rate (r=0.596 10 mGy d^{-1}; r=0.936 20 mGy d^{-1}). The strength of correlation between the fraction of total ^{55}Fe and ^{239}Pu activity in cell pellets also increases with increasing total dose (r=0.493 10 mGy d^{-1}; r=0.757 20 mGy d^{-1}). While it is generally assumed that these accumulation patterns are the result of chemical characteristics of Fe and Pu, this data may provide limited evidence that there is a radiological component to the patterns of accumulation. More likely, the differences can be attributed to increased ^{239}Pu in the cultures. Pellet ^{239}Pu activity concentration is correlated with the fraction of total ^{239}Pu activity found in cell pellets (^{239}Pu only r=0.781; ^{239}Pu + stable Fe r=0.839, ^{55}Fe+^{239}Pu 10 mGy d^{-1} r=0.835, ^{55}Fe+ ^{239}Pu 5 mGy d^{-1} r=0.732). Pellet ^{55}Fe activity concentration is not correlated with the fraction of total ^{55}Fe activity found in cell pellets in any case. This is consistent with **Figure 10** and **Figure 11** which show the fraction of total ^{239}Pu activity in cell pellets increasing over time while the fraction of total ^{55}Fe activity in cell pellets remains fairly stable.

RNA Extraction Sample Analysis

The analysis of RNA extraction samples was instructive when considering our hypotheses regarding ^{239}Pu's potential use of Fe pathways such that uptake of ^{239}Pu into the cells occurs in addition to sorption. Reports of bioavailable metals binding to electron-rich sites on both phosphate-backbones and nucleotide bases of DNA and RNA have been reported in the

literature [47], and this behavior has specifically been observed with both Fe [48,49] and Pu [50]. Because *P. putida* is a prokaryotic organism that lacks a cell nucleus and genetic material floats freely inside the cell, ^{55}Fe and ^{239}Pu found in RNA extraction samples is likely the result of ^{55}Fe and ^{239}Pu that became bound to RNA after uptake into the cells when the metals were in a bioavailable form.

Analysis of ^{239}Pu in RNA extraction samples is shown in **Figure 15**. Because of the low activity of the samples, the slope of linear regression models for ^{239}Pu activity in cultures with and without Fe was not statistically different from zero ($p = 0.07$ for samples from cultures containing Fe and $p = 0.11$ for samples without Fe). However, for ^{239}Pu activity in RNA extractions there was a significant interaction between sample day and whether the cultures contained Fe.

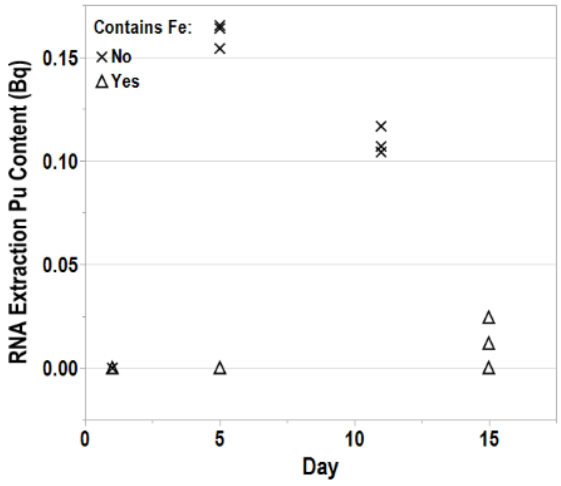

Figure 15 Plutonium-239 activity (Bq) over the sampling period found in RNA extraction samples performed on samples of bacteria from cultures containing ^{239}Pu in the presence of Fe, as well as with no additional Fe added to culture media.

The activity of ^{55}Fe in RNA extraction samples, shown in **Figure 16**, is even more instructive. When ^{239}Pu is not present, ^{55}Fe activity in RNA extraction samples grows over the

sampling period (p = 0.002, R^2=0.77) whereas linear regression analysis of ^{55}Fe activity in RNA extractions when ^{239}Pu is present does not indicate a slope that is significantly different from zero (p = 0.425, R^2=0.09).

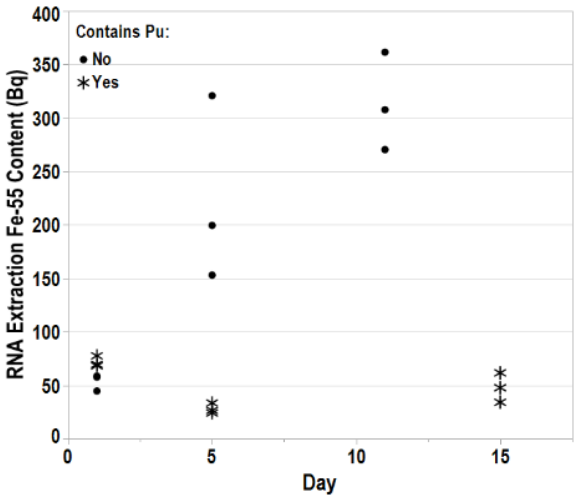

Figure 16 Iron-55 activity (Bq) over the sampling period found in RNA extraction samples performed on samples of bacteria from cultures containing ^{55}Fe in the presence of ^{239}Pu, as well as with no ^{239}Pu added to culture media.

The analysis of ^{239}Pu content was less quantitatively conclusive than analysis of ^{55}Fe, though this is to be expected in a radiological analysis as a result of their extremely different specific activities. The increasing quantity of ^{55}Fe over time when ^{239}Pu is not present versus the low ^{55}Fe activity when ^{239}Pu is present that has no apparent relationship to sample day supports our hypothesis that ^{239}Pu is competing with Fe and using Fe pathways to enter the cells. While the measurement of ^{239}Pu when Fe is present in cultures than when it is not might require a larger sample cell culture to demonstrate a truly quantitative measurement, the existing data suggests that more ^{239}Pu is present in RNA samples where Fe was added to cultures, and this is also supportive of our hypothesis that the presence of Fe is triggering different pathways for ^{239}Pu to use.

Conclusions

The results of this study demonstrate a measurable impact of ^{239}Pu on the uptake of Fe in *P. putida*. The results also suggest the presence of Fe may provide additional pathways and mechanisms for the uptake and sorption of ^{239}Pu in *P. putida*. Comparing the results of this work to transcriptional results may further explain the patterns of accumulation of both radionuclides based on the induction of metabolically intensive processes like flagella formation / use. While this study cannot quantify or definitively determine uptake vs. sorption of radionuclides, the differences in accumulation patterns suggest that both mechanisms are in play in many of our cultures and the collection of RNA extraction data provided additional support for this theory. The analysis of RNA extraction samples was a process initially proposed for the purpose of radiological safety, and, as such, RNA extractions for this study were performed to mirror the extraction of RNA for transcriptomic analysis. For transcriptomic analysis, bacteria culture sample volumes are selected based on optical density to ensure an appropriate quantity of RNA that allows for quality data collection. The analysis of RNA extraction samples, however, provided an instructive set of data for our investigation and may prove useful in future investigations. However, if this method were to be applied in future investigations, we would advise the use of a larger sample for radiological analysis to improve counting statistics instead of mirroring the sample volumes used for transcriptomic analysis.

Because both radionuclides deposit their energy over short distances relative to the size of *P. putida,* evidence of uptake will influence the development of our microdosimetric models such that multiple locations for radionuclides will be considered. The information provided by the present study, including its implications on dosimetry, will provide a necessary bridge as we

work to translate the results of transcriptomic analysis into implications regarding effects of low doses of ionizing radiation on bacteria.

CHAPTER FOUR

FLOWTHROUGH OF ^{239}PU AND ^{55}FE DURING RNA EXTRACTION

Abstract

Analysis of gene expression has become an important tool in understanding low-dose effect mechanisms of ionizing radiation at the cellular level. Metal binding to nucleic acids needs to be considered when interpreting these results, as some radioactive metals, particularly actinides, may produce free radicals and cause oxidative stress damage via chemical means at rates much higher than free radical formation related to their radiological properties. Bacteria exposed *in situ* to low dose rates of plutonium-239 (^{239}Pu) and iron-55 (^{55}Fe) were previously analyzed for gene expression. The work herein was motivated by an interest in more precisely identifying the distribution of radionuclides in these bacteria as well as the practical need to ensure appropriate transport and handling of the associated ribonucleic acid (RNA) extractions. RNA extractions were performed on bacteria growth media with and without bacteria cells (i.e., with and without RNA) at several different concentrations of ^{239}Pu and ^{55}Fe to inform the level of specificity of the extraction membrane as well as provide insight into internal (uptake) vs external (sorption) accumulation of these radionuclides in bacteria cells. Results of the study suggest that ^{239}Pu and ^{55}Fe detected in RNA extraction samples during long term cell studies is the result of binding to RNA prior to the time of extraction, as opposed to flow through or binding after cell lysis, and it highlights the practical importance of nucleic acid sample characterization to radiation protection more generally.

Introduction

Ionizing radiation effects

The genome of a cell, made of deoxyribonucleic acid (DNA), contains the full set of genetic information for living organisms, with sequences that control everything from morphology to function[51]. If ionizing radiation interacts with DNA, any resultant damage that is not successfully repaired by the cell may cause cell death or produce a non-fatal mutation.[52,53] In humans, excessive cell death associated with high dose-rate exposures to ionizing radiation results in tissue reactions which may occur acutely or years after exposure as observed in radiation therapy patients[54], while non-fatal mutations, under the right conditions, may result in carcinogenesis.[55–57] Studies of effects in individual cells cannot be used directly to develop a dose-response relationship for carcinogenesis in humans, that belongs in the realm of epidemiology,[58] but cellular studies are important in understanding fundamental mechanisms, particularly for low doses and low dose rates.[59]

Radiobiological studies indicate that a combination of events may better explain low dose radiation response, especially when there is damage to proteins, the cell membrane, and mitochondria.[18] One popular field for examining cellular response to damage is transcriptomics, a branch of biological study that examines response through gene expression.[51] An impacted cell may differentially express (e.g. “turn off” or “turn on”) genes coded on its genome in response to damage or stress to open repair pathways, protect the cell, send extra-cellular messages, etc. Gene expression includes the transcription of ribonucleic acid (RNA) from DNA, and differentially expressed genes are quantified by analysis of RNA produced in populations of cells through sequencing or amplification of previously identified genes of interest.[51]

Fe and Pu binding to nucleic acids

In general, DNA has a strong negative charge and consists of a cyclic sugar (deoxyribose), purine (adenine and guanine) and pyrimidine (cytosine and thymine) bases, and a

phosphate group. DNA is usually found in a double strand, where hydrogen bonds between the purine and pyrimidine groups connect the two molecules. RNA is found in a single strand form and is otherwise similar to DNA except that the cyclic sugar is ribose and uracil is used instead of thymine.[47] The potential for redox-active species of Fe to bind to DNA in cells has been studied because of Fe's ability to accelerate free radical reactions that cause DNA damage. Iron is known to bind to multiple sites on DNA molecules under physiologically relevant chemical conditions.[49] Both Fe(II) and Fe(III) bind to DNA at sites located on the phosphate backbone as well as the guanine base, where the strongest affinity is between Fe(III) and phosphate groups.[60] Potential binding sites for Fe on DNA also apply to RNA molecules. Additionally, binding sites on RNA for Mg related to RNA folding can also be used by Fe.[61,62] Plutonium(IV) often follows the biochemistry associated with Fe(III), so it is expected that many binding sites available to Fe will also be available to Pu when uptake occurs in cells.[50,63]

Low-dose exposures to high energy, low-LET radiation can be achieved through external irradiation with radiation generating devices or sources, such that only radiological interactions occur without the introduction of direct chemical stressors. Studying the response of cells to low doses of alpha emissions or low-energy electrons, however, requires the introduction of radiological materials directly to the cell culture environment because of the short path length of these types of radiations. DNA and RNA are likely to bond with metal cations, with evidence in the literature of bonding to radiologically relevant metals besides Fe and Pu, such as Y, Ce, Sm, Sr, Cs, U, and Pb.[47] As we strive to better understand low-dose effect mechanisms of ionizing radiation, metal binding to DNA and RNA cannot be ignored, especially for actinides like U and Pu which may produce free radicals and cause oxidative stress damage via chemical means at rates much higher than free radical formation related to their radiological properties.[64,65]

Relevance for radiological materials handling

The work presented herein was spurred by the practical need to radiologically characterize RNA extraction samples from bacteria cultures exposed to ^{55}Fe and ^{239}Pu, because they would be removed from a radiologically controlled laboratory and brought to a shared, non-radiological facility for quality control and sequencing processes for transcriptomic analysis. To ensure high quality data, DNA and RNA extraction processes are designed to be highly selective for DNA or RNA so that the extraction product contains few impurities, though physical efficiency values are not generally available due to the proprietary nature of these extraction processes. Because of this selectivity, it was expected that the RNA extractions would contain little to no detectable radiological content. But an initial semi-quantitative analysis suggested otherwise. Thus, the investigation was expanded, and RNA extraction samples were appropriately characterized so that proper transport and handling procedures could be developed.

After considering the affinity of DNA and RNA for metal cations, I postulated that the radiological content of our RNA extraction samples could be used to gain insight into internal (uptake) vs external (sorption) accumulation of ^{55}Fe and ^{239}Pu in the bacteria cultures. The use of the RNA extraction radiological data for this purpose, however, depended on demonstrating evidence that the ^{55}Fe and ^{239}Pu found in RNA extractions samples was bound to RNA when the cell cultures were being incubated and studied. It was determined that there were two other potential routes for how the ^{55}Fe and ^{239}Pu could end up in the RNA extraction samples:

1. Process flowthrough: Because of the previously mentioned lack of physical efficiency data for impurity removal, it was possible that the ^{55}Fe and ^{239}Pu may end up in the RNA extraction samples as impurities directly from the growth media.

2. Binding with RNA during the extraction process: I also considered the possibility that metals present in the growth media or released from the cell surface when the cells were lysed as part of the extraction process could quickly bind to RNA at that point.

To determine if these two pathways better explained the quantities of ^{239}Pu and ^{55}Fe in our RNA extraction samples, I designed an experiment that considered process flowthrough by completing RNA extractions on solutions containing radioactive material spikes in growth media with no cells. I also considered metal binding with RNA during the extraction process by using cell culture samples and spiking them with ^{239}Pu immediately before the cell lysing step.

Materials and methods

The methods applied to this study sought, primarily, to mimic previous studies with *Pseudomonas putida* and *Escherichia coli* exposed to ^{239}Pu and ^{55}Fe in their growth media.[66,67] As such, sample volumes and radionuclide concentrations were selected to be relevant to previous work.

RNA extraction process overview

For clarity, the RNA extraction process is graphically described in in **Figure 17**. The RNA extraction process begins with a 100-400 μL aliquot collected from a liquid culture of bacteria, where the volume of which is based on the optical density (OD) of the culture (OD600). Solutions used to lyse the cells (which releases RNA from the cells) and preserve the RNA are added. The solution is run through a proprietary exchange column that is centrifuged. During this step, RNA and other compounds bind to the exchange column. The exchange column is then washed with various solutions to remove non-RNA content before a final wash with the goal of producing an aqueous RNA sample with few impurities. Non-RNA content is either released in

the effluent of the process or remains on the exchange column. All RNA extraction simulations were performed using a Qiagen RNeasy kit. Extractions were performed according to manufacturer instructions.

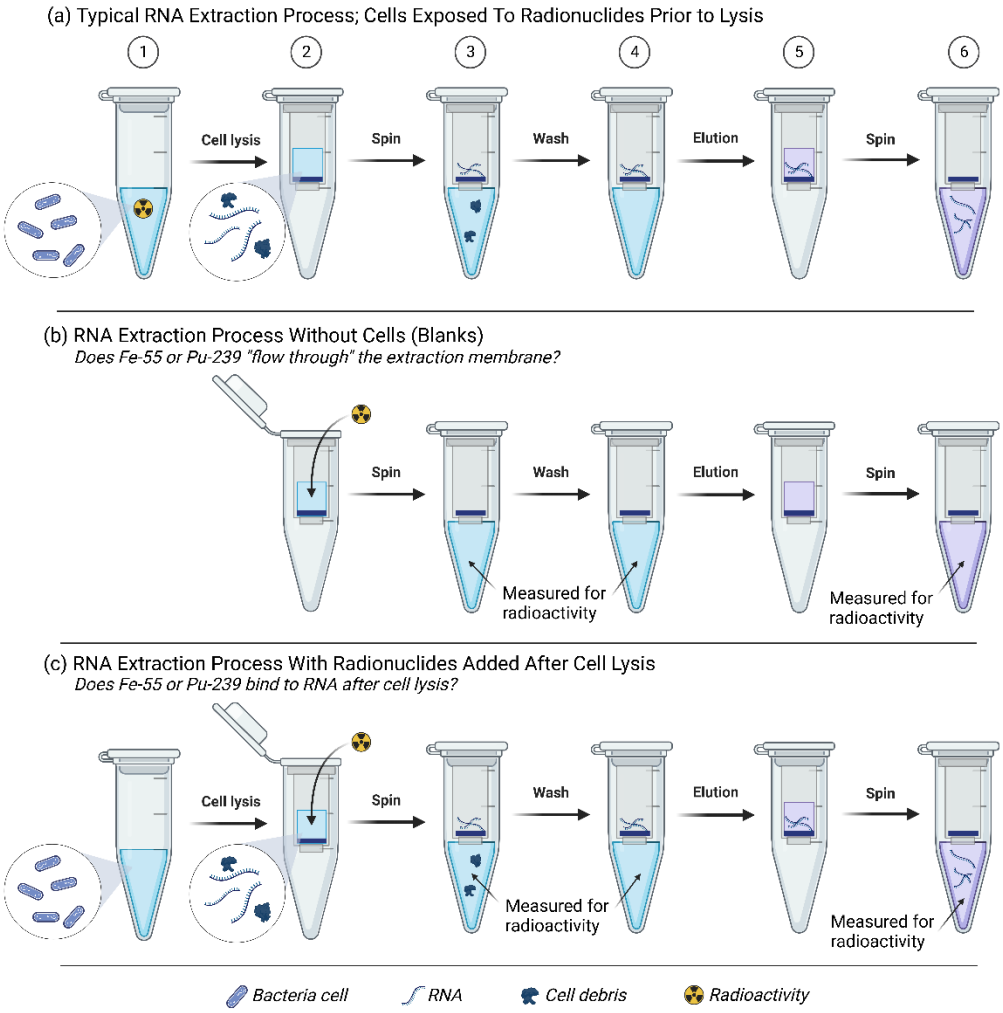

Figure 17 (a) Illustration of the general RNA extraction process as compared to the processes completed for this work; (b) testing for potential process flow through by performing an "RNA extraction" without cells; (c) testing for potential binding with RNA during the extraction process by adding the radionuclide after cell lysis. Created with BioRender.

Plutonium solution preparation

Plutonium solutions were prepared from two working solutions of ^{239}Pu in 0.01 M HCl, one solution where ^{239}Pu was complexed with citrate in a ratio of 1000:1 and another without

citrate complexation. The solution of ^{239}Pu complexed with citrate was diluted with 0.01 M HCl to produce a working solution with an activity concentration of 1.37×10^{1} kBq mL^{-1}. Using this working solution, four additional solutions were produced via serial dilution (with 0.01 M HCl) with activity concentrations of 1.37 kBq mL^{-1}, 1.37×10^{-1} kBq mL^{-1}, 1.37×10^{-2} kBq mL^{-1}, and 1.37×10^{-3} kBq mL^{-1}. The dilution process was also completed using the ^{239}Pu solution that was not complexed with citrate. There were 10 total ^{239}Pu solutions used as ^{239}Pu -spiked process blanks: 5 complexed with citrate and 5 without. The activity of solutions used for each experiment conducted is summarized in **Table 3**.

Iron-55 solution preparation

Process blanks for ^{55}Fe were made from a stock solution of $^{55}FeCl_3$. An aliquot of the stock solution was diluted to a concentration of 1.81×10^{4} kBq mL^{-1} in approximately 0.01 M HCl. Four additional working solutions were prepared as process blanks via serial dilution (with 0.01 M HCl) with concentrations of 1.81×10^{3} kBq mL^{-1}, 1.81×10^{2} kBq mL^{-1}, 1.81×10^{1} kBq mL^{-1}, and 1.81 kBq mL^{-1}. The process resulted in 5 total ^{55}Fe blanks with different concentrations that were used (**Table 3**).

Table 3 Summary of the Radiological Solution Activity Concentrations Used

Experiment	*Activity Concentrations (kBq mL^{-1})*				
RNA extraction without cells					
Process Blank ^{239}Pu	1.37×10^{1}	1.37	1.37×10^{-1}	1.37×10^{-2}	1.37×10^{-3}
Process Blank ^{239}Pu with citrate	1.37×10^{1}	1.37	1.37×10^{-1}	1.37×10^{-2}	1.37×10^{-3}
Process Blank $^{55}FeCl_3$	1.81×10^{4}	1.81×10^{3}	1.81×10^{2}	1.81×10^{1}	1.81
RNA extraction with radionuclide spike after cell lysis					
P. putida and ^{239}Pu		1.37	1.37×10^{-1}	1.37×10^{-2}	
P. putida and ^{239}Pu with citrate		1.37	1.37×10^{-1}	1.37×10^{-2}	

Sample preparation for ^{239}Pu and ^{55}Fe blanks

The RNA extraction process was first completed using solution blanks to examine flow-through of ^{239}Pu and ^{55}Fe from the extraction process without the presence of cells. Activity concentration for both ^{239}Pu and ^{55}Fe solutions were based on laboratory experiments conducted in our laboratory with different microorganisms. The middle concentration of the five concentrations used for each radionuclide was chosen to reflect the approximate activity concentration of bacteria solutions used in previous experiments (1.37×10^{1} kBq mL^{-1} for ^{239}Pu solutions and 1.81×10^{2} kBq mL^{-1} for $^{55}FeCl_3$), such that our experiment included solutions two orders of magnitude greater and two orders of magnitude lesser than the bacteria cultures previously studied. The activity concentration of each solution used was verified by Liquid Scintillation Counting (LSC) analysis of an aliquot of each solution.

The RNA extraction process was completed according to manufacturer's instructions starting with the transfer of 100 µL of ^{239}Pu or ^{55}Fe solution to a 2 mL microcentrifuge tube. The process is outlined in **Figure 17**(b). Solutions containing ^{239}Pu, ^{239}Pu complexed with citrate, or $^{55}FeCl_3$ were added to the ion exchange column in step 2 of the RNA extraction process (step 1 of Figure 17 was not completed for process blanks, as there were no cells used). The process was completed in triplicate for each concentration used.. Throughout the RNA extraction process, ~2 mL of liquid effluent waste was produced (steps 3 and 4, **Figure 17**). The waste effluent from each extraction column was collected in a 20 mL LSC vial for the purpose of activity / mass balance. The final liquid effluent from the RNA extraction process, which under normal circumstances would contain the RNA sample to be used for bioinformation analysis, was collected in a separate 20 mL LSC vial (step 6, Figure 17)

Plutonium and P. putida sample preparation

To address the potential for radionuclides to bind to RNA as a result of the chemical changes inherent to the RNA extraction process, several control bacteria samples were spiked with ^{239}Pu prior to RNA extraction. The process used for the ^{239}Pu and *P. putida* samples is outlined in **Figure 17**(c). Aliquots (150 µL) were collected from bacteria cultures grown with no radiological contaminants and prepared for RNA extraction. After the cell lysing agent was added, the samples were spiked with 10 µL of the previously prepared Pu solutions with activity concentrations of 1.37 kBq mL^{-1}, 1.37×10^{-1} kBq mL^{-1}, and 1.37×10^{-2} kBq mL^{-1} of ^{239}Pu complexed with citrate and 1.37 kBq mL^{-1}, 1.37×10^{-1} kBq mL^{-1}, and 1.37×10^{-2} kBq mL^{-1} of ^{239}Pu without citrate complexation creating six different exposure scenarios (step 2, **Figure 17**). As completed in the process blank investigations, the waste effluent was collected for LSC analysis

(steps 3 and 4, **Figure 17**), in addition to the RNA extraction product (step 6, **Figure 17**). The mass of samples was collected for mass balance and quality analysis.

Liquid Scintillation Counting

All samples were prepared for LSC with 10 mL of Optiphase HiSafe 3 (Perkin Elmer) liquid scintillation cocktail. Plutonium-239 samples were quantified based on activity from alpha emissions assuming 100% efficiency. Iron-55 samples were quantified based on activity from electron emissions, assuming an efficiency of 42%. All samples were corrected for variation in volume based on their mass.

Sample Terminology

Two samples were produced for each RNA extraction performed. The first sample, collected in steps 3 and 4 of the process as illustrated in **Figure 17**, is referred to as an effluent sample. The second sample, collected in step 6 of the process as illustrated in **Figure 17**, is referred to as an RNA extraction sample. While most of the samples considered in this work were blanks, processed exclusively to examine the flow-through of radionuclides, and thus contain little to no RNA, this terminology will be used for all samples as they were intended to represent the product of the RNA extraction process.

Results and Discussion

While the radiological content of RNA samples was initially analyzed for the purpose of developing appropriate protocols for the handling of radiological materials, the discovery of ^{239}Pu and ^{55}Fe in RNA samples lead to the decision to collect RNA extraction samples specifically for the purpose of radiological characterization during experiments. In Chapter 3, I

use the radiological content of RNA samples as evidence to differentiate uptake of ^{239}Pu and ^{55}Fe into the cells, versus sorption to the outside of the cell membrane. To use the RNA extractions as evidence of uptake, however, it was necessary to rule out that the presence of ^{239}Pu and ^{55}Fe was not the result of something related to the extraction process. By examining process blanks, with no cellular content including RNA, I was able to demonstrate that the presence of ^{239}Pu and ^{55}Fe in our RNA extractions was not the result of process flow through.

There was no detectable ^{239}Pu in any RNA extraction sample analyzed when ^{239}Pu was complexed with citrate. When process blanks for ^{239}Pu without citrate complexation were analyzed, Pu was detected in only one RNA extraction sample. The sample with detectable ^{239}Pu was from the sample-blank concentration, 1.37×10^{1} kBq mL^{-1}, and had an activity of 0.87±0.04 Bq. The activity of the RNA extraction sample represents 0.064% of the total activity in this sample. The results of this part of the experiment demonstrated that the presence of ^{239}Pu in RNA extraction samples in the previous work is not reasonably attributed to process flow-through.

By studying the radiological content of the extraction process effluent samples, the movement of the radionuclides was observed through the extraction process and improved understanding of where radiological waste may be produced. Plutonium-239 was detected in effluent samples from sample blanks containing ^{239}Pu complexed with citrate from the three largest concentrations (1.37×10^{1} kBq mL^{-1}, 1.37 kBq mL^{-1}, and 1.37×10^{-1} kBq mL^{-1}), with no ^{239}Pu detected in effluent samples from the 1.37×10^{-2} kBq mL^{-1} and 1.37×10^{-3} kBq mL^{-1} blanks. The activity of ^{239}Pu found in these samples varied between blank concentrations by about a factor of 10, which is consistent with the serial dilution method used to create the working solutions. Note that 1 of the 3 effluent replicates for the 1.37×10^{1} kBq mL^{-1} was excluded from

the data set as the sample was spilled during processing. The Pu activity of the effluent samples for blanks containing Pu complexed with citrate are provided in **Figure 18**.

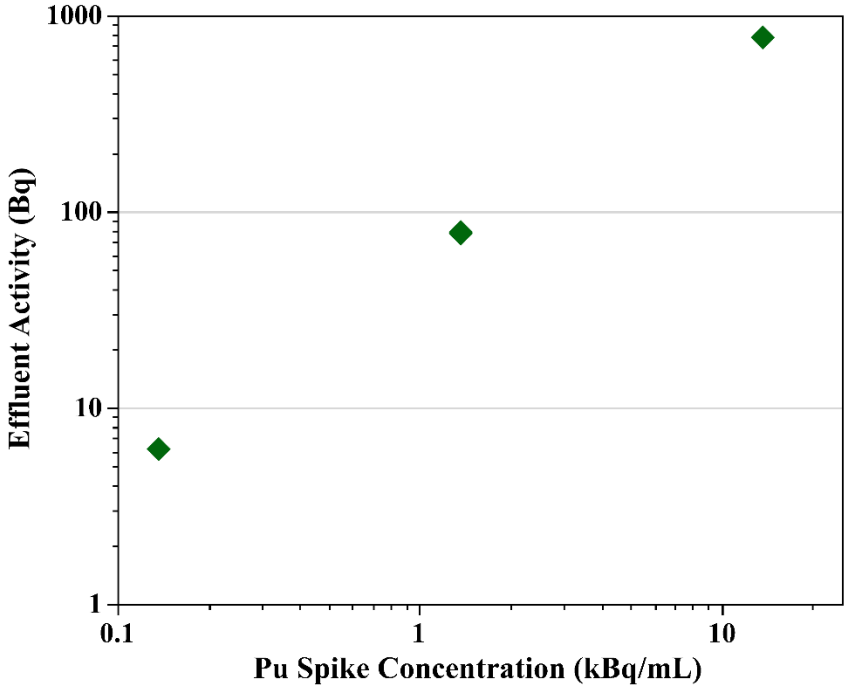

Figure 18 Activity of Effluent Samples for RNA extraction blanks using Pu complexed with citrate. Data points represent individual data points but overlap in most cases.

When considering the total activity contained in each sample analyzed, the effluent blanks left about half of the ^{239}Pu unaccounted for in samples where ^{239}Pu was complexed with citrate for the three highest concentrations used. We assume that the exchange column used in this process has some affinity for Pu and the remaining activity was disposed of with the exchange columns. The percent of Pu activity that was assumed to remain on the exchange column at the end of the RNA extraction process is provided in **Figure 19.**

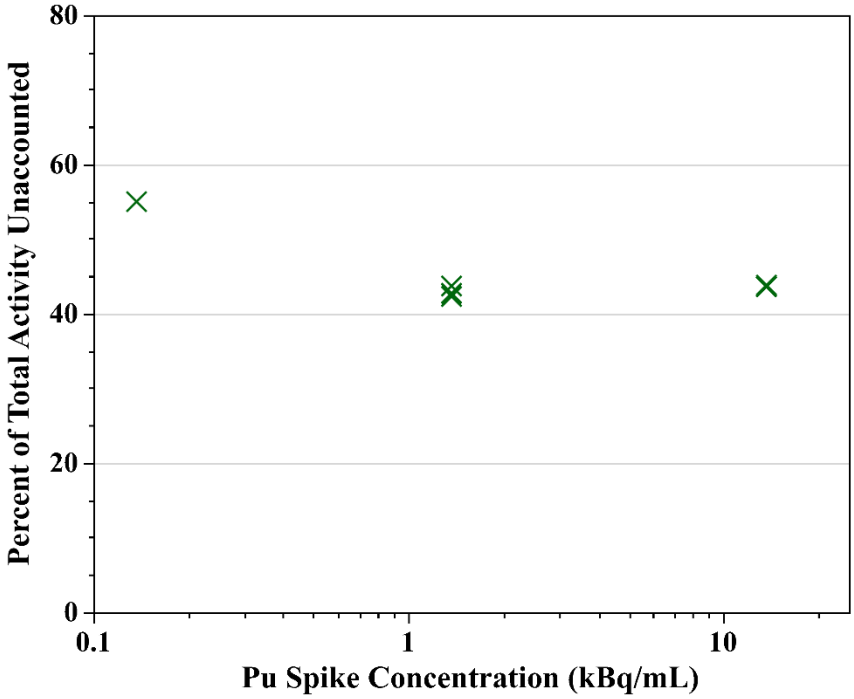

Figure 19 Percent of total sample activity that was not accounted in the RNA extraction or effluent samples. Data points represent individual data points but overlap in many cases.

When effluent samples from process blanks containing ^{239}Pu that was not complexed with citrate were analyzed, ^{239}Pu was detected only in effluent samples from the blanks containing 1.37×10^{1} kBq mL^{-1} ^{239}Pu. The effluent samples from 1.37×10^{1} kBq mL^{-1} ^{239}Pu without citrate also contained a lower concentration of ^{239}Pu when compared to effluent samples from the same ^{239}Pu concentration complexed with citrate. In all three replicates, 99.5% of the activity was unaccounted for and assumed to have remained on the exchange column when the 1.37×10^{1} kBq mL^{-1} blanks were processed, with 100% remaining on the exchange column for all other concentrations.

Iron-55 was detected in RNA extraction samples for all replicates of blanks with the highest concentration of ^{55}Fe, 1.81×10^{4} kBq mL^{-1}, as well as in one sample from the 1.81×10^{3} kBq mL^{-1} set of blanks, and one sample from the lowest concentration, 1.81 kBq mL^{-1}. All other

RNA extraction samples did not contain detectable quantities of ^{55}Fe. The results are provided in **Figure 20.**

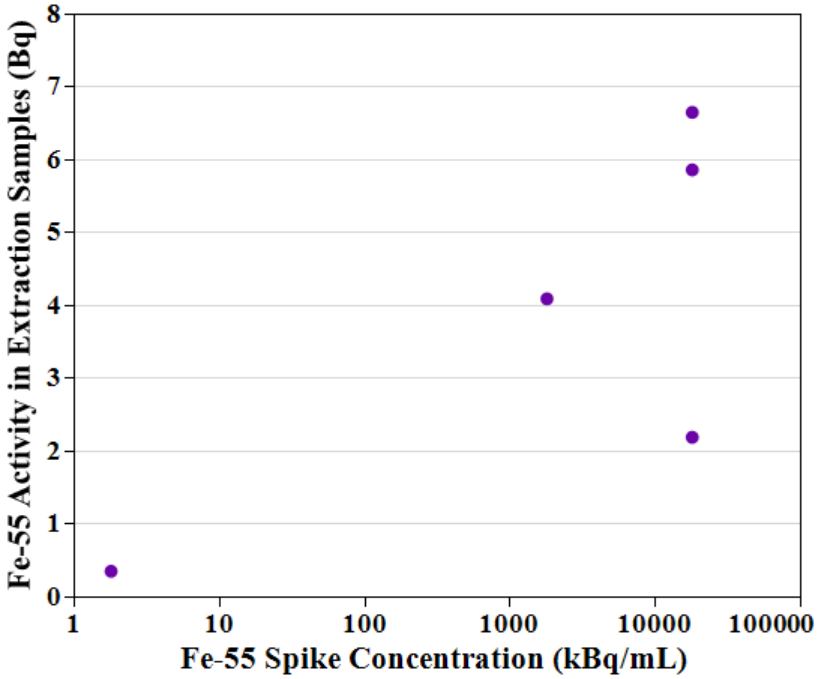

Figure 20 Iron-55 content of RNA extraction samples for RNA extraction completed with ^{55}Fe process blanks.

The detected ^{55}Fe in the RNA extraction sample from a 1.81 kBq mL^{-1} blank is inconsistent with two replicate data points and also inconsistent with triplicate data from two higher concentrations of ^{55}Fe blanks. Furthermore, the activity in the 1.81 kBq mL^{-1} extraction sample that was reported is 1.92% of the total activity in the sample analyzed. In other RNA extraction samples where ^{55}Fe was detected, the extraction sample activity represented between 0.00121% and 0.0226% of the total activity in the samples analyzed. The results have been presented in their complete form for the purpose of transparency; however, it is most likely that the RNA extraction result related to the 1.81 kBq mL^{-1} sample is the result of cross contamination during the RNA extraction process because of its lack of consistency with all other data, which was collected in triplicate. The content of ^{55}Fe in RNA extraction samples also

demonstrate that ^{55}Fe content in our previous RNA extraction studies was not the result of process flow through.

Iron-55 was detected in all effluent samples, where the ^{55}Fe activity in effluent samples increased by a factor of about 10 for each concentration of ^{55}Fe used as a process blank. The ^{55}Fe activity in effluent samples for process blanks is provided in **Figure 21**.

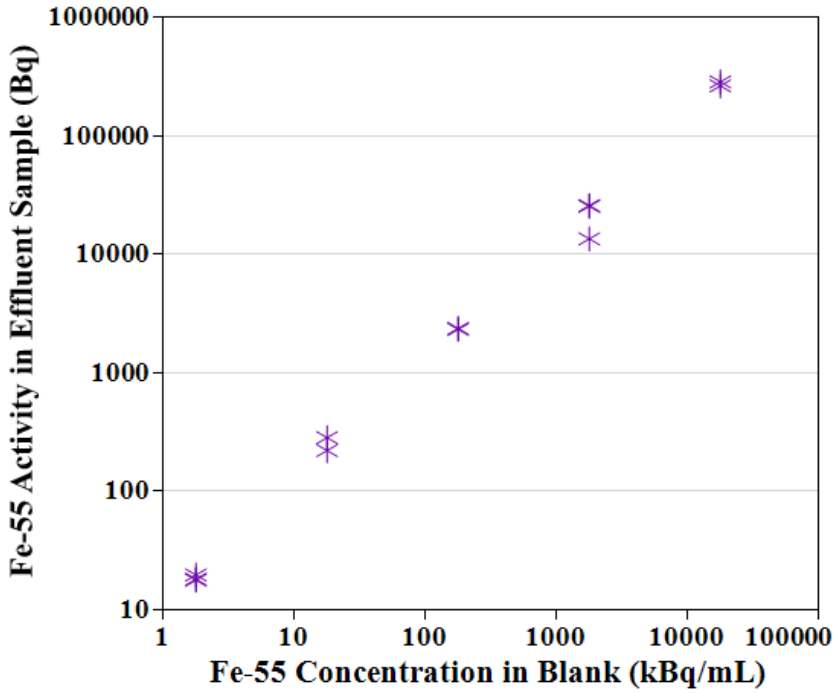

Figure 21 Concentration of ^{55}Fe in effluent samples. Data points represent individual data points but overlap in most cases.

As observed with the ^{239}Pu blank effluent samples, the total quantity of activity from the original sample is not accounted for by the RNA extraction and effluent samples, so it is assumed the remainder of activity remained on the extraction column. The amount of ^{55}Fe that was assumed to remain on the extraction column more closely resembles the activity balance results from ^{239}Pu without citrate complexation, where the percent of ^{55}Fe that was unaccounted for ranged from 97.1%-99.3% across all samples. As stable Fe would be likely be found in trace quantities in normal cell culture studies, and the RNA extraction process strives to produce an

extract that contains few impurities, the extraction column is likely designed to have an affinity for Fe.

In addition to process flow through, we also prepared an experiment to = examine if ^{239}Pu bound to RNA after the cells were lysed, during the RNA extraction process. RNA extraction samples were collected from *P. putida* samples spiked after lysing cells with 1.37 kBq mL^{-1}, 1.37×10^{-1} kBq mL^{-1}, and 1.37×10^{-2} kBq mL^{-1} ^{239}Pu complexed with citrate. The experiment was also completed with the same concentrations of ^{239}Pu without citrate complexation. There were no extraction samples that contained detectable quantities of ^{239}Pu. Only one effluent sample, effluent from the *P. putida* sample spiked with the greatest quantity of Pu complexed with citrate, the 1.37 kBq mL^{-1} spike, contained detectable ^{239}Pu. The results of this analysis indicate that ^{239}Pu found in RNA extraction samples is not the result of ^{239}Pu binding to RNA after the cell is lysed.

Due to the number of samples where no radiological material was detected, all results are provided in a tabular format in Appendix E.

Conclusions

Plutonium-239 was only found in one set of RNA extraction replicates, the set containing over 100 times the quantity of ^{239}Pu without citrate complexation that would be expected in cell studies conducted as a part of my work. Iron-55 was only consistently found in extraction samples with 100 times the quantity of ^{55}Fe used in cell cultures for this work, and in one replicate with 10 times more ^{55}Fe. The results of this work show that process flow through is not a significant pathway for ^{239}Pu or ^{55}Fe in RNA extraction samples as observed in our previous work. By analyzing the radiological content of effluent samples, the study also demonstrated that the extraction columns used have an affinity for both Pu and Fe. The study supports the

assumption that ^{55}Fe and ^{239}Pu detected in RNA extraction samples during long term cell studies is the result of ^{55}Fe and ^{239}Pu that was bound to RNA prior to the time of extraction.

Validating a model for radiation protection for doses less than about 150 mGy remains a priority in the field of radiological science, and the use of -omics technologies to understand low dose effects, especially transcriptomics and proteomics, will likely increase in the coming years. A 2022 Consensus Study of the National Academy of Sciences reaffirms the prioritization of a low dose research program in the United States of America for radiological doses below 100 mGy and dose rates of 5 mGy h^{-1} or less[39]. Specifically, the report calls for leveraging modern biological research techniques for the study of low dose and low dose-rate mechanisms of effect and integrating this data with epidemiological studies to examine risk assessment models.[39] The relevance of the observations regarding the radiological content of RNA samples is two-fold. The first area of relevance of this work is the practical concern of handling radiologically contaminated samples. Biological equipment utilized for transcriptomic research, especially equipment used for RNA sequencing, is costly and requires specialized training to use. Sequencing equipment is often located in centralized facilities at laboratories and universities, and, in some cases, sequencing is completed off-site. Researchers preparing RNA or DNA extraction samples from cells exposed to radiological contaminants, especially metals, should take care to characterize samples so that appropriate procedures for transport and handling are developed in accordance with federal, state, and facility regulations. Appropriate characterization will also help prevent contamination of specialized equipment.

This work also highlights the importance of considering how effects may be impacted when radiological metals are bound to DNA and RNA. Radiologically characterizing the content of DNA and RNA samples may provide quantitative data needed to differentiate between

chemical and radiological response in low-dose research efforts. Separating chemical and radiological effects will not only be useful when attempting to identify unique responses to radiation exposure, it may also help identify responses related to specific radiological contaminants. Finally, radiological content found in DNA and RNA samples may also be useful in quantifying uptake rates which could have implications for dosimetry, as advanced biological assessment techniques should be matched with fine-tuned dose estimates if dose-effect relationships are developed.

CHAPTER 5

CONCLUSION

The experiments presented in this work provide sufficient evidence to move forward with the development of refined dosimetry models. A review of the history and current state of microdosimetry efforts related to the development of a single cell model for bacteria is provided as Appendix A. In summary, microdosimetry efforts for individual, low-dose cell models are still in their infancy, but the study of both ^{239}Pu and ^{55}Fe fractionation between the growth media and cells in this work demonstrates a variety of scenarios that can be used to inform model development. In future work, I hope to expand the existing literature by examining the performance of GEANT4-DNA for alpha energies related to ^{239}Pu in liquid water. I also hope to apply both alpha and low-energy electron emissions in liquid water with varying densities of 1.1-2.0 g cm^{-3} to better represent the organelles of individual cells. The efforts described will entail comparing the performance of at least two of GEANT4-DNA's physic models so that an appropriate model can be chosen after the results of the work undergo peer-review. The use of a freely available, open-source modeling code like GEANT4-DNA is ideal for my research career at a predominantly undergraduate university for both my own research as well as the inclusion of student researchers.

Utilizing microdosimetric models for the purpose of developing a true dose-response model in the future would require further benchtop experiments. Specifically, experiments would be needed to provide a sufficient gradient of doses from which to develop a dose-response model. The data collected in this dissertation and in other works stemming from the research project demonstrates that there are effects at 10 mGy d^{-1} dose rates, but to create a relationship

between occurrence or severity of effects, multiple dose rates must be considered. When an appropriate model is achieved, it would be best paired with data from experiments with a minimum of 5 dose rates so that a relationship between dose and response can be achieved with significance. In addition to adding more dose rates, if more experiment data is collected in future work, I recommend a more comprehensive analysis of the bacteria that differentiates uptake versus sorption in a definitive manner. For example, suspension of cell pellets in EDTA with washing steps added can remove surface bound Pu[8]. Completing a step to remove surface bound Pu prior to lysing the cells would allow for quantitative analysis of sorption vs uptake. Additional experiments with *P. putida* may also consider analysis for siderophore production via fluorescence measurements. The pyoverdine produced by *P. putida* is green, fluorescent siderophore[34] and fluorescence measurements may provide for a more cost-effective method for monitoring pyoverdine production.

Perhaps the most surprising contribution to this dissertation is the material included in Chapter 4 related to the characterization of RNA extraction samples for radiological content. The work originated from a simple experiment for the purposes of radiological materials handling, with the hypothesis that RNA extracts from samples containing ^{239}Pu and ^{55}Fe would not contain detectable levels of radiological materials. When I concluded that the hypothesis was incorrect, however, it opened the door for further analysis. From the perspective of radiological protection and operational health physics, the results of the experiment were sufficient to conclude the researchers using unsealed radiological materials in experiments that require the analysis of RNA should consider RNA extraction samples for their potential to contaminate scientific measurement equipment that may be shared between non-radiological and radiological experiments.

The experiments presented also examined RNA extracts for their potential to differentiate uptake versus sorption of radionuclides. While the data presented was not sufficient to conclude the analysis of RNA extracts for this purpose in a quantitative way, they support the assertation that RNA extracts could be a useful tool for the purpose of differentiating sorption versus uptake in the future. I feel that it would be interesting to consider further examination of the use of both RNA and DNA extractions when uptake of radionuclides is suspected. Though DNA was not used in these experiments, extraction of DNA is cheaper and often more simple than RNA extraction, which could further improve the utility of methods related to RNA/DNA extractions for determining uptake of radionuclides.

As an aside, I found the problem and subsequent the analysis of RNA for radiological content to be ideal from the perspective of the scientific method, especially as an educator. While the scientific method was long taught as a five to six step, linear process, a more modern perspective opts to present the method as a cycle or on-going process, as shown in **Figure 22**. The idea of an ongoing process is more easily reconciled with critiques of the scientific method that have led to inquiry-based scientific teaching techniques[68].

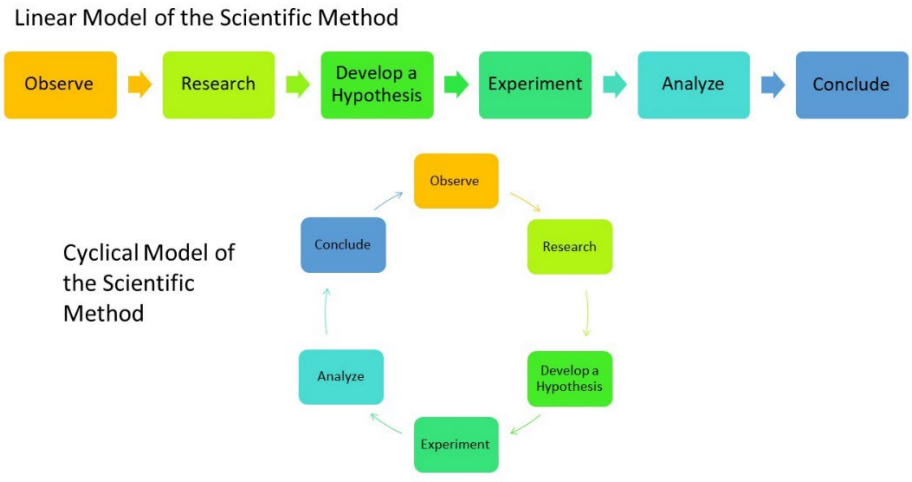

Figure 22 A visualization of the scientific method both as a linear process and as a cycle.

APPENDICES

APPENDIX A

CONSIDERATIONS FOR THE DEVELOPMENT OF A MICRODOSIMETRIC MODEL FOR ROD-SHAPED BACTERIA

Background

A fundamental area of interest to the scientific community is to examine the dose-effect relationship when bacteria are exposed to low doses of ionizing radiation[27], which requires an accurate estimate of dose in addition to the observation of effect. "Dosimetry" refers generally to the determination and/or assessment of radiation dose, whether by model, measurement, or a combination of the two. The dosimetric quantity of interest in this work is absorbed dose; although technically a point quantity, for practical purposes absorbed dose is typically averaged over a volume of interest.[38] For example, the dose estimates for bacteria in a 100 mL volume of liquid culture were averages of total energy deposition over the entire volume. Without specific evidence for how radionuclides distribute within the solution, it must be assumed that the radionuclides of interest, in this case ^{55}Fe and ^{239}Pu, are homogenously distributed throughout the culture volume. However, the investigations in the previous chapters demonstrated that ^{239}Pu and ^{55}Fe accumulated internally and/or externally on cells in both *P. putida* and *E.coli*, motivating consideration of a more refined dosimetric model.

As mentioned previously, ^{239}Pu was selected because of its specific connection to the production of nuclear weapons, while serving as a representative of high linear energy transfer (LET) radiation for dosimetry and potential dose-effect efforts with a range of approximately 40 μm in water.[69] Iron-55 is a common activation product that undergoes electron capture.[38] Iron-55 produces x-rays, 5.9 (25%) and 6.5 (3.4%) keV, as well as auger electrons with an average

energy of 5.2 keV(61%) making it representative of low-LET radiation.[19] The mean free path of ^{55}Fe x-rays is about 400 μm in water; however, the range of the auger electrons is approximately 0.6 μm in water.[69,70] The concentration of either radionuclide on or in cells, which have an average length of about 1-5 μm[71], (i.e., internal or extremal accumulation) would indicate that the absorbed dose would not actually be homogeneously delivered within the liquid cell culture due to the short range of the ^{239}Pu and ^{55}Fe emissions. Thus, a more complex assessment of dosimetry is warranted, and this project's design supports such an assessment by applying sensitive biological tools to analyze the response of microorganisms to ionizing radiation.

Considerations for internal and external accumulation

As previously discussed, in addition to damage to DNA, radiological interactions with the cell membrane, proteins, mitochondria, cell signaling pathways, and other organelles may also be responsible for inducing effects as a result of ionizing radiation, and these effects may be highly relevant to understanding the mechanisms of effect at low doses of radiation.[18] Bacteria are prokaryotic organisms that lack a true cell nucleus, and as such this is one factor that differentiates them from traditional cellular models. Plutonium-239 and ^{55}Fe concentrated within the cells internally (via uptake) or externally on the cell surfaces (sorption) would mean that a larger portion of alpha interactions will occur at sensitive locations within the cells including, but not limited to, bacterial DNA, the nucleoid region, the cell membrane, and other organelles. In general, our investigations of *E. coli* exposed to both ^{239}Pu and ^{55}Fe showed increased biosynthetic burdens and stress response, consistent with prevailing theories related to low-dose response to ionizing radiation. Investigations of RNA expression in the cell cultures studied for the project also found upregulation of six6 genes related to the production of enterobactin in *E. coli* cultures exposed to ^{239}Pu as compared to both control cultures and cultures that contain

^{55}Fe.[72] As enterobactin is a siderophore that mediates iron transfer and has been implicated as a transfer mechanism for transporting Pu into cells, the hypothesis that ^{239}Pu is internally accumulating in cell cultures is further supported.

Microdosimetry computational techniques

Microdosimetry is a type of radiological dosimetry that examines energy deposition in a stochastic manner on microscopic scale and is aimed at more precise understanding of radiation interactions and effects in living tissue.[73] Microdosimetric methods are the ideal methods when considering dose from ionizing radiation to small targets as opposed to large volumes. Experimental microdosimetry began in the 1950's with Rossi and Rosenzweig's development of tissue equivalent proportional counters (TEPCs)[74]. TEPCs use plastics and gases with a molecular content that is approximately equivalent to human tissue to simulate targets at a macro-scale that approximate mammalian cells.[74] Experimental methods rather than computational methods were the primary methods used in the field of microdosimetry for many decades, as computational methods require many iterations of the same events to provide statistically rigorous answers, a calculation methodology best achieved with computers.

In recent decades, the prevalence of increasingly powerful and accessible computing technology has shifted the field's focus to computational microdosimetry methods. Computational microdosimetry is primarily conducted with Monte Carlo-based computer codes that are designed to simulate the interactions in matter resulting from individual radiological events by using random number generators to model the stochastic nature of particle interactions.[75] Monte Carlo methods can then be used to calculate a variety of dosimetric quantities to a target area. Monte Carlo codes like PENELOPE, MCNP, and GEANT4 were initially developed to take on this task with a condensed history (CH) approach. CH models do

not model all interactions, but rather condense several interactions into a single step by using stopping power to calculate energy loss and distributing that energy in a local region instead of modeling the path of all secondary particles.[76] As microdosimetry has traditionally focused on radiation interactions in living tissue, CH methods have been successfully deployed as the standard for measuring energy deposition in targets related to mammalian cells, which generally range from 10-100 μm. Another common target has been the mammalian cell nucleus, the largest organelle in the mammalian cell with a diameter of 5-20 μm.[77] While it would be impossible to list all the applications of these codes for cell-level dosimetry in the literature, some recent advanced examples of these applications include: the use of GEANT4 to accurately describe radiobiological response to cancer cells irradiated with monochromatic and clinical proton beams[78], examining the distribution of radiopharmaceuticals in clusters of tumor cells using MCNP6[79], and development of an algorithm that creates quasi-realistic cancerous tumor volumes from individualized cells to study radiation damage using MATLAB and GEANT4.[80]

The CH approach still has a wide variety of useful applications in the field of dosimetry, but studies in low-dose radiation research have found limitations in this approach. Investigations involving organelles like the mitochondria, cell membranes, and endoplasmic reticulum, create targets in the nanometer range, and researchers found it prudent to question the utility of CH models at such small sizes. How small is too small for a CH model? Unsurprisingly, the answer is complicated, but, generally, target size is a key factor in model for very small target. Specifically, when targets are smaller than the track length but larger than the mean free path (mfp) of incident charged particle radiation, CH models must be used with extreme caution, and when the target is smaller than the mfp, CH models are no longer accurate.[76] Ideally, CH codes should not be used to model electrons in liquid water with energies below 1 keV.[81]

The other factor that pushed the limits of CH models is related to complex investigations of DNA damage. While double stand breaks (DSBs) are still considered to be the major indicator used for cell survival, it is theorized that one key to understanding low-dose biological effects requires examination of cluster damage to DNA. Cluster damage is defined as any combination of DSBs, single strand breaks (SSBs), change or loss of a base, damage to the deoxyribose backbone, or cross-link[82], as demonstrated in **Figure 23**.

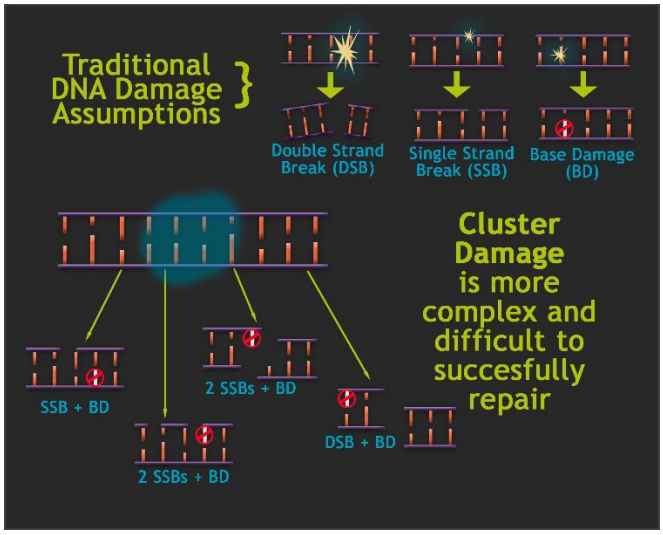

Figure 23 A visualization of DNA cluster damage.

To understand cluster damage, we cannot ignore the paths of secondary particles as is done in CH models, as we must know more spatial information about interactions to predict the occurrence of different cluster damage types / combinations. An interest in modeling secondary particle interactions has been especially supported by the increased use of Heavy Ion Therapy (HIT), such as proton and carbon-ion radiation therapy, for cancer treatment. As proton and carbon-ion treatments have been used and studied, the effects observed were not sufficiently predicted by microdosimetric efforts, and it became evident that further investigation of the relative biological effectiveness (RBE) of HIT modalities was warranted, which included examination of secondary particle interactions.[83]

To meet the new needs of the microdosimetry field, a new type of model is required, Track Structure (TS) codes. While more computationally intensive than CH codes, TS codes provide resolution to the nanometer scale by tracking secondary particles. An ideal TS model used for microdosimetry is capable of considering very low energy electrons, because over 90% of cluster damage is caused by energy depositions less than 150 eV.[84] Many TS codes have been developed and deployed, such as the PARTRAC and KURBUC codes, however the GEANT4-DNA package for the GEANT4 code has become a dominant player in the literature.

GEANT4 with GEANT4-DNA

GEANT4 (Geometry ANd Tracking) is a Monte Carlo toolkit designed to simulate the passage of particles through matter using object-oriented (C++) programming.[85] The code is developed through a consortium of many laboratories and research groups and is primarily maintained by the European Council for Nuclear Research (CERN). GEANT4 was initially developed for high-energy, particle physics research; however, its design is useful for a variety of research functions in the fields of radiation physics, space research, and medical physics. GEANT4 has been maintained as an open-source code which has paved the way for a variety of add-ons, packages, and analysis options to improve its utility in specific fields. A set of physics models, termed GEANT4-DNA, is one such add-on.

The goal of the GEANT4-DNA project, initiated by the European Space Agency (ESA), was to develop a set of physics models appropriate for simulating biological effects at the molecular and cellular scale.[86] GEANT4-DNA has become an important code in microdosimetry for many reasons, though an undeniable contributor to its popularity is that it is the only appropriate TS code that is open access and open source.[87] While it does not provide the plethora of materials that can be used as a target found in most CH models, the GEANT4-DNA package

can effectively manage interactions of low-energy electrons in water as well as in the four DNA constituent materials (adenine, guanine, thymine, and cytosine), a sufficient set of materials for biological study.[86,88]

Low energy electron modeling in liquid water

To track secondary and other low-energy electrons in a TS code, appropriate models for physical interactions must be applied. It has been known for some time that low-energy electrons were likely responsible for large portions (50%+) of energy deposition in biological materials,[89] however the field was technologically limited, both in a computational and experimental sense, and adequate efforts to address this only began about 20 years ago. High-energy approximation methods common to CH codes fail at low-energies because they do not sufficiently account for the impact of atomic/electric properties of target materials on interaction cross-sections.[90] The use of TS codes has become the state of the art method for evaluating low-energy interactions, and continued attempts to validate and use these models are expected in future research on low-dose radiation effects.[91]

Relevance of this work

The focus of cellular-level modeling to date has been primarily focused on mammalian cells due to interest in and relevance to human health, although a model that is representative of a common environmental microorganism has similar, albeit indirect, relevance. Many bacteria have a strong propensity for accumulating radiological contaminants from the environment, which is why they are used for bioremediation at impacted sites. The accumulation of material results in bacteria serving as an important pathway to the food chain in ecosystems.[28] Of course, the qualifications that necessitate the move to TS models for human cells are of particular

relevance to this work. Our targets are located within prokaryotic cells with average sizes of 1-5 μm, much smaller than the 10-100 μm eukaryotic cells generally considered with microdosimetry models. Accordingly, all potential sub-cellular targets defined for an *E. coli* or *P. putida* cell would be in the nanometer range.

Challenges When Developing a Modeling Methodology

Radionuclides of Interest

The range of ^{55}Fe auger electrons is 0.6 μm, smaller than our cell of interest and potentially smaller than other targets considered, which is the relative size range where CH models must be used cautiously or not at all. In the last 20 years, much attention has been drawn to low-energy, low-LET radiation, like the auger electrons produced by ^{55}Fe, as many radiobiological studies have indicated that the relative RBE of low-energy, low-LET radiation might be as high as four4 when compared to gamma radiation from ^{60}Co (where RBE of low-LET radiation has conventionally been assumed to be one).[17] One of the most commonly examined radionuclides is ^{3}H, a beta-emitter with an average energy of 5.69 keV, because ^{3}H is the dominant release from nuclear power plants, with an estimated 100 PBq of ^{3}H released world-wide on an annual basis.[92] RBE is often consulted and used for the development of appropriate radiation weighting factors (w_R), which are used to compute dose when using radiation protection quantities. In 2008, when the ICRP affirmed their position that a w_R of 1 is an appropriate simplifying assumption for the purpose of calculating radiation protection quantities, despite recognized differences in RBE, interest in the matter continued to grow.[93] Examination of evidence regarding the relationship of ^{3}H exposure to cancer incidence in humans supported the International Commission on Radiological Protection (ICRP) position,

because, while some data suggest a potential sensitivity for breast and thyroid cancer development with low-energy, low-LET radiation exposure,[94] epidemiological evidence did not support a statistically significant increase in cancer incidence from ^{3}H exposure as compared to gamma exposure.[95] Investigations into the RBE of ^{3}H in tissue continued to support the evidence that the RBE for tritium is greater than 1, and attempted to explain the observed variation in this value.[96] The discrepancy in observed RBE in experimental studies as compared to predicted RBE from models has been an impetus for applying TS models to ^{3}H microdosimetry studies as the resolution provided by TS models may provide insight that CH models have historically lacked.

An observed increase in RBE for low-energy, low-LET radiation is more relevant to this work than w_R because there are various potential end points that might be used to determine effect at the cellular level in bacteria. The w_R would only hold relevance if the end point of concern was cancer incidence, and would be specific to human tissue, not bacteria. Iron-55 does not have a strong presence in the literature regarding the study of low-energy, low-LET radiation, but the evidence related to ^{3}H is highly applicable to special considerations for ^{55}Fe. The 5.2 and 6.1 keV auger electrons produced by ^{55}Fe are close in energy to the 5.7 keV beta produced by ^{3}H. As such, if a TS model is needed to accurately examine the short and tortuous path of ^{3}H beta emissions in tissue, this would also be necessary to study ^{55}Fe's auger electrons. Another interesting connection between ^{3}H and ^{55}Fe microdosimetry is that the variation in ^{3}H RBE values in experimental studies has been explained, in large part, by differentiating exposure from tritiated water (HTO) and organically bound tritium (OBT). In general, the RBE for OBT is about twice that of HTO, such that the recommended RBE for HTO is about 2, while it is about 4 for OBT.[97] Because of the relatively short range of low-energy electrons and beta particles in water, when ^{3}H is in an OBT form, the RBE is much higher because of the increased likelihood

of an interaction with targets located in the cells themselves. Considering that this work found that around 80% of ^{55}Fe in the cell cultures was accumulated in the bacteria cells, either internally or externally, the high propensity for uptake makes the study of ^{55}Fe reasonably analogous to OBT for this work.

Alpha particles produced by ^{239}Pu represent high-LET radiation in this study but attempts to understand low-dose effects from alpha-emitters still are tied to the understanding of low-energy electron interactions. The 5.14 MeV alpha particle from ^{239}Pu will primarily lose energy by ionization interactions, such that alphas lose, on average, 35.5 eV per ion pair produced (in liquid water), resulting in the formation of hundreds of thousands of ion pairs in tissue over its relatively short track.[98] Many of the secondary electrons produced are capable of ionizing water, with an ionization threshold of about 12.6 eV,[99] and will thus deposit much energy locally, necessitating the use of TS models when considering clustered DNA damage or interactions with other organelles.

Physics Models

When TS codes were first developed, experimental data for scattering of electrons in liquid water was not available, and early models were validated with data from water vapor using a linear extrapolation for density to transform the data for liquid water. Experimental studies with liquid water, however, showed that there are phase effects in condensed matter that are not sufficiently explained by the linear extrapolations from gas-phase data.[100] While some interactions are still based on water vapor data, solutions have been developed for the phase effect issue in some cases, though liquid water data is still sparse for very low-energy electrons, especially those under 100 eV.

To overcome the phase issues for inelastic interactions, several research groups developed solutions to the dielectric response function for liquid water with varying sets of limited optical data from liquid water experiments. One such model, the Emfietzoglou model, was used to develop the ionization and electronic excitation physics processes for GEANT4-DNA.[86,90,100,101] While less energy will be deposited from elastic collisions, they are important for the spatial distribution of electrons in TS models, and are modeled using a partial wave calculation computed by Champion et.al. designed specifically for use in the GEANT4-DNA code.[102] As advances in both experimental data and computing power have allowed for more options to validate TS codes, the GEANT4-DNA development team has responded with improved models. Kryriakou et al. developed an algorithm to improve the Emfietzoglou models to make the model more accurate for electrons below 10 keV, and this model is now included as an alternative to the default in the GEANT4-DNA code, as part of the "option 4" models.[90] The option 4 models only provide improvements for ionization and excitation interactions. GEANT4-DNA also includes a full alternative set of physics models for inelastic and elastic scattering implemented from a specialized TS code, CPA-100, included as the "option 6" models.[103,104] CPA-100 is a Fortran based microdosimetry code, and the option 6 models use the CPA-100 cross section data for elastic scattering, excitation, and ionization to provide an alternative route for using this program's models.[104]

When choosing a set of physics models for use in a GEANT4-DNA simulation, the limitations of each model set should be carefully considered for each scenario. The use of option 4 or option 6 models is recommended for low-energy electrons over default models[105] though option 4 models are only applicable below 10 keV and option 6 models are only applicable below 255 keV, while option 2 (default) GEANT4-DNA models are applicable up to 1 MeV.

While option 4 or option 6 models would both be sufficient for ^{55}Fe auger electron TS modeling, a combination of models would be required for ^{239}Pu to cover the entire energy ranged needed. There is currently insufficient data to determine which set of models, option 4 or option 6, is the best performing for electrons up to 10 keV and both models are used in the current literature.[87] Constructors for each set of models are provided by GEANT4-DNA, however generally any combination of model sets would need to be coded manually. A recent addition to the GEANT-DNA code, however, is a constructor called "G4EmDNAPhysicsActivator" which provides a combined set of models and eliminates the need for a manual combination. When using the "G4EmDNAPhysicsActivator" constructor, the model will use option 4 models for electrons below 10 keV, default GEANT4-DNA models between 10 keV and 1 MeV, and standard GEANT4 electromagnetic models (EM) over 1 MeV. The use of the "G4EmDNAPhysicsActivator" would allow for a consistent physics model choice for both ^{239}Pu alphas and ^{55}Fe auger electrons.

Option 4 model cross sections have shown better agreement with a large range of experimental water vapor data, however limited sets of liquid water data suggest that there is better alignment of liquid water cross sections with option 6 models[104]. Additionally, the CPA-100 code, where the option 6 model originated, included cross sections for a wider variety of biological materials. Currently, molecular cross sections that allow for the use simulation of DNA targets have been added to GEANT4-DNA and it is likely that other biologically relevant materials may be added in future updates.[104] Considering the experimental uncertainty regarding which set of physics models is the best model, development of an appropriate bacteria model for dosimetry should consider the use of both the option 4 and option 6 physics models, with a comparison of the results for each to be presented in the literature. Option 6 models may have a

more varied utility in the future; however, to date, the only attempt at developing a model for bacteria (*E. coli,* specifically) and very low-energy electrons, utilized option 4 models.[106]

Validation Considerations for an Appropriate Physiological Model

Two other attempts at GEANT4-DNA for a bacteria model (*E. coli* in both cases) have been published. A 2022 model published by Rafiepour et al. considered "low-energy" electron and photon exposures, however the electrons used in this study were 50, 100, and 150 keV which is of minimal relevance to this work.[107] Another model from Lampe et al. considered exposures with electrons from 1-990 keV and protons from 500 keV to 30 MeV[106], which is more relevant to this work. In both studies, the focus of modeling was a physiochemical output that was specifically aimed at characterizing complex damages to DNA only. In both cases, an appropriate physiological bacterial cell was not considered, and in Lampe et al.'s study only a bacteria nucleoid was used. The bacteria nucleoid was packed with an elegant DNA construction that might have potential use in combination with a physiological model of the cell in future work; however, the study was published in 2018 and the authors do not appear to be pursuing future work with this model. As is, the model would be insufficient for computing a dose calculation for the purpose of developing a dose-effect relationship.

There is a great need for physics models in a variety of targets beyond liquid water and DNA bases, including high-Z materials for biomedical applications and other biological compounds like amino acids to improve cell models.[103] The current models, however, lack validation for these types of materials. One way to improve simple cellular modeling efforts such as the one presented in this work without constructing new materials might be to examine the models with different density values for liquid water that are closer to the density of areas like the cytoplasm and nucleoid to provide more accurate differentiation of the targets. While a

common assumption for cells is to approximate density with water (1 g cm^{-3}), the overall density of *E. coli* cells is found to be in the range of 1.09 – 1.11 g cm^{-3}.[108] Additionally the cell consists of about 55% protein and 20% RNA[109], which have densities of 1.38 g cm^{-3} [110] and 2.0 g cm^{-3} [111], respectively.[112] The use of varying densities might provide a sufficient physiological model, however considering the uncertainty regarding the validation of ionization cross sections for liquid water at 1 g cm^{-3}, a study on this variation in density with multiple physics models is necessary and should undergo successful peer review prior to application in a model.

Practical Challenges

The Palmetto Research Cluster has a large number of users, so users do not have administrative privileges to install software or needed dependencies on the main path for use by all users. When using the cluster, users must request a set of computing nodes to use for all operations, including file installation, and it is challenging / discouraged to attempt to use the same nodes during every session as they are generally distributed on a "first come, first served" basis to users to maximize availability. For reasons that have still not been identified by this author or the staff charged with maintaining the Palmetto Cluster, GEANT4 seems to struggle with developing paths to dependencies that are stored on the user's allocated drive in a way that they can be used from any computing node. If attempting to use GEANT4 on a large computing cluster, it may be advisable to request that the cluster administrators add all dependencies to the primary module list (where they would be available to all users) as a way of avoiding this issue.

Conclusion

The development of a novel and physiologically adequate bacteria model for establishing dose comes with abundant challenges when the need for TS modeling of very low-energy electrons is considered. While it is possible to overcome some of these challenges in the coming

years, currently, more validation of fundamental physics models will be needed to create the needed model. A simplified CH model for bacteria cells would be neither novel nor accurate, though a future TS model will have utility in the literature beyond the scope of this study.

APPENDIX B

PLUTONIUM OXIDATION STATE ANALYSIS

To verify the oxidation state analysis of the plutonium stock after complexing with citrate that was used for the experiments presented in this dissertation, a duplicate experiment was carried out in February and March of 2021 to create representative samples for analysis. The primary goal was to examine the oxidation state of ^{239}Pu in cell culture media at the beginning of experiment periods. Samples were collected from the culture media after it was spiked with ^{239}Pu stock that had been complexed with citrate but before they were inoculated with bacteria. Additionally, representative samples of *P. putida* and *E. coli* were grown with ^{239}Pu complexed with citrate. Culture flasks prepared for *P. putida* and *E. coli* were spiked with 194 µL of a solution of ^{239}Pu stock complexed with citrate that contains 12.6 kBq mL^{-1} ^{239}Pu following the same procedures found in Chapter 1. The activity of the cultures was 24 Bq mL^{-1}. An extra set of culture flasks that were inoculated with *P. putida* were spiked with 388 µL of the same ^{239}Pu solution such that these cultures contained 48 Bq mL^{-1} of ^{239}Pu. It is important to note that these cultures were grown as a representative of previous experiments, however the cultures were grown specifically for the purpose of examining oxidation states and were not used in any fractionation analysis. Samples were collected from bacteria cultures 1 day and 5 days after inoculation. A volume of 1 mL was collected for analysis. Oxidation state analysis of a set of representative samples was completed by James Foster at Clemson University in May 2021. Plutonium(IV) content was determined based on the results of extraction using 1-phenyl-3-methyl-4-benzoylpyrazol-5-one (PMBP), where the percent of total extraction product activity found in the organic phase is the percent of the sample that is Pu(IV). Plutonium (V) content was

determined based on the results of extraction using Bis(2-ethylhexyl)phosphoric acid (HDEHP) where the percent of total extraction product activity found in the aqueous phase is the percent of the sample that is Pu(V). Plutonium(VI) content was determined based on the result of subtracting the percent of total activity found in the aqueous phase during HDEHP extraction from the percent of total activity found in the aqueous phase during PMBP extraction. When this value was a negative value, it was determined that the samples contained little to no Pu(VI). The results of this analysis are found in **Table 4** with reported standard error.

Table 4 Reported results of oxidation state analysis for cell culture media and cell culture samples.

	Pu(IV)	Pu(V)	Pu(VI)
Cell Culture Media 24 Bq mL^{-1} ^{239}Pu	78 ± 1.1 %	35±0.7%	-
Cell Culture Media 48 Bq mL^{-1} ^{239}Pu	77 ± 0.8%	21 ± 0.4%	2 ± 0.6%
P. putida sample, 1 day after inoculation, 24 Bq mL^{-1} ^{239}Pu	27 ± 2.8%	84 ±3.0%	-
P. putida sample, 5 days after inoculation, 24 Bq mL^{-1} ^{239}Pu	4±0.6%	95±2.3%	1±3.0%
P. putida sample, 1 day after inoculation, 48 Bq mL^{-1} ^{239}Pu	13±1.4%	96±2.9%	-
P. putida sample, 5 days after inoculation, 48 Bq mL^{-1} ^{239}Pu	10±1.1%	95±1.5%	-
E. coli sample, 1 day after inoculation, 24 Bq mL^{-1} ^{239}Pu	74±1.9%	2±0.1%	25±0.9%
E. coli sample, 5 days after inoculation, 24 Bq mL^{-1} ^{239}Pu	72±1.5%	9±0.8%	19±1.1%

APPENDIX C

M9 MINIMAL MEDIA RECIPE

M9 Minimal Growth Medium (Liquid)

The M9 minimal growth media was created with the following, standard, components:

M9 minimal salts, 5X (BD Difco),

1M $MgSO_2*7H_2O$ (Sigma-Aldrich),

1M $CaCl_2$ supplemented with 0.5% glucose (Sigma-Aldrich),

1% thiamine hydrochloride (Spectrum), and

1% (w/v) casamino acids (Bacto)

If prepared with above stock concentrations, the following will produce 1 L of medium.

Table 5 M9 stock solution components.

Stock concentration component	Volume of stock added
Sterilized ddH20	759.95 mL *Use this to bring volume to 1L
Sterile 5X M9 Salts	220.12 mL
1M Calcium chloride (CaCl2)	110.06 µL
1M Magnesium sulfate ($MgSO4*7H_2O$)	2.2 mL
1% Thiamine HCl (Vitamin B12)	1 mL
*40% Glucose	12.5 mL
20 % Casamino acids	5.5 mL

APPENDIX D

CORRECTIONS FOR INGROWTH OF PROGENY IN PLUTONIUM STOCK

The ^{239}Pu stock provided by the Powell Radiochemistry group was stated to contain 99.919% ^{239}Pu by mass as of July 15th, 2015. While the stock contained only 0.012% ^{241}Pu, by mass, the short half-life and associated high-specific activity of ^{241}Pu. The stock underwent chemical separation to separate Pu from its progeny in the laboratory, as well. The contents of the stock at the time of chemical separation are provided in **Table 6.**

Table 6 Reported Pu Stock Contents and Associated Radiological Data

	Reported percent by mass	***Half-life (years)***	***Specific activity (TBq g^{-1})***	***Emission type***	***Emission energy (MeV)***
^{238}Pu	0.002	87.74	6.34×10^{-1}	Alpha	5.48
^{239}Pu	99.919	24,065	2.30×10^{-3}	Alpha	5.14
^{240}Pu	0.055	6,537	8.43×10^{-3}	Alpha	5.16
^{241}Pu	0.012	14.4	3.81	Beta	5.2 (average)
^{242}Pu	0.012	380,000	1.48×10^{-4}	Alpha	4.91

Isotopes of Pu were decay corrected based on the date of July 15th, 2015. Additionally, ^{234}U, ^{235}U, ^{236}U, ^{241}Am, and ^{238}U were considered as associated progeny based on the last date of radiochemical separation. When the stock solution was analyzed via LSC, two alpha peaks were observed in association with the Pu isotopes and their progeny, one peak that encompassed all detectable alpha emissions from 4.4-5.16 MeV, and a second peak representing the two highest-energy emissions from ^{238}Pu and ^{241}Am (5.48 and 5.4 MeV, respectively). The beta peak from ^{241}Pu was also characterized.

By using the date of ^{239}Pu measurement, the date of last chemical separation, and the date of measurement by LSC in the experiments, correction factors to activity attributed to ^{239}Pu were calculated. The correction factors, of course, varied for all experiments based on the dates of chemical separation and experiment. In general, ^{241}Pu accounted for 12-16% of total activity, which was found in the beta peak. In cases where ^{55}Fe was considered in combination with ^{239}Pu, the results were corrected based on this as there is overlap in the peaks formed from the ^{55}Fe electrons and ^{241}Pu betas. A copy of the spreadsheet used to calculate these ratios is provided as **Figure 24** to provide more clarity on the process used.

Background informatiion

Date Pu Seperation Occurred	12-Apr-18	Years Since Seperation	1.61533196	3 Peaks were quantified: 1) 5 keV beta peak, channels 1-32 2) Alpha Peak 1 in the range of 5.1 MeV, channels 153-467 and 3) Alpha Peak 2, for alphas in the range of 5.5 MeV, channels 468:766
Date Isotopic Composition Confirmed	7-Jul-15	Years Since Composition Confirmed	4.38056126	
		Years Between Composition Confirmation and Seperation		
Date of Meaurements	23-Nov-19		2.7652293	

Radioisotope Data

	Half Life (years)	Decay Constant	Specific Activity (TBq/g)	Average Alpha Energy (MeV)	Associated Peak
Pu-238	87.74	0.00790001	0.634	5.48	Alpha 2
Pu-239	24065	2.8803E-05	2.30E-03	5.14	Alpha 1
Pu-240	6537	0.00010603	8.43E-03	5.16	Alpha 1
Pu-241	14.4	0.04813522	3.81	-	Beta
Pu-242	380000	1.8241E-06	0.000148	4.91	Alpha 1

Isotopic Composition

Plutonium Isotope	Reported Percent by Mass	Activity in 100 g 7-Jul-15 (Bq)	Decay Corrected Activity in 100 g on 12-Apr-18	Decay Corrected Activity 27-Apr-18 (Bq)
238	0.002	1.27E+09	1.22E+09	1.24E+09
239	99.919	2.30E+11	2.30E+11	2.30E+11
240	0.055	4.64E+08	4.63E+08	4.64E+08
241	0.012	4.57E+10	3.70E+10	4.00E+10
242	0.012	1.78E+06	1.78E+06	1.78E+06
243	0	-		
244	0	-		

Ingrowth Products

Isotope	Half-Life (years)	Decay Constant	Average Alpha Energy (MeV)	Ingrowth since seperation (Bq)	Associated Peak
U-234	2.45E+05	2.82E-06	4.8	5.62E+03	Alpha 1
U-235	7.04E+08	9.85E-10	4.4	3.66E+02	Alpha 1
U-236	2.34E+07	2.96E-08	4.48	2.22E+01	Alpha 1
Am-241	432.2	1.60E-03	5.4	9.96E+07	Alpha 2
U-238	4.47E+09	1.55E-10	4.18	4.45E-04	Alpha 1

$$A_2(t) = \frac{\lambda_2}{\lambda_2 - \lambda_1} A_t^0 (e^{-\lambda_1 t} - e^{-\lambda_2 t})$$

TOTAL ACTIVITY

Total Activity of 100 g on 12-APR-2018 (Bq)	**2.69E+11**

Beta Peak

Isotope	Activity (Bq)	Percent Total Activity
Pu-241	3.70E+10	13.79%
Beta Peak Percent Total Activity		13.79%

Alpha Peak 1

Isotope	Activity (Bq)	Percent Total Activity
Pu-239	2.30E+11	85.55%
Pu-240	4.63E+08	0.17%
Pu-242	1.78E+06	0.00%
U-234	5.62E+03	0.00%
U-235	3.66E+02	0.00%
U-236	2.22E+01	0.00%
U-238	4.45E-04	0.00%
Alpha Peak 1 Percent Total Activity		85.72%

Alpha Peak 2

Isotope	Activity (Bq)	Percent Total Activity
Pu-238	1.22E+09	0.46%
Am-241	9.96E+07	0.04%
Alpha Peak 2 Percent Total Activity		0.49%

***The efficency for alpha counting in liquid scintillation is close to 100% and measured to be around 40.8% for 5 keV beta/gamma counting. As a result, the beta peak value divided by 0.408 to roughly account for this difference.**

Figure 24 An example of a spreadsheet used for determining Pu and progeny content.

APPENDIX E

RESULTS OF RNA FLOWTHROUGH ANALYSIS

Table 7 RNA Extraction and Effluent Activities for Flowthrough Experiments using ^{239}Pu Complexed with Citrate. Only samples in bold were reported as having detectable quantities of ^{239}Pu

Blank Concentration	**Replicate**	**RNA Extraction Activity (Bq)**	**Error (Bq)**	**MDA**	**Effluent Activity (Bq)**	**Error (Bq)**	**MDA**
	1	4.58E-02	3.33E-02	1.25E-01	**7.73E+02**	**1.74E+00**	3.46E+00
1.37x10^{1} kBq mL^{-1}	2	1.37E-02	3.29E-02	1.25E-01	**7.71E+02**	**1.74E+00**	3.45E+00
	3	-1.96E-03	3.28E-02	1.25E-01	**3.65E+02**	**1.20E+00**	2.56E+00
	1	-9.15E-03	3.27E-02	1.24E-01	**7.71E+01**	**5.52E-01**	1.50E+00
1.37 kBq mL^{-1}	2	-2.61E-03	3.28E-02	1.24E-01	**7.91E+01**	**5.59E-01**	1.52E+00
	3	3.27E-03	3.28E-02	1.25E-01	**7.85E+01**	**5.57E-01**	1.51E+00
	1	6.54E-04	3.28E-02	1.25E-01	**6.15E+00**	**1.62E-01**	8.65E-01
1.37x10^{-1} kBq mL^{-1}	2	0.00E+00	3.28E-02	1.25E-01	**6.17E+00**	**1.62E-01**	8.66E-01
	3	-5.88E-03	3.27E-02	1.24E-01	**6.16E+00**	**1.62E-01**	8.65E-01
	1	0.00E+00	3.28E-02	1.25E-01	**5.74E-01**	**6.53E-02**	7.07E-01
1.37x10^{-2} kBq mL^{-1}	2	-1.18E-02	3.27E-02	1.24E-01	**6.88E-01**	**6.87E-02**	7.13E-01
	3	8.50E-03	3.29E-02	1.25E-01	**6.41E-01**	**6.73E-02**	7.10E-01
	1	6.54E-03	3.29E-02	1.25E-01	**6.80E-02**	**4.78E-02**	6.78E-01
1.37x10^{-3} kBq mL^{-1}	2	1.31E-02	3.29E-02	1.25E-01	**1.03E-01**	**4.92E-02**	6.81E-01
	3	-1.05E-02	3.27E-02	1.24E-01	**-2.58E-01**	**3.18E-02**	6.52E-01

Table 8 RNA Extraction and Effluent Activities for Flowthrough Experiments using ^{239}Pu without complexation. Only samples in bold were reported as having detectable quantities of ^{239}Pu.

Blank Concentration	**Replicate**	**RNA Extraction Activity (Bq)**	**Error (Bq)**	**MDA**	**Effluent Activity (Bq)**	**Error (Bq)**	**MDA**
	1	**8.73E-01**	**4.06E-02**	1.37E-01	**6.39E+00**	**1.65E-01**	8.70E-01
1.37x10^{1} kBq mL^{-1}	2	-2.61E-02	3.25E-02	1.24E-01	**6.33E+00**	**1.64E-01**	8.69E-01
	3	-9.15E-03	3.27E-02	1.24E-01	**6.78E+00**	**1.69E-01**	8.77E-01
	1	1.31E-02	3.29E-02	1.25E-01	4.72E-01	6.22E-02	7.02E-01
1.37 kBq mL^{-1}	2	-4.58E-03	3.28E-02	1.24E-01	5.27E-01	6.39E-02	7.05E-01
	3	9.15E-03	3.29E-02	1.25E-01	4.84E-01	6.26E-02	7.03E-01
	1	1.57E-02	3.30E-02	1.25E-01	-6.54E-03	4.46E-02	6.73E-01
1.37x10^{-1} kBq mL^{-1}	2	-1.63E-02	3.26E-02	1.24E-01	9.15E-02	4.88E-02	6.80E-01
	3	7.19E-03	3.29E-02	1.25E-01	4.44E-02	4.68E-02	6.77E-01
	1	-1.83E-02	3.26E-02	1.24E-01	-2.61E-02	4.38E-02	6.72E-01
1.37x10^{-2} kBq mL^{-1}	2	-5.88E-03	3.27E-02	1.24E-01	2.09E-02	4.58E-02	6.75E-01
	3	-6.54E-03	3.27E-02	1.24E-01	1.70E-02	4.57E-02	6.75E-01
	1	-6.54E-04	3.28E-02	1.25E-01	9.15E-03	4.53E-02	6.74E-01
1.37x10^{-3} kBq mL^{-1}	2	3.27E-03	3.28E-02	1.25E-01	-1.05E-02	4.45E-02	6.73E-01
	3	-3.27E-03	3.28E-02	1.24E-01	-4.18E-02	4.31E-02	6.71E-01

Table 9 RNA Extraction and Effluent Activities for Flowthrough Experiments using ^{55}Fe. Only samples in bold were reported as having detectable quantities of ^{55}Fe.

Blank Concentration	**Replicate**	**RNA Extraction Activity (Bq)**	**Error (Bq)**	**MDA (Bq)**	**Effluent Activity (Bq)**	**Error (Bq)**	**MDA (Bq)**
1.81x10^4 kBq mL^{-1}	1	**2.19E+00**	**1.63E-01**	1.76E+00	**2.80E+05**	**4.63E+01**	7.76E+01
	2	**5.86E+00**	**2.34E-01**	1.88E+00	**2.59E+05**	**4.45E+01**	7.46E+01
	3	**6.65E+00**	**2.46E-01**	1.90E+00	**2.62E+05**	**4.48E+01**	7.51E+01
1.81x10^3 kBq mL^{-1}	1	**4.09E+00**	**2.03E-01**	1.83E+00	**2.50E+04**	**1.38E+01**	2.43E+01
	2	1.56E-01	1.05E-01	1.67E+00	**2.53E+04**	**1.39E+01**	2.45E+01
	3	1.94E-01	1.06E-01	1.67E+00	**1.33E+04**	**1.01E+01**	1.82E+01
1.81x10^2 kBq mL^{-1}	1	8.68E-02	1.02E-01	1.66E+00	**2.34E+03**	**4.24E+00**	8.57E+00
	2	3.24E-01	1.11E-01	1.68E+00	**2.33E+03**	**4.23E+00**	8.55E+00
	3	1.17E-01	1.04E-01	1.66E+00	**2.29E+03**	**4.19E+00**	8.48E+00
1.81x10^1 kBq mL^{-1}	1	4.09E-02	1.01E-01	1.66E+00	**2.18E+02**	**1.30E+00**	3.75E+00
	2	7.15E-02	1.02E-01	1.66E+00	**2.79E+02**	**1.47E+00**	4.02E+00
	3	1.02E-02	9.95E-02	1.66E+00	**2.17E+02**	**1.29E+00**	3.74E+00
1.81 kBq mL^{-1}	1	1.25E-01	1.04E-01	1.66E+00	**1.94E+01**	**3.99E-01**	2.27E+00
	2	-1.28E-01	9.41E-02	1.65E+00	**1.76E+01**	**3.81E-01**	2.24E+00
	3	3.47E-01	1.12E-01	1.68E+00	**1.79E+01**	**3.84E-01**	2.25E+00

Table 10 RNA Extraction and Effluent Activities for Flowthrough Experiments where cells were spiked with ^{239}Pu with and without citrate complexation after lysing. Only samples in bold were reported as having detectable quantities of ^{239}Pu.

Spike Concentration	**With citrate?**	**RNA Extraction Activity (Bq)**	**Error (Bq)**	**MDA (Bq)**	**Effluent Activity (Bq)**	**Error (Bq)**	**MDA (Bq)**
1.37 kBq mL^{-1}	Yes	1.76E-02	3.30E-02	1.25E-01	**8.37E+00**	**1.87E-01**	9.06E-01
1.37x10^{-1} kBq mL^{-1}	Yes	1.50E-02	3.29E-02	1.25E-01	6.99E-01	6.90E-02	7.13E-01
1.37x10^{-2} kBq mL^{-1}	Yes	1.31E-02	3.29E-02	1.25E-01	4.05E-02	4.67E-02	6.77E-01
1.37 kBq mL^{-1}	No	1.37E-02	3.29E-02	1.25E-01	1.70E-02	4.57E-02	6.75E-01
1.37x10^{-1} kBq mL^{-1}	No	2.09E-02	3.30E-02	1.25E-01	2.09E-02	4.58E-02	6.75E-01
1.37x10^{-2} kBq mL^{-1}	No	8.50E-03	3.29E-02	1.25E-01	5.62E-02	4.73E-02	6.78E-01

REFERENCES

(1) Beck, H. L.; Bennett, B. G. A Historical Overview of Atmosphere Nuclear Weapons Testing and Estimates of Fallout in the Continental United States. *Health Physics* **2002**, *82* (5), 591–608. https://doi.org/10.1097/00004032-200205000-00007.

(2) Maher, K.; Bargar, J. R.; Brown, G. E. Environmental Speciation of Actinides. *Inorganic Chemistry* **2013**, *52* (7), 3510–3532. https://doi.org/10.1021/ic301686d.

(3) Silva, R. J.; Nitsche, H. Actinide Environmental Chemistry. *Radiochimica Acta* **1995**, *70–71*, 377–396.

(4) Steinhauser, G.; Brandl, A.; Johnson, T. E. Comparison of the Chernobyl and Fukushima Nuclear Accidents: A Review of the Environmental Impacts. *Science of The Total Environment* **2014**, *470–471*, 800–817. https://doi.org/10.1016/j.scitotenv.2013.10.029.

(5) Whicker, F. W.; Schultz, V. *Radioecology: Nuclear Energy and the Environment*; CRC Press, 1982; Vol. 1.

(6) Kaplan, D. I.; Demirkanli, D. I.; Molz, F. J.; Beals, D. M.; Cadieux, J. R.; Halverson, J. E. Upward Movement of Plutonium to Surface Sediments during an 11-Year Field Study. *Journal of Environmental Radioactivity* **2010**, *101* (5), 338–344. https://doi.org/10.1016/j.jenvrad.2010.01.007.

(7) Romanchuk, A. Y.; Kalmykov, S. N.; Kersting, A. B.; Zavarin, M. Behavior of Plutonium in the Environment. *Russian Chemical Reviews* **2016**, *85* (9), 995–1010. https://doi.org/10.1070/RCR4602.

(8) Boggs, A.; Yonggin, J.; Zurong, D.; Zavarin, M.; Kersting, A. B. Interactions of Plutonium with Pseudomonas Sp. Strain EPS-1W and Its Extracellular Polymeric Substances. *Applied and Environmental Microbiology* **2016**, *82* (24), 7093–7101. https://doi.org/10.1128/AEM.02572-16.

(9) Ewing, R. C. Nuclear Waste Forms for Actinides. *Proceedings of the National Academy of Sciences* **1999**, *96* (7), 3432–3439. https://doi.org/10.1073/pnas.96.7.3432.

(10) Bachmann, B. J. Pedigrees of Some Mutant Strains of Escherichia Coli K-12. **1972**, *36*, 33.

(11) Alberts, B.; Johnson, A.; Lewis, J.; Raff, M.; Roberts, K.; Walter, P. *Molecular Biology of The Cell*, Fifth Edition.; Garland Science: New Tork, 2008.

(12) Durfee, T.; Nelson, R.; Baldwin, S.; Plunkett, G.; Burland, V.; Mau, B.; Petrosino, J. F.; Qin, X.; Muzny, D. M.; Ayele, M.; Gibbs, R. A.; Csörgő, B.; Pósfai, G.; Weinstock, G. M.; Blattner, F. R. The Complete Genome Sequence of Escherichia Coli DH10B: Insights into

the Biology of a Laboratory Workhorse. *JB* **2008**, *190* (7), 2597–2606. https://doi.org/10.1128/JB.01695-07.

(13) Riley, M. *Correlates of Smallest Sizes for Microorganisms. Size Limits of Very Small Microorganisms.*; Proceedings of a Workshop of the National Research Council; National Academies of Science: Washington D.C., 1999; pp 21–25.

(14) Singh, P.; Saini, H.; Kahlon, R. Pseudomonas: The Versatile and Adaptive Metabolic Nework. In *Pseudomonas: Molecular and Applied Biology*; Springer International Publishing, 2016; pp 81–126.

(15) Weinel, C.; Nelson, K. E.; Tummler, B. Global Features of the Pseudomonas Putida KT2440 Genome Sequence. *Environmental Microbiology* **2002**, *4* (12), 809–818. https://doi.org/10.1046/j.1462-2920.2002.00331.x.

(16) Davis, M. L.; Mounteer, L. C.; Stevens, L. K.; Miller, C. D.; Zhou, A. 2D Motility Tracking of Pseudomonas Putida KT2440 in Growth Phases Using Video Microscopy. *Journal of Bioscience and Bioengineering* **2011**, *111* (5), 605–611. https://doi.org/10.1016/j.jbiosc.2011.01.007.

(17) *ICRP Publication 103 The 2007 Recommendations of the International Commission on Radiological Protection*; International Commission on Radiological Protection, 2007.

(18) Dauer, L. T.; Brooks, A. L.; Hoel, D. G.; Morgan, W. F.; Stram, D.; Tran, P. Review and Evaluation of Updated Research on the Health Effects Associated with Low-Dose Ionising Radiation. *Radiation Protection Dosimetry* **2010**, *140* (2), 103–136. https://doi.org/10.1093/rpd/ncq141.

(19) Shleinen, B. *The Health Physics and Radiological Health Handbook*, Revised.; Scinta, Inc., 1992.

(20) Phillips, S. H.; Donaher, S. E.; Powell, B. A.; Tharayil, N.; Martinez, N. E. The Influence of Iron and Ligand Type on Plutonium Uptake in Two Strains of Hydroponically Grown Corn (Zea Mays). *Health Phys* **2022**. https://doi.org/10.1097/HP.0000000000001638.

(21) *Speciation of Plutonium and Americium in Ground Waters from the Radioactive Waste Management Complex, Idaho National Engineering Laboratory, Idaho*; 1993. https://doi.org/10.3133/wri934035.

(22) Pardo, R.; Herguedas, M.; Barrado, E.; Vega, M. Biosorption of Cadmium, Copper, Lead and Zinc by Inactive Biomass of Pseudomonas Putida. *Analytical and Bioanalytical Chemistry* **2003**, *376* (1), 26–32. https://doi.org/10.1007/s00216-003-1843-z.

(23) Neu, M. P.; Icopini, G. A.; Boukhalfa, H. Plutonium Speciation Affected by Environmental Bacteria. *Radiochimica Acta* **2009**, *93* (11), 705–714. https://doi.org/10.1524/ract.2005.93.11.705.

(24) Francis, A. J.; Dodge, C. J.; Gillow, J. B. Biotransformation of Plutonium Complexed with Citric Acid. *Radiochimica Acta* **2006**, *94* (9–11), 731–737.

(25) Lin, P.; Xu, C.; Kaplan, D. I.; Chen, H.; Yeager, C. M.; Xing, W.; Sun, L.; Schwehr, K. A.; Yamazaki, H.; Saito-Kokubu, Y.; Hatcher, P. G.; Santschi, P. H. Nagasaki Sediments Reveal That Long-Term Fate of Plutonium Is Controlled by Select Organic Matter Moieties. *Science of The Total Environment* **2019**, *678*, 409–418. https://doi.org/10.1016/j.scitotenv.2019.04.375.

(26) D'Arrigo, I.; Cardoso, J. G. R.; Rennig, M.; Sonnenschein, N.; Herrgård, M. J.; Long, K. S. Analysis of *Pseudomonas Putida* Growth on Non-trivial Carbon Sources Using Transcriptomics and Genome-scale Modelling. *Environmental Microbiology Reports* **2019**, *11* (2), 87–97. https://doi.org/10.1111/1758-2229.12704.

(27) Blount, Z. D.; Borland, C. Z.; Lenski, R. E. Historical Contingency and the Evolution of a Key Innovation in an Experimental Population of Escherichia Coli. *Proceedings of the National Academy of Sciences* **2008**, *105* (23), 7899–7906. https://doi.org/10.1073/pnas.0803151105.

(28) Lacoue-Labarthe, T.; Warnau, M.; Beaugeard, L.; Pascal, P.-Y. Trophic Transfer of Radioisotopes in Mediterranean Sponges through Bacteria Consumption. *Chemosphere* **2016**, *144*, 1885–1892. https://doi.org/10.1016/j.chemosphere.2015.10.046.

(29) U.S. Department of Energy. *A Graded Approach For Evaluating Radiation Doses to Aquatic and Terrestrial Biota*; DOE-STD-1153-2019; Washington, D.C., 2019.

(30) United Nations; United Nations. *Sources and Effects of Ionizing Radiation, UNSCEAR 2008 Report.*; 2011.

(31) Fesenko, S. Review of Radiation Effects in Non-Human Species in Areas Affected by the Kyshtym Accident. *Journal of Radiological Protection* **2019**, *39* (1), R1–R17. https://doi.org/10.1088/1361-6498/aafa92.

(32) Lewis, C. L.; Craig, C. C.; Senecal, A. G. Mass and Density Measurements of Live and Dead Gram-Negative and Gram-Positive Bacterial Populations. *Applied and Environmental Microbiology* **2014**, *80* (12), 3622–3631. https://doi.org/10.1128/AEM.00117-14.

(33) Joshi, H.; Dave, R.; Venugopalan, V. P. Pumping Iron to Keep Fit: Modulation of Siderophore Secretion Helps Efficient Aromatic Utilization in Pseudomonas Putida KT2440. *Microbiology* **2014**, *160* (7), 1393–1400. https://doi.org/10.1099/mic.0.079277-0.

(34) Boukhalfa, H. Siderophore Production and Facilitated Uptake of Iron and Plutonium in P. Putida. In *AIP Conference Proceedings*; AIP: Albuquerquer, New Mexico (USA), 2003; Vol. 673, pp 343–344. https://doi.org/10.1063/1.1594658.

(35) Ratledge, C.; Dover, L. G. Iron Metabolism in Pathogenic Bacteria. *Annual Review of Microbiology* **2000**, *54* (1), 881–941. https://doi.org/10.1146/annurev.micro.54.1.881.

(36) Raymond, N.; Cass, M. E.; Evans, S. L. Metal Sequestering Agents in Bioinorganic Chemistry: Enterobactin Mediated Iron Transport in E. Coil and Biomimetic Applications. *Pure and Applied Chemistry* **1987**, *59* (6), 771–779.

(37) *Pseudomonas: Molecular and Applied Biology*; Kahlon, R. S., Ed.; Springer International Publishing: Cham, 2016. https://doi.org/10.1007/978-3-319-31198-2.

(38) Eckerman, K.; Endo, A. ICRP Publication 107. Nuclear Decay Data for Dosimetric Calculations. *Annals of the International Commission on Radiological Protection* **2008**, *38*.

(39) Committee on Developing a Long-Term Strategy for Low-Dose Radiation Research in the United States; Nuclear and Radiation Studies Board; Division on Earth and Life Studies; National Academies of Sciences, Engineering, and Medicine. *Leveraging Advances in Modern Science to Revitalize Low-Dose Radiation Research in the United States*; National Academies Press: Washington, D.C., 2022; p 26434. https://doi.org/10.17226/26434.

(40) Hoelbling, S. Competitive Uptake of Plutonium and Iron in Corn (Zea Mays). Masters Thesis, Clemson University, 2016.

(41) Ott, R. L.; Longnecker, M. *In Introduction to Statistical Methods and Data Analysis*, Sixth Edition.; Brooks/Cole: Belmont, CA, 2010.

(42) Cornelis, P. Iron Uptake and Metabolism in Pseudomonads. *Applied Microbiology and Biotechnology* **2010**, *86* (6), 1637–1645. https://doi.org/10.1007/s00253-010-2550-2.

(43) Matilla, M. A.; Ramos, J. L.; Duque, E.; de Dios Alché, J.; Espinosa-Urgel, M.; Ramos-González, M. I. Temperature and Pyoverdine-Mediated Iron Acquisition Control Surface Motility of *Pseudomonas Putida*: Swarming in *Pseudomonas Putida*. *Environmental Microbiology* **2007**, *9* (7), 1842–1850. https://doi.org/10.1111/j.1462-2920.2007.01286.x.

(44) Kang, D.; Kirienko, D. R.; Webster, P.; Fisher, A. L.; Kirienko, N. V. Pyoverdine, a Siderophore from *Pseudomonas Aeruginosa* , Translocates into *C. Elegans* , Removes Iron, and Activates a Distinct Host Response. *Virulence* **2018**, *9* (1), 804–817. https://doi.org/10.1080/21505594.2018.1449508.

(45) Lin, P.; Xu, C.; Kaplan, D. I.; Chen, H.; Yeager, C. M.; Xing, W.; Sun, L.; Schwehr, K. A.; Yamazaki, H.; Saito-Kokubu, Y.; Hatcher, P. G.; Santschi, P. H. Nagasaki Sediments Reveal That Long-Term Fate of Plutonium Is Controlled by Select Organic Matter Moieties. *Science of The Total Environment* **2019**, *678*, 409–418. https://doi.org/10.1016/j.scitotenv.2019.04.375.

(46) Neu, M. P.; Boukhalfa, H.; Merroun, M. L. Biomineralization and Biotransformations of Actinide Materials. *MRS Bull.* **2010**, *35* (11), 849–857. https://doi.org/10.1557/mrs2010.711.

(47) Kanellis, V. G.; dos Remedios, C. G. A Review of Heavy Metal Cation Binding to Deoxyribonucleic Acids for the Creation of Chemical Sensors. *Biophys Rev* **2018**, *10* (5), 1401–1414. https://doi.org/10.1007/s12551-018-0455-y.

(48) Ma, J.; Haldar, S.; Khan, M. A.; Sharma, S. D.; Merrick, W. C.; Theil, E. C.; Goss, D. J. Fe2+ Binds Iron Responsive Element-RNA, Selectively Changing Protein-Binding Affinities and Regulating MRNA Repression and Activation. *Proceedings of the National Academy of Sciences* **2012**, *109* (22), 8417–8422. https://doi.org/10.1073/pnas.1120045109.

(49) Netto, L. E. S.; Da Costa Ferreira, A. M.; Augusto, O. Iron(III) Binding in DNA Solutions: Complex Formation and Catalyric Activity in the Oxidation of Hydrazine Derivatives. *Chemico-Biological Interactions* **1991**, *79* (1), 1–14. https://doi.org/10.1016/0009-2797(91)90048-C.

(50) Andreev, G.; Budantseva, N.; Sokolova, M.; Tananaev, I.; Myasoedov, B. Interaction of Transuranium Elements with Biologically Important Ligands: Structural and Spectroscopic Evidence for Nucleotide Coordination to Plutonium. *Inorg. Chem.* **2009**, *48* (6), 2343–2345. https://doi.org/10.1021/ic802053s.

(51) Liang, K. H. *Bioinformatics for Biomedical Science and Clinical Applicaitons*; Woodhead Publishing: Oxford, 2013.

(52) Hoeijmakers, J. H. Genome Maintenance Mechanisms for Preventing Cancer. *Nature* **2001**, *411* (6835), 366–374. https://doi.org/10.1038/35077232.

(53) von Sonntag, C. *Free-Radical-Induced DNA Damage and Its Repair A Chemical Perspective*; Springer: Berlind, 2006.

(54) Wei, J.; Meng, L.; Hou, X.; Qu, C.; Wang, B.; Xin, Y.; Jiang, X. Radiation-Induced Skin Reactions: Mechanism and Treatment. *CMAR* **2018**, *Volume 11*, 167–177. https://doi.org/10.2147/CMAR.S188655.

(55) Clement, C. H.; Stewart, F. A.; Akleyev, A. V.; Hauer-Jensen, M.; Hendry, J. H.; Kleiman, N. J.; MacVittie, T. J.; Aleman, B. M.; Edgar, A. B.; Mabuchi, K.; Muirhead, C. R.; Shore, R. E.; Wallace, W. H. ICRP PUBLICATION 118: ICRP Statement on Tissue Reactions and Early and Late Effects of Radiation in Normal Tissues and Organs — Threshold Doses for Tissue Reactions in a Radiation Protection Context. *Annals of the ICRP* **2012**, *41* (1–2), 1–322. https://doi.org/10.1016/j.icrp.2012.02.001.

(56) Arena, C.; De Micco, V.; Macaeva, E.; Quintens, R. Space Radiation Effects on Plant and Mammalian Cells. *Acta Astronautica* **2014**, *104* (1), 419–431.

(57) Hall, E. J.; Giaccia, A. J. *Radiobiology for the Radiologist*, Seventh.; Wolters Kluwer, 2012.

(58) Boice Jr., J. D.; Bouville, A.; Dauer, L. T.; Golden, A. P.; Wakeford, R. Introduction to the Special Issue on the US Million Person Study of Health Effects from Low-Level Exposure to Radiation. *International Journal of Radiation Biology* **2022**, *98* (4), 529–532. https://doi.org/10.1080/09553002.2021.1989906.

(59) Brooks, A. L.; Hoel, D. G.; Preston, R. J. The Role of Dose Rate in Radiation Cancer Risk: Evaluating the Effect of Dose Rate at the Molecular, Cellular and Tissue Levels Using Key Events in Critical Pathways Following Exposure to Low LET Radiation. *Int J Radiat Biol* **2016**, *92* (8), 405–426. https://doi.org/10.1080/09553002.2016.1186301.

(60) Ouameur, A. A.; Arakawa, H.; Ahmad, R.; Naoui, M.; Tajmir-Riahi, H. A. A Comparative Study of Fe(II) and Fe(III) Interactions with DNA Duplex: Major and Minor Grooves Bindings. *DNA and Cell Biology* **2005**, *24* (6), 394–401. https://doi.org/10.1089/dna.2005.24.394.

(61) Berens, C.; Streicher, B.; Schroeder, R.; Hillen, W. Visualizing Metal-Ion-Binding Sites in Group I Introns by Iron(II)-Mediated Fenton Reactions. *Chemistry and Biology* **1998**, No. 5, 163–175.

(62) Honda, K.; Smith, M. A.; Zhu, X.; Baus, D.; Merrick, W. C.; Tartakoff, A. M.; Hattier, T.; Harris, P. L.; Siedlak, S. L.; Fujioka, H.; Liu, Q.; Moreira, P. I.; Miller, F. P.; Nunomura, A.; Shimohama, S.; Perry, G. Ribosomal RNA in Alzheimer Disease Is Oxidized by Bound Redox-Active Iron. *Journal of Biological Chemistry* **2005**, *280* (22), 20978–20986. https://doi.org/10.1074/jbc.M500526200.

(63) Aryal, B. P.; Paunesku, T.; Woloschak, G. E.; He, C.; Jensen, M. P. A Proteomic Approach to Identification of Plutonium-Binding Proteins in Mammalian Cells. *Journal of Proteomics* **2012**, *75* (5), 1505–1514. https://doi.org/10.1016/j.jprot.2011.11.023.

(64) Claycamp, H. G.; Luo, D. Plutonium-Catalyzed Oxidative DNA Damage in the Absence of Significant Alpha-Particle Decay. *Radiation Research* **1994**, *137* (1), 114. https://doi.org/10.2307/3578799.

(65) Miller, A.; Stewart, M.; Brooks, K.; Shi, L.; Page, N. Depleted Uranium-Catalyzed Oxidative DNA Damage: Absence of Significant Alpha Particle Decay. *Journal of Inorganic Biochemistry* **2002**, No. 91, 246–252.

(66) Manglass, L.; Wintenberg, M.; Blenner, M.; Martinez, N. Pu-239 Accumulation in E. Coli and P. Putida Grown in Liquid Cultures. *Health Physics* **2021**, *121* (5).

(67) Manglass, L. M.; Wintenberg, M.; Vogel, C.; Blenner, M.; Martinez, N. E. Accumulation of Radio-Iron and Plutonium, Alone and in Combination, in Pseudomonas Putida Grown in

Liquid Cultures. *Journal of Radiological Protection* **2021**, *41* (4), 1199–1212. https://doi.org/10.1088/1361-6498/ac2f86.

(68) Windschitl, M.; Thompson, J.; Braaten, M. Beyond the Scientific Method: Model-Based Inquiry as a New Paradigm of Preference for School Science Investigations. *Science Education* **2008**, *92* (5), 941–967. https://doi.org/10.1002/sce.20259.

(69) Berger, M. J.; J. Coursey; Zucker, M. A.; Chang, J. *Stopping Power and Range Tables for Electrons, Protons, and Helium Ions*; NIST Standard Reference Database 124; National Institute of Standards and Technology, 2017. https://dx.doi.org/10.18434/T4NC7P.

(70) Meesungnoen, J.; Jay-Gerin, J.-P.; Filali-Mouhim, A.; Mankhetkorn, S. Low-Energy Electron Penetration Range in Liquid Water. *Radiation Research* **2002**, *158* (5), 657–660. https://doi.org/10.1667/0033-7587(2002)158[0657:LEEPRI]2.0.CO;2.

(71) Neidhart, F. C.; Ingraham, J. L.; Schaechter, M. Composition and Organization of the Bacterial Cell. In *Physiology of the Bacterial Cell A Molecular Approach*; Sineauer Associates, Inc., 1990.

(72) Wintenberg, M. E. Effects of Continuous in Situ Low-Dose Ionizing Radiation on Microorganisms. dissertation, Clemson University, 2022. https://tigerprints.clemson.edu/all_dissertations/3025.

(73) Santa Cruz, G. A. Microdosimetry: Principles and Applications. *Reports of Practical Oncology & Radiotherapy* **2016**, *21* (2), 135–139. https://doi.org/10.1016/j.rpor.2014.10.006.

(74) Braby, L. A. Experimental Microdosimetry: History, Applications and Recent Technical Advances. *Radiat Prot Dosimetry* **2015**, *166* (1–4), 3–9. https://doi.org/10.1093/rpd/ncv137.

(75) INCERTI, S.; BALDACCHINO, G.; BERNAL, M.; CAPRA, R.; CHAMPION, C.; FRANCIS, Z.; GUÈYE, P.; MANTERO, A.; MASCIALINO, B.; MORETTO, P.; NIEMINEN, P.; VILLAGRASA, C.; ZACHARATOU, C. THE GEANT4-DNA PROJECT. *International Journal of Modeling, Simulation, and Scientific Computing* **2010**, *01* (02), 157–178. https://doi.org/10.1142/S1793962310000122.

(76) Lazarakis, P.; Incerti, S.; Ivanchenko, V.; Kyriakou, I.; Emfietzoglou, D.; Corde, S.; Rosenfeld, A. B.; Lerch, M.; Tehei, M.; Guatelli, S. Investigation of Track Structure and Condensed History Physics Models for Applications in Radiation Dosimetry on a Micro and Nano Scale in Geant4. *Biomed. Phys. Eng. Express* **2018**, *4* (2), 024001. https://doi.org/10.1088/2057-1976/aaa6aa.

(77) Lammerding, J. Mechanics of the Nucleus. In *Comprehensive Physiology*; Terjung, R., Ed.; Wiley, 2011; pp 783–807. https://doi.org/10.1002/cphy.c100038.

(78) Petringa, G.; Romano, F.; Manti, L.; Pandola, L.; Attili, A.; Cammarata, F.; Cuttone, G.; Forte, G.; Manganaro, L.; Pipek, J.; Pisciotta, P.; Russo, G.; Cirrone, G. A. P. Radiobiological Quantities in Proton-Therapy: Estimation and Validation Using Geant4-Based Monte Carlo Simulations. *Physica Medica* **2019**, *58*, 72–80. https://doi.org/10.1016/j.ejmp.2019.01.018.

(79) Di Maria, S.; Belchior, A.; Romanets, Y.; Paulo, A.; Vaz, P. Monte Carlo Dose Distribution Calculation at Nuclear Level for Auger-Emitting Radionuclide Energies. *Applied Radiation and Isotopes* **2018**, *135*, 72–77. https://doi.org/10.1016/j.apradiso.2018.01.013.

(80) Douglass, M.; Bezak, E.; Penfold, S. Development of a Randomized 3D Cell Model for Monte Carlo Microdosimetry Simulations: Development of a Randomized 3D Cell Model. *Med. Phys.* **2012**, *39* (6Part1), 3509–3519. https://doi.org/10.1118/1.4719963.

(81) Fernández-Varea, J. M.; González-Muñoz, G.; Galassi, M. E.; Wiklund, K.; Lind, B. K.; Ahnesjö, A.; Tilly, N. Limitations (and Merits) of PENELOPE as a Track-Structure Code. *International Journal of Radiation Biology* **2012**, *88* (1–2), 66–70. https://doi.org/10.3109/09553002.2011.598209.

(82) Nikitaki, Z.; Nikolov, V.; Mavragani, I. V.; Mladenov, E.; Mangelis, A.; Laskaratou, D. A.; Fragkoulis, G. I.; Hellweg, C. E.; Martin, O. A.; Emfietzoglou, D.; Hatzi, V. I.; Terzoudi, G. I.; Iliakis, G.; Georgakilas, A. G. Measurement of Complex DNA Damage Induction and Repair in Human Cellular Systems after Exposure to Ionizing Radiations of Varying Linear Energy Transfer (LET). *Free Radical Research* **2016**, *50* (sup1), S64–S78. https://doi.org/10.1080/10715762.2016.1232484.

(83) Palmans, H.; Rabus, H.; Belchior, A. L.; Bug, M. U.; Galer, S.; Giesen, U.; Gonon, G.; Gruel, G.; Hilgers, G.; Moro, D.; Nettelbeck, H.; Pinto, M.; Pola, A.; Pszona, S.; Schettino, G.; Sharpe, P. H. G.; Teles, P.; Villagrasa, C.; Wilkens, J. J. Future Development of Biologically Relevant Dosimetry. *BJR* **2015**, *88* (1045), 20140392. https://doi.org/10.1259/bjr.20140392.

(84) Liu, W.; Tan, Z.; Zhang, L.; Champion, C. Investigation on the Correlation between Energy Deposition and Clustered DNA Damage Induced by Low-Energy Electrons. *Radiation and Environmental Biophysics* **2018**, *57* (2), 179–187. https://doi.org/10.1007/s00411-018-0730-0.

(85) Agostinelli, S.; Allison, J.; Amako, K.; Apostolakis, J.; Araujo, H.; Arce, P.; Asai, M.; Axen, D.; Banerjee, S.; Barrand, G.; Behner, F.; Bellagamba, L.; Boudreau, J.; Broglia, L.; Brunengo, A.; Burkhardt, H.; Chauvie, S.; Chuma, J.; Chytracek, R.; Cooperman, G.; Cosmo, G.; Degtyarenko, P.; Dell'Acqua, A.; Depaola, G.; Dietrich, D.; Enami, R.; Feliciello, A.; Ferguson, C.; Fesefeldt, H.; Folger, G.; Foppiano, F.; Forti, A.; Garelli, S.; Giani, S.; Giannitrapani, R.; Gibin, D.; Gómez Cadenas, J. J.; González, I.; Gracia Abril, G.; Greeniaus, G.; Greiner, W.; Grichine, V.; Grossheim, A.; Guatelli, S.; Gumplinger, P.; Hamatsu, R.; Hashimoto, K.; Hasui, H.; Heikkinen, A.; Howard, A.; Ivanchenko, V.; Johnson, A.; Jones, F. W.; Kallenbach, J.; Kanaya, N.; Kawabata, M.; Kawabata, Y.;

Kawaguti, M.; Kelner, S.; Kent, P.; Kimura, A.; Kodama, T.; Kokoulin, R.; Kossov, M.; Kurashige, H.; Lamanna, E.; Lampén, T.; Lara, V.; Lefebure, V.; Lei, F.; Liendl, M.; Lockman, W.; Longo, F.; Magni, S.; Maire, M.; Medernach, E.; Minamimoto, K.; Mora de Freitas, P.; Morita, Y.; Murakami, K.; Nagamatu, M.; Nartallo, R.; Nieminen, P.; Nishimura, T.; Ohtsubo, K.; Okamura, M.; O'Neale, S.; Oohata, Y.; Paech, K.; Perl, J.; Pfeiffer, A.; Pia, M. G.; Ranjard, F.; Rybin, A.; Sadilov, S.; Di Salvo, E.; Santin, G.; Sasaki, T.; Savvas, N.; Sawada, Y.; Scherer, S.; Sei, S.; Sirotenko, V.; Smith, D.; Starkov, N.; Stoecker, H.; Sulkimo, J.; Takahata, M.; Tanaka, S.; Tcherniaev, E.; Safai Tehrani, E.; Tropeano, M.; Truscott, P.; Uno, H.; Urban, L.; Urban, P.; Verderi, M.; Walkden, A.; Wander, W.; Weber, H.; Wellisch, J. P.; Wenaus, T.; Williams, D. C.; Wright, D.; Yamada, T.; Yoshida, H.; Zschiesche, D. Geant4—a Simulation Toolkit. *Nuclear Instruments and Methods in Physics Research Section A: Accelerators, Spectrometers, Detectors and Associated Equipment* **2003**, *506* (3), 250–303. https://doi.org/10.1016/S0168-9002(03)01368-8.

(86) Incerti, S.; Ivanchenko, A.; Karamitros, M.; Mantero, A.; Moretto, P.; Tran, H. N.; Mascialino, B.; Champion, C.; Ivanchenko, V. N.; Bernal, M. A.; Francis, Z.; Villagrasa, C.; Baldacchino, G.; Guèye, P.; Capra, R.; Nieminen, P.; Zacharatou, C. Comparison of GEANT4 Very Low Energy Cross Section Models with Experimental Data in Water. *Medical Physics* **2010**, *37* (9), 4692–4708. https://doi.org/10.1118/1.3476457.

(87) Incerti, S.; Kyriakou, I.; Bernal, M. A.; Bordage, M. C.; Francis, Z.; Guatelli, S.; Ivanchenko, V.; Karamitros, M.; Lampe, N.; Lee, S. B.; Meylan, S.; Min, C. H.; Shin, W. G.; Nieminen, P.; Sakata, D.; Tang, N.; Villagrasa, C.; Tran, H. N.; Brown, J. M. C. Geant4-DNA Example Applications for Track Structure Simulations in Liquid Water: A Report from the Geant4-DNA Project. *Medical Physics* **2018**, *45* (8), e722–e739. https://doi.org/10.1002/mp.13048.

(88) Salim, R.; Taherparvar, P. Monte Carlo Single-Cell Dosimetry Using Geant4-DNA: The Effects of Cell Nucleus Displacement and Rotation on Cellular S Values. *Radiat Environ Biophys* **2019**, *58* (3), 353–371. https://doi.org/10.1007/s00411-019-00788-z.

(89) Nikjoo, H.; Goodhead, D. T. Track Structure Analysis Illustrating the Prominent Role of Low-Energy Electrons in Radiobiological Effects of Low-LET Radiations. *Phys. Med. Biol.* **1991**, *36* (2), 229–238. https://doi.org/10.1088/0031-9155/36/2/007.

(90) Kyriakou, I.; Emfietzoglou, D.; Ivanchenko, V.; Bordage, M. C.; Guatelli, S.; Lazarakis, P.; Tran, H. N.; Incerti, S. Microdosimetry of Electrons in Liquid Water Using the Low-Energy Models of Geant4. *Journal of Applied Physics* **2017**, *122* (2), 024303. https://doi.org/10.1063/1.4992076.

(91) Massillon-JL, G. Future Directions on Low-Energy Radiation Dosimetry. *Sci Rep* **2021**, *11* (1), 10569. https://doi.org/10.1038/s41598-021-90152-3.

(92) Eyrolle, F.; Ducros, L.; Le Dizès, S.; Beaugelin-Seiller, K.; Charmasson, S.; Boyer, P.; Cossonnet, C. An Updated Review on Tritium in the Environment. *Journal of*

Environmental Radioactivity **2018**, *181*, 128–137. https://doi.org/10.1016/j.jenvrad.2017.11.001.

(93) Preston, R. C., Hans-Georg Menzel and Ju. Internal Dosimetry and Tritium—the ICRP Position. *Journal of Radiological Protection* **2008**, *28* (2), 131–135. https://doi.org/10.1088/0952-4746/28/2/E02.

(94) Hunter, N.; Muirhead, C. R. Review of Relative Biological Effectiveness Dependence on Linear Energy Transfer for Low-LET Radiations. *J. Radiol. Prot.* **2009**, *29* (1), 5–21. https://doi.org/10.1088/0952-4746/29/1/R01.

(95) *Health Effects, Dosimetry and Radiological Protection of Tritium: Part of the Tritium Studies Project*; Canadian Nuclear Safety Commission: Ottawa, Ont., 2010.

(96) ICRP. ICRP Publication 148. Radiation Weighting for Reference Animals and Plants. *Annals of the International Commission on Radiological Protection* **2021**, *50* (2).

(97) Chen, J. Radiation Quality of Tritium A Comparison with Cobalt-60 Gamma Rays. *Radiation Protection Dosimetry* **2013**, *122* (1–4), 546–548. https://doi.org/10.1093/rpd/ncl411.

(98) Johnson, T. E. *Introduction to Health Physics*, Fifth.; McGraw Hill Medical: New York, 2017.

(99) Lias, S. G.; Liebman, J. F. Ion Energetics Data. In *NIST Chemisty WebBook, NIST Standard Reference Database 69*; National Institute of Standards and Technology: Gaithersburg, MD.

(100) Emfietzoglou, D. Inelastic Cross-Sections for Electron Transport in Liquid Water: A Comparison of Dielectric Models. *Radiation Physics and Chemistry* **2003**, *66* (6), 373–385. https://doi.org/10.1016/S0969-806X(02)00504-2.

(101) Emfietzoglou, D.; Nikjoo, H. The Effect of Model Approximations on Single-Collision Distributions of Low-Energy Electrons in Liquid Water. *Radiation Research* **2005**, *163* (1), 98–111. https://doi.org/10.1667/RR3281.

(102) Champion, C.; Incerti, S.; Aouchiche, H.; Oubaziz, D. A Free-Parameter Theoretical Model for Describing the Electron Elastic Scattering in Water in the Geant4 Toolkit. *Radiation Physics and Chemistry* **2009**, *78* (9), 745–750. https://doi.org/10.1016/j.radphyschem.2009.03.079.

(103) Bernal, M. A.; Bordage, M. C.; Brown, J. M. C.; Davídková, M.; Delage, E.; El Bitar, Z.; Enger, S. A.; Francis, Z.; Guatelli, S.; Ivanchenko, V. N.; Karamitros, M.; Kyriakou, I.; Maigne, L.; Meylan, S.; Murakami, K.; Okada, S.; Payno, H.; Perrot, Y.; Petrovic, I.; Pham, Q. T.; Ristic-Fira, A.; Sasaki, T.; Štěpán, V.; Tran, H. N.; Villagrasa, C.; Incerti, S. Track Structure Modeling in Liquid Water: A Review of the Geant4-DNA Very Low Energy

Extension of the Geant4 Monte Carlo Simulation Toolkit. *Physica Medica* **2015**, *31* (8), 861–874. https://doi.org/10.1016/j.ejmp.2015.10.087.

(104) Bordage, M. C.; Bordes, J.; Edel, S.; Terrissol, M.; Franceries, X.; Bardiès, M.; Lampe, N.; Incerti, S. Implementation of New Physics Models for Low Energy Electrons in Liquid Water in Geant4-DNA. *Physica Medica* **2016**, *32* (12), 1833–1840. https://doi.org/10.1016/j.ejmp.2016.10.006.

(105) Sakata, D.; Lampe, N.; Karamitros, M.; Kyriakou, I.; Belov, O.; Bernal, M. A.; Bolst, D.; Bordage, M.-C.; Breton, V.; Brown, J. M. C.; Francis, Z.; Ivanchenko, V.; Meylan, S.; Murakami, K.; Okada, S.; Petrovic, I.; Ristic-Fira, A.; Santin, G.; Sarramia, D.; Sasaki, T.; Shin, W.-G.; Tang, N.; Tran, H. N.; Villagrasa, C.; Emfietzoglou, D.; Nieminen, P.; Guatelli, S.; Incerti, S. Evaluation of Early Radiation DNA Damage in a Fractal Cell Nucleus Model Using Geant4-DNA. *Physica Medica* **2019**, *62*, 152–157. https://doi.org/10.1016/j.ejmp.2019.04.010.

(106) Lampe, N.; Karamitros, M.; Breton, V.; Brown, J. M. C.; Sakata, D.; Sarramia, D.; Incerti, S. Mechanistic DNA Damage Simulations in Geant4-DNA Part 2: Electron and Proton Damage in a Bacterial Cell. *Physica Medica* **2018**, *48*, 146–155. https://doi.org/10.1016/j.ejmp.2017.12.008.

(107) Rafiepour, P.; Sina, S.; Tavakolialahabadi, Z. A Comparison of DNA Damages in an E. Coli Bacterium Induced by Low-Energy X-Ray and Electron Beam, Using Geant4-DNA.

(108) Baldwin, W. W.; Myer, R.; Powell, N.; Anderson, E.; Koch, A. L. Buoyant Density of Escherichia Coli Is Determined Solely by the Osmolarity of the Culture Medium. *Arch Microbiol* **1995**, *164* (2), 155–157. https://doi.org/10.1007/s002030050248.

(109) Moran, U.; Phillips, R.; Milo, R. SnapShot: Key Numbers in Biology. *Cell* **2010**, *141* (7), 1262-1262.e1. https://doi.org/10.1016/j.cell.2010.06.019.

(110) Howard, J.; Clark, R. Mechanics of Motor Proteins and the Cytoskeleton. *Applied Mechanics Reviews* **2002**, *55* (2), B39–B39. https://doi.org/10.1115/1.1451234.

(111) Feijó Delgado, F.; Cermak, N.; Hecht, V. C.; Son, S.; Li, Y.; Knudsen, S. M.; Olcum, S.; Higgins, J. M.; Chen, J.; Grover, W. H.; Manalis, S. R. Intracellular Water Exchange for Measuring the Dry Mass, Water Mass and Changes in Chemical Composition of Living Cells. *PLoS One* **2013**, *8* (7), e67590. https://doi.org/10.1371/journal.pone.0067590.

(112) Milo, R.; Jorgensen, P.; Moran, U.; Weber, G.; Springer, M. BioNumbers--the Database of Key Numbers in Molecular and Cell Biology. *Nucleic Acids Res* **2010**, *38* (Database issue), D750-753. https://doi.org/10.1093/nar/gkp889.